Automated Integrated Microfluidic Device for DNA Cloning

Zur Erlangung des akademischen Grades eines
DOKTORS DER INGENIEURWISSENSCHAFTEN (Dr.-Ing.)

von der KIT-Fakultät für Maschinenbau des
Karlsruher Instituts für Technologie (KIT)
angenommene

DISSERTATION

von

M.Sc. Daniela Sánchez

aus Mexiko

Hauptreferent: Prof. Dr. Andreas E. Guber

Korreferent: Prof. Dr. Jan G. Korvink

Korreferent: Prof. Dr. Uwe Strähle

Tag der mündlichen Prüfung:

19. November 2018

Karlsruher Institut für Technologie
Institut für Mikrostrukturtechnik
H.-v.-Helmholtz Platz 1
76344 Eggenstein-Leopoldshafen

To my mom

To Namo and my sister

And Bita and Mono

And to all future girls in science and engineering. *Dare to do it!*

Para mi ma

Para Namo y mi hermana

Y para Bita y Mono

Y para todas las futuras niñas en la ciencia e ingeniería. *¡Atrévanse!*

I hereby declare that I have developed and written the enclosed thesis completely by myself, and have not used sources or means without declaration in the text. Furthermore, I have respected the statue of KIT, in its current version, to ensure good scientific practice.

Hiermit erkläre ich, dass ich die vorliegende Arbeit selbständig angefertigt und keine anderen als die angegebenen Quellen und Hilfsmittel benutzt sowie die wörtlich und inhaltlich übernommenen Stellen als solche kenntlich gemacht und die Satzung des KIT zur Sicherung guter wissenschaftlicher Praxis in der jeweils gültigen Fassung beachtet habe.

Karlsruhe, September 24th, 2018

. . . . . .

(Daniela Sánchez)

Hiermit erkläre ich, dass für mich Promotionsverfahren außerhalb der Fakultät für Maschinenbau des Karlsruher Instituts für Technologie (KIT) weder anhängig sind noch erfolglos abgeschlossen wurden.

Karlsruhe, 24. September, 2018

. . . . . .

(Daniela Sánchez)

Abstract

DNA cloning is one of the most important techniques of the molecular biology. Its main goal is to obtain identical copies of DNA fragments and consists on isolating the DNA fragment of interest from the original organism and insert it into host organisms to multiply it. These organisms, normally bacteria, have the ability to replicate foreign DNA as they replicate their own. Almost every molecular biologist must perform such a procedure in the lab; however, it is a tedious, time-consuming process. Therefore, it is striven for its automation. Different groups have performed molecular cloning steps on-chip with favorable results. However, these systems are either difficult to integrate with other steps, are not automated or have very complex structures.

In this work the development of an Automated Integrated Microfluidic Device (AIMD) for DNA cloning is presented. Three steps of the molecular cloning process were to be performed on-chip, namely digestion, ligation, and transformation. The device was designed with a modular structure to enable each step to be performed independently or together with the others. Moreover, the design allows the parallelization of up to four different cloning processes of different DNA fragments, but the same vector and competent bacteria. The multilayered modules are fabricated with Polydimethylsiloxane (PDMS) using standard techniques for PDMS casting. The negative structures are micro-milled in Polymethyl methacrylate (PMMA) molds. Plasma bonding is used as the bonding technique and alignment holders ensure the proper positioning of the layers to each other.

Different microfluidic components, employed in all modules, were designed and characterized. With simulation support as well as optical characterization, a micromixer with cylindrical obstacles was chosen as the mixing system. An extracting system was developed for dosing the reagents directly from the Eppendorf® tube (Eppi). Moreover, a dosing system, based on geometry to meter the exact amount of volume to be dosed, was conceived. This microfluidic component was tested with water and a water-glycerin solution to reproduce the properties of the ligase. A distribution system, used to divide the volume evenly within all processes, is also part of the system. Using delay and blocking valves based on geometric changes, a homogenous, bubble-free distribution was achieved without problems. Water, a water-glycerin solution, and a bacteria solution were examined for its characterization. These components were combined to create the layers of the modules. To pump the reagents and control the flow, only one micropump and one directional valve was required.

Furthermore, a heat shock mechanism was developed for transformation. Thermoelectric coolers (TECs) were implemented as heating and cooling systems. For cooling, appropriate heat dissipation mechanisms were evaluated to select the most efficient one. Different tests were performed to characterize both mechanisms. A standard protocol was performed to have results as basis for the next ones. A comparison between the behavior of distilled water and bacteria was made to ensure the results of the further tests, which

were performed with distilled water. Heating procedures were tested for 45 s, the temperature rise as well as the temperature stability were examined. The test for the cooling procedures were tested for 2-30 minutes, examining the same parameters as for heating. In additions, the accuracy of the Temperature Control System (TCS) was also determined during these tests.

Various biological tests were performed on-chip. The components of the pGEM®-T Easy Vector System I, with a total volume reduction of 60% compared to the standard protocol, were used for the ligation. By means of the blue-white selection, which can provide a quick indication of the ligation success, it was proven that ligation can be performed on the AIMD. The transformation was carried out with nearly 75% less competent bacteria and slight modifications to the standard protocol for culturing the bacteria. The results obtained showed that bacteria can be successfully transformed on the AIMD. These tests were carried out semi-automatically as the control valve, the micropump and the on/off switching of the TECs were done manually.

The proposed system enables a parallel ligation and transformation of up to four different DNA fragments. A reduction of the total volume of 60% for the ligation and ~75% for the competent bacteria was achieved. Finally, it was proven that both ligation and transformation procedures with few modifications to the standard protocol can be successfully performed on the AIMD.

Kurzfassung

Eine der wichtigsten und am häufigsten verwendeten Methoden der Molekularbiologie ist die DNA-Klonierung, deren Ziel es ist, gleiche DNA-Fragmente in großen Mengen zu gewinnen. Dabei wird das zu klonierende DNA-Fragment aus dem ursprünglichen Organismus isoliert und in Wirtsorganismen zur Replikation eingebracht. Diese sind in der Lage, fremde DNA zu replizieren, während sie sich vermehren und ihre eigene replizieren. Es ist ein zeitaufwändiges Verfahren, das in jedem molekularbiologischen Labor immer wieder durchgeführt werden muss. Deshalb wird nach einer Automatisierung gesucht. Verschiede Arbeitsgruppen haben bereits alle Einzelschritte des Klonierungsprozesses auf mikrofluidischen Chips durchgeführt und dabei richtungsweisende Ergebnisse erzielt. Allerdings arbeiten diese Systeme bisher nur partiell bzw. teilautomatisiert, sind nicht in einem hochintegrierten Gesamtsystem zusammengeführt oder haben einen sehr komplexen Aufbau.

Im Rahmen dieser Arbeit wird die Entwicklung eines automatisierten, integrierten mikrofluidischen Systems (AIMD *Automated Integrated Microfluidic Device*) vorgestellt. Drei Schritte des molekularen Klonierungsprozesses, nämlich enzymatische Verdauung, Ligation und Transformation, sollen on-chip durchgeführt werden. Das angestrebte mikrofluidische System ist modular aufgebaut, um einerseits die Einzelmodule separat testen zu können und um anderseits eine integrative Zusammenführung der drei Module zu realisieren. Darüber hinaus ermöglicht das Design die Parallelisierung von bis zu vier verschiedenen Klonierungsprozessen verschiedener DNA-Fragmente, aber gleichen Vektors und kompetenten Bakterien. Die mehrschichtigen mikrofluidischen Module sind aus PDMS hergestellt, unter Verwendung von Standardtechniken des PDMS-Gießens. Die negativen Strukturen sind in PMMA-Formeinsätze mikrogefräst. Als Verbindungstechnik wird das Plasmabonden verwendet. Dabei werden Positionierungshalter verwendet, um die verschiedenen Schichten richtig zueinander zu positionieren.

Verschiedene mikrofluidische Komponenten, die in allen Modulen eingesetzt werden, wurden entworfen und charakterisiert. Mit Unterstützung von Simulationsrechnungen und optischer Charakterisierung wurde ein Mikromischer mit zylindrischen Hindernissen als Mischsystem ausgewählt. Für die Dosierung der Reagenzien direkt aus dem Eppendorf® Mikroreaktionsgefäß (Eppi) wurde ein Extraktionssystem entwickelt. Darüber hinaus wurde ein Dosiersystem realisiert. Es basiert auf die Geometrie des Kanals, um exakte Mengenvolumen zu dosieren. Diese mikrofluidische Komponente wurde mit Wasser und einer Wasser-Glycerin-Lösung getestet, um die Eigenschaften der Ligase zu reproduzieren. Ein Verteilersystem, mit dem das Volumen gleichmäßig verteilt wird, ist ebenfalls Teil des Systems. Durch Verzögerungs- und Absperrventile, die ebenfalls auf geometrischen Veränderungen basieren, konnte eine homogene, blasenfreie Verteilung problemlos erreicht werden. Wasser, eine Wasser-Glycerin-Lösung und eine Bakterien-Lösung wurden zur Charakterisierung untersucht. Alle mikrofluidischen

Komponenten wurden zusammengefügt, um die einzelnen Module zu bilden. Um die Reagenzien zu pumpen und den Durchfluss zu steuern, wurden nur eine Mikropumpe und ein 3/2-Wegeventil benötigt.

Darüber hinaus wurde ein Hitzeschockmechanismus zur Transformation entwickelt. Peltier Elemente (TEC *Thermoelectric cooler*) wurden als Heiz- und Kühlsysteme eingesetzt. Für die Kühlung wurden geeignete Wärmeableitungsmechanismen evaluiert, um den effizientesten auszuwählen. Es wurden verschiedene Tests ausgeführt, um beide Mechanismen zu charakterisieren. Ein Standardprotokoll wurde durchgeführt, um Ergebnisse als Grundlage für die nächsten Tests zu erhalten. Ein Vergleich zwischen dem Verhalten von DI-Wasser und Bakterien wurde durchgeführt, um die Ergebnisse der weiteren Tests, die mit DI-Wasser ausschließlich durchgeführt wurden, sicherzustellen. Das Heizverfahren wurde für 45 s getestet, dabei wurden sowohl der Temperaturanstieg sowie die Temperaturstabilität untersucht. Zum Testen des Kühlverfahrens wurden Versuche mit verschiedenen Zeitfenstern (2-30 Minuten) durchgeführt. Hierbei wurden die gleichen Parameter wie beim Heizen untersucht. Zusätzlich wurde bei diesen Tests die Genauigkeit der Temperaturregelung (TCS *Temperature Control System*) bestimmt.

Verschiedene biologische Tests wurden on-chip durchgeführt. Die Komponenten vom pGEM®-T Easy Vector System I, mit einer Gesamtvolumenreduktion von 60% gegenüber den Standardprotokoll, wurden für die Ligation verwendet. Mittels der Blue-Weiß Selektion, die eine schnelle Aussage über den Erfolg der Ligation liefern kann, wurde nachgewiesen, dass die Ligation auf dem AIMD durchgeführt werden kann. Die Transformation wurde mit fast 75% weniger kompetenten Bakterien und kleinen Änderungen des Standardprotokolls zur Kultivierung der Bakterien aufgeführt. Die erzielten Ergebnisse zeigten, dass Bakterien auf dem AIMD erfolgreich transformiert werden können. Diese Tests wurden halbautomatisch durchgeführt, da das Steuerventil, die Mikropumpe und das Ein- und Ausschalten der Peltier Elemente manuell erfolgte.

Das entwickelte System ermöglicht daher eine parallele Ligation und Transformation von bis zu vier verschiedenen DNA-Fragmenten. Eine Reduktion des Gesamtvolumens von 60% für die Ligation und ca. 75% für die kompetenten Bakterien wurde erreicht. Schließlich wurde nachgewiesen, dass sowohl Ligations- als auch Transformationsverfahren mit wenigen Änderungen des Standardprotokolls erfolgreich auf dem AIMD durchgeführt werden können.

Acknowledgment

This written thesis is the proof that I accomplished a goal I set to myself a few years ago. During this time, I have learned much, not only on the scientific level, but also personally. Nonetheless, all this would have been impossible without the aid and support of everyone involved in this project. First and foremost, I am deeply grateful to Prof. A. Guber for giving me the opportunity to work under his supervision. It was really a pleasure to be part of the Bio-MEMS group, and take part in different activities such as the long oral exam-days. My sincere thanks go also to Prof. J. Korvink for showing interest in my work and accepting to be part of my project as a reviewer. I would also like to express my gratitude to Prof. U. Strähle for introducing me to the interesting world of the molecular cloning and setting the basis for the cooperation between the Institute of Toxicology and Genetics (ITG) and the Institute of Microstructure Technology (IMT). Without his idea and vision, this work would had never happened. I am also grateful for his acceptance to be my reviewer.

Furthermore, I sincerely appreciate the financial support provided by the Molecular Interaction Engineering (MIE) research project. Additionally, I would like to thank the BioInterfaces International Graduate School (BIF-IGS), that introduced me to a very interesting interdisciplinary environment, which I did really enjoyed during my project.

I would as well like to express my deepest appreciation to Dr. Ralf Ahrens. He was always very cooperative and supportive and gave me insightful comments and suggestions, not only by proof-reading different reports and also this work, but throughout the entire project. He was available even at unusual working hours and was even willing to interrupt his vacation. Thanks also to Ms. Ida Humbert, who was always ready to show her support, particularly regarding adhesive technique. Heartfelt thanks go to Prof. Strähle's work group, led by Dr. Sepand Rastegar. Especially, I'm extremely grateful to Ms. Vanessa Gerber for her invaluable contribution regarding the biological part of my work. She always answered gladly and patiently all biological questions I had and supported me unconditionally during the execution of the biological tests.

I would like to extend my sincere thanks to all the employees of the IMT, who supported me through this process. Many thanks to Ms. A. Moritz and his staff for their support by milling the molds and other tasks related with the mechanical workshop. She always received me at her office with a smile, something I will always appreciate. I would also like to acknowledge the assistance of Mr. U. Köhler with the plasma bonding machine; Mr. U. Klein with any IT problems; Ms. K. Klein with the organization of student theses; and Ms. N. Giraud for her help within any organizational stuff. Many thanks also to Mr. A. Voigt and Mr. L. Witt for their support by the development of the temperature control system. My thanks should go too to Mr. Florian Brüderlin, Dr. Hinnerk Oßmer, and Dr. Marcel Gültig for their support with different machines and measuring instruments.

My thanks go as well to my students Ying Zhan, Manuela Sevilla, Ye Xu, Nicolas Siegel, Martin Bailey, Hannah Soergel, and Erika Bárcena. Your ideas, hard work, and support were very valuable for the outcome of this work.

I would also like to offer my deepest gratitude to my work group. Dr. Tala Rajabi was always willing to share her knowledge and experience with me. My fellow PhD students, Mr. Patrick Doll, Mr. Tim Finkbeiner, Mr. Ruben Garschagen, and Ms. Helena Melzer, always offered me insightful thoughts and gave me supportive advice. We also encouraged each other at times when difficulties arose. Sharing an office with most of them was a great pleasure. Also, I enjoyed sharing time with them, not only at a professional level, but privately as well. Furthermore, I am deeply grateful for their support during my *crutches-time*. It facilitated those difficult times and made them go more smoothly.

Por último, pero no menos importante, me gustaría dar las gracias a mi familia y amigos. En especial quiero agradecerle a Elvia Valadez y a Ángel González por su apoyo y comprensión ya que también son doctorantes. Siempre estuvieron dispuestos a responder cualquier pregunta o ayudar a encontrar la respuesta, de ser necesario, principalmente con mis problemas con LaTeX. Voy a extrañar nuestras comidas y viajes hacia el Campus Nord. También quiero agradecer al resto de mi familia y amigos, quiénes siempre me han apoyado.

No sé cómo expresar con palabras mi agradecimiento hacia mi esposo Pablo Name, mi hermana Alejandra Sánchez y a mi cuñado Sebastian Geißenhöner. Su apoyo jugó un papel decisivo en la finalización de esta meta, desde el principio hasta, literalmente, el último momento. Siempre me han apoyado incondicionalmente, no sólo en lo que respecta a mi tesis, sino también en ámbito personal. Sin su apoyo no hubiera logrado lo que estoy a punto de lograr. Finalmente, me gustaría agradecer a mi mamá, cuyo apoyo quizás no está directamente relacionado con mi tesis; sin embargo, con su positivismo siempre me ha ayudado a sobrepasar los momentos difíciles, ya que siempre ha creído en mí y me impulsa a dar lo mejor de mí misma. No estaría en este momento de mi vida sin ella. Y, Bita, su apoyo incondicional ha estado presente en toda mi vida y siempre lo hará. Nunca olvidaré lo que ella y Mono han hecho por mí.

Contents

1. Introduction

Molecular biology deals with the study of biological activities at molecular level. Mainly, it focuses on the interactions within the cell as well as its structure, and the understanding of how Deoxyribonucleic acid (DNA), Ribonucleic acid (RNA), and protein function. Hence, this field studies, mainly, how genetic processes work on molecular basis by locating the genes on specific chromosome and identifying its relationship with specific behaviors or characteristics of an organism [1, 2].

In the early 1970s, this field gained interest as the recombinant DNA technology was discovered, i.e. enzymes were found that could cut DNA sequences at specific sites and recombine these cut fragments to other DNA segments. This technique changed the world of biology as it allowed gene manipulation. In the past decades, the genetic research has leaped incredibly forward as biologist are able to study more complex organisms, understand genetic diseases in more detail, start gene therapy, create proteins synthetically and commercialize them, such as synthetic insulin, and much more [1].

All this is possible due to the different techniques that have been developed through the years, such as Polymerase chain reaction (PCR) or molecular cloning. PCR is a method to rapidly produce up to billions of identical copies of DNA fragments within hours. It is well widespread among research labs, but also finds application in other fields such as diagnostics or forensic science [3]. Using PCR has become extremely important; therefore, modern machines that automate this process are commercially available and are used in almost every biology lab.

Nonetheless, the error rate of this method is not low. For some applications, the enormous amounts of identical fragments neglect the defective or incorrect ones. However, other applications cannot afford a high error rate and need a high DNA fidelity. Hence, another technique is used, i.e. molecular cloning. This method is used for obtaining identical copies of DNA fragments as well. This procedure is, though, quite different from the PCR. This consists on isolating the DNA of interest from the original organism and introducing it to a host organism, which is in charge of replicating it [1]. Nevertheless, in the present time, the DNA of interest is synthesized and commercially available for biological labs.

The DNA of interest, called **insert**, must be first ligated to a molecule, whose function is solely to carry the insert into the host organism. Normally, this molecule, called **cloning vector**, is round-shaped; therefore, it is first linearized, i.e. cut at specific sites, to be able to match the insert. Restriction enzymes are responsible for the linearizing of the vector. They perform this during a reaction called **digestion**. Once the vector is opened, it is brought in contact with the insert. They combine each other to form a new molecule called **recombinant DNA**. This term defines a molecule consisting of DNA fragments of more than one source [4]. An enzyme, **DNA ligase**, act as "glue" to bond the insert with the vector together. This refers to the process known as **ligation**. Finally, once

the recombinant DNA is created, it must be introduced into the host cells. Normally, bacteria act as host organism. The process of inserting foreign DNA into an organism is the **transformation** and is the last step of the cloning process. Bacteria are not naturally able to take up foreign DNA; hence, this process must be induced. There are different techniques to achieve this, being the most popular exposing the bacteria to a heat shock or to electroporation. Using these techniques, the cell membrane of the bacteria becomes permeable for DNA for a short time [1].

This process is used almost in every biology lab as well. However, contrary to PCR, it is still done manually. This is a very tedious and time-consuming procedure that almost every molecular biologist must perform in their labs, some even in daily basis. It consists primarily on pipetting the reagents into a common Eppendorf® tube (Eppi). Then, the transformation must also be conducted manually. By the heat shock, the Eppi is placed on a water bath or heating block for a certain period of time and then placed shortly on ice. Afterwards, the mixture must be incubated and spread on agar plates for cell culture. All these steps must be done for each independent DNA fragment that should be cloned. Automating and/or parallelizing this process represents a great advance in the molecular biology research.

In the past few decades, automation solutions in the molecular biology field have rapidly progressed. Robotics for pipetting or high-throughput screening are well established in both the industrial as well as in the academic field. However, these systems are limited to certain applications. In the molecular cloning, they have not yet found their proper use. Robotically driven pipetting systems are very cumbersome, space-consuming, and, in a field where the reagents are extremely costly, have relatively high investment costs. Therefore, new methods for automation are being searched, particularly in the Bio-Micro-Electro-Mechanical Systems (MEMS) field.

Bio-MEMS focuses on microsystems and their fabrication technologies designed for biomedical or biological applications. These new technologies have supported, particularly, the increasing advance in microfluidics. Microfluidics refers to the study field focused on the behavior and control of fluids in volumes smaller than a microliter range as well as the fabrication methods and techniques of the micro-spaces the fluid flows through [5]. Developing microfluidic devices is challenging as the fluid behavior differs from the “normal” behavior known from the macroworld. Nevertheless, in the past two decades considerable advances have been made in this field as Manz et al. [6] introduced the concept of Micro Total Analysis System (μ-TAS). They proposed that one of the most important, if not the most important, application of microfluidics was in life-science. Moreover, that developing fully integrated and automatic systems which comprise all the steps of a biological or chemical process, such as dispensing, transporting, mixing, filtering, detecting, and any other step required, was the key to automate these procedures, and thus, accelerate the research in this field.

Several groups have developed microfluidic devices for genetic analysis, synthetic biology, and diagnostics and medical applications [7–16]. However, despite some exceptions such as PCR and DNA sequencing machines, most devices remain on the academic field. Specific to molecular cloning, all steps of the process, namely digestion, ligation, and transformation, have been performed on a microfluidic device, i.e. on-chip [17–28]. Promising results have been obtained from these systems; however, those systems are

only partially automated and are not integrated with each other. Samples must be prepared off-chip, the reaction products must be taken manually for the next step, or the procedure itself is done manually, e.g. placing the chip manually on the heating block and then on ice for transformation. Furthermore, the design and fabrication of these systems are rather complex.

After an intensive literature review, it was determined that a fully automated integration of the molecular cloning process with a simple structure is still missing. Hence, the aim of this project was to develop an Automated Integrated Microfluidic Device (AIMD) for high-throughput cloning. This work was part of a cooperation between the Institute of Microstructure Technology (IMT) and the Institute of Toxicology and Genetics (ITG), both from the Karlsruhe Institute of Technology (KIT), within the Helmholtz Synthetic Biology Initiative.

The device has a modular structure to be able to perform each step independently or integrated, if required. It allows the parallelization of up to four cloning processes. Hereby, up to four different inserts can be cloned with the same vector and competent bacteria type simultaneously. The entire system consists of different layers, each comprised of different microfluidic components: micromixers for mixing the reagents, dosing components for an exact reagent metering directly from the Eppis, and distribution components, which allow the equal distribution of the dosed volume to the four different processes. Moreover, a heating and cooling system enables the exposure of the bacteria to a heat shock.

The device and its components were fabricated in Polydimethylsiloxane (PDMS) as this material allows the fabrication of different structures in low time frames. Different components were to be developed rapidly; therefore, this was the best option. Moreover, Polymethyl methacrylate (PMMA) was the material chosen for the PDMS casting molds. Using plasma bonding, the PDMS layers were bonded to obtain closed structures.

The design, fabrication and characterization of the microfluidic components and the entire device were done at the IMT. The biological tests were performed at the ITG as well as at the IMT. The experiments performed at the IMT were constantly supported by the ITG.

The development progress of the AIMD and its components as well as the biological results performed on it are described in this thesis, structured as follows: In Chapter 2 the fundamental biological as well as technical background required for understanding this thesis are provided. In Chapter 3 the overall system, its materials and fabrication are introduced. In Chapter 4 the microfluidic components used in every module are described and discussed. In Chapter 5 the structure of the modules and its biological implementation are presented. Finally, in Chapter 6 a brief summary and future related improvements and works are described.

2. Theory

As an interdisciplinary project, this thesis wraps different, but specific, topics. First and foremost, the biological process to be transferred on-chip must be properly understood to fully comprehend the complete development cycle. Therefore, in this chapter, the molecular cloning process is insightfully explained. Moreover, the microfluidics fundamentals describe the fluid behavior as well as its transport on a microscale, backing up the decisions made throughout the development. These are then presented as well. Finally, the fabrication methods relevant for this work are clarified.

2.1. Background: Molecular Biology

Molecular biology is the field of study regarding the molecular reactions and interaction in any biological function. Mainly, it focuses on the structural basis of the cell and how the information is processed inside it as well as on the development of useful techniques to research and analyze such topics. However, as no defining line can be traced between the biological field of study, it often overlaps with biochemistry and genetics [1, 2].

In the late 1970s, the so-called DNA recombinant technology was developed. This permits not only the isolation of specific DNA sequences, but also its sequencing and modification. Additionally, these could be transferred to foreign organisms. This technological breakthrough has supported a faster and more detailed understanding of the cell structure and functions, the correction of genetic diseases, and probably soon, the complete sequencing of an individual genome [1].

PCR, used to copy specific DNA sequences; DNA sequencing, employed to obtain the order of the nucleotides of a specific DNA sequence; and DNA or molecular cloning, another technique to replicate a specific DNA sequence, are the most widespread techniques in the molecular biology. PCR is the oldest and the most widespread one [3]. In this work, only the molecular cloning technique is relevant, thus, this is the only one that will be explained in detail.

2.1.1. DNA Cloning

Analyzing proteins or other components of complex organisms in detail is a difficult task. As the gene or genes of interest occur only once or twice on a cell, it is extremely difficult to extract it from the organism and purify it. The recombinant DNA technology offers a solution to this problem. This technique allows to combine the DNA of interest to another DNA piece, and then replicate normally inside a host organism. These DNA molecules composed of DNA fragments from different sources are called recombinant DNA [1,4]. As

the host organism replicates, the new organisms are genetically identical, called clones. Hence, this process is called DNA cloning [1].

This well widespread technique can be found in numerous applications such as partial or total DNA sequencing of a genome; protein function research; identification of mutation in human beings and other organisms; production of proteins or biological molecules commercially available; gene therapy, etc [1].

Briefly, a conventional cloning process is carried out as follows (Figure 2.1):

1. DNA of interest, called **insert**, is isolated from the original organism
2. The inserts are combined with **cloning vectors**, commonly round-shaped DNA molecules, to form recombinant DNA.
3. These molecules are inserted into a **host organism**, normally bacteria, which replicate the recombinant DNA as they replicate their own DNA.
4. The host organisms that contain the recombinant DNA are selected for further use.

The vector is foreign to the host organism; however, they have genes that provide new characteristics to the host organism such as antibiotic-resistance [4]. This property is used later to determine the success of the process. If the bacteria did not transform correctly, i.e. if the bacteria did not take the vector in, they do not present antibiotic resistance, and therefore, cannot grow on an agar plate with antibiotics. On the contrary, if the bacteria did take the vector in, are now resistant against the antibiotics and can grow on the agar plate.

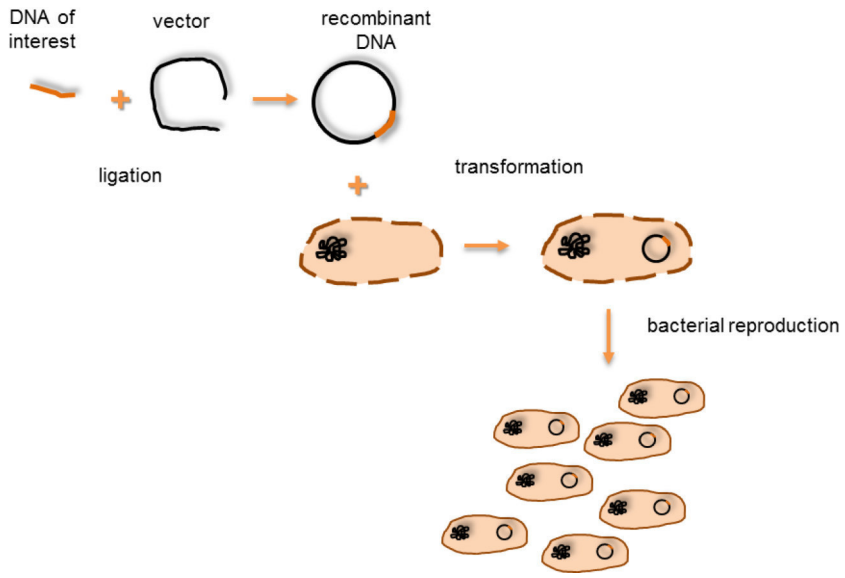

Figure 2.1. Cloning process. The DNA of interest, called insert, is combined with cloning vectors, normally round-shaped molecules. These are then inserted into host organism, generally bacteria, which replicate the foreign DNA as they replicate their own.

The process of isolating the insert as well as preparing the vector to accept the insert is called **digestion**. Creating the recombinant DNA, i.e. combining the insert with the

cloning vector, is a process called **ligation**. **Transformation** is the process that occurs when the recombinant DNA is inserted into the host organism.

2.1.1.1. Digestion

There are several approaches to obtain the DNA of interest. It can be copied using PCR, synthesized from individual oligonucleotides, or removed from the source DNA by *digestion*. For the latter, the DNA molecule is cleaved at specific sites by restriction enzymes. These recognize only these specific sites. Hence, the DNA of interest has at its ends a specific sequence that was recognized by the restriction enzyme. Moreover, the cloning vector is also digested by the same restriction enzymes. Thus, the vector is now linear and has at its ends the same specific sequence as the DNA of interest [29].

For this work, how the inserts are isolated is not relevant, as the biologist at the ITG use different techniques to obtain them. However, digesting the vector is indeed relevant. Therefore, a general digestion protocol for cloning vectors is briefly explained [30]:

After selecting the restriction enzymes to digest the vector,

1. Pipette the vector, restriction enzyme, buffer, and water into an Eppi
2. Mix gently
3. Incubate at an appropriate temperature, normally 37 °C for 1 h
4. Perform a gel electrophoresis analysis to determine the success of the digestion or perform size separation

This is a general protocol that uses a total volume of 30 µl. The amount of vector and restriction enzyme depend on the type of these and their manufacturer. The incubation temperature as well as the incubation time also depends on the manufacturer.

2.1.1.2. Ligation

Once the insert and the vector are cleaved, they are brought together to ligate. As they come in contact, their complementary cleaved ends formed hydrogen bonds. An enzyme called *DNA ligase*, responsible of forming covalent bonds between the hybridized ends, is then mixed together with the insert and the vector. As the three reagents meet each other, a new circular molecule, the recombinant DNA, is created [1, 29].

During this reaction, two processes can occur. The best-case scenario is, as mentioned, that the ends of the insert meet the ends of the vector. However, another possibility exists, namely, that the vector ends find themselves, i.e. the vector bonds with itself. This is a common problem that reduces the ligation efficiency [29].

The ligation procedure is performed manually in any biology laboratory. A standard protocol taken form the pGEM®-T Easy Vector System I[1] [31] is performed as follows:

1. Centrifuge the Vector and Control Insert tubes to collect the contents at the bottom of the tube

[1]Promega Corporation

2. Add to an 0.5 ml Eppi:
    - 1 µl Vector
    - 2 µl Control Insert
    - 1 µl T4 DNA Ligase
    - 5 µl 2x Rapid Ligation Buffer
    - 1 µl deionized water
3. Mix by pipetting
4. Incubate for 1 h at room temperature (or overnight at 4 °C)

Although these are the only steps for the ligation, the process is always followed by transformation as there is no other method to analyze or prove the ligation results. If more than one DNA of interest must be cloned, this process must be performed as many times as needed.

2.1.1.3. Transformation

After the ligation, the recombinant DNA must be inserted into a host organism to be replicated. The process of inserting a foreign DNA to a cell is called transformation. Mostly, *Escherichia coli (E. coli)* are used as host organisms; however, eukaryotic cells such as yeast are also used [29]. The ability of the cells to undergo transformation is called competence. Although some bacteria are naturally competent, most species cannot do this under normal circumstances. Therefore, for molecular cloning, transformation is artificially induced with different physical and/or chemical methods, e.g. heat shock or electroporation [32]. The former consists on exposing the bacteria to abrupt temperature changes, whereas the latter, on applying an electrical pulse at high voltages to the cells. These methods allow the cell membrane to be momentarily permeable to DNA molecules [27, 29].

As mentioned, exposing the bacteria to a heat shock increases their competence, i.e. increasing the transformation efficiency. Different protocols exist for heat shock; however, the principal idea is to bring together the recombinant DNA and the competent bacteria, and then incubate this mixture at lower temperatures, e.g. on ice, for 20-30 minutes. Mixing must be done extremely gently as competent bacteria are very delicate. Then, the bacteria are exposed to temperatures between 42-50 °C for 45-90 s. As the time elapses, the bacteria are again incubated shortly, i.e. 2-5 minutes, on ice. At this point, the bacteria are even more delicate as this process weakens them. Therefore, culture medium is then added to the bacteria, and an incubation for 1 h proceeds to let them recover from the heat shock. Finally, the bacteria are placed on agar plates with a corresponding antibiotic and incubated overnight at 37 °C to let them grow.

A standard protocol followed by the biologists at the ITG is as follows:

1. Select the competent bacteria (50 µl): XL 1 blue or Top 10. Both types are stored at −80 °C.

2. Add 10 µl of ligation mixture to the bacteria without mixing, as the bacteria are very sensitive. This should be done near a turned-on Bunsen burner to keep the area sterile, and, thus preventing other bacteria to overcome the transformed bacteria.
3. Place the mixture on ice for ~20 minutes.
4. Expose the bacteria to a heat shock by placing the Eppi on a heating block set at 42 °C for 45 s.
5. Put the Eppi on ice for 2 minutes.
6. Add 250 µl Lysogeny broth (LB)[2] medium to the bacteria.
7. Incubate at 37 °C while shaking vigorously for 1 h.
8. Warm up the agar plates, containing the appropriate antibiotics, by placing them at 37 °C without shaking for ~15 minutes.
9. Put 70 µl of X-gal[3] on the agar plates. (This step is relevant for the Blue-white-Screening explained in Chapter 2.1.2.1.)
10. Put ~8 small, sterile crystal balls on the agar plate, close it, and shake to spread the X-gal homogenously all over the plate.
11. Take out the crystal balls and place them on disinfectant to autoclave later.
12. Pipette the bacterial mixture on the agar plate.
13. Put again ~8 small, sterile crystal balls on the agar plate, close it, and shake to spread the bacteria, just as done for the X-gal.
14. Incubate at 37 °C overnight.

2.1.2. Methods for identification of recombinant DNA

After the ligation and transformation steps, it is necessary to determine if the ligation was successful, and if the recombinant DNA was indeed inserted in the host cells. For this purpose, a few methods are available. Most of them rely on the expression or non-expression of certain characteristics, and in one process different methods can be used.

One extremely common method is to insert a gene resistant to the antibiotic ampicillin or tetracycline in the vector. Bacteria, which have taken up the vector, will grow normally on agar plates prepared with ampicillin as the vector offers them an antibiotic resistance. On the contrary, bacteria without the vector die on the agar plate due to the ampicillin. Hence, to use this method, the vector must contain the specific gene and the agar plates must be prepared with the corresponding antibiotic.

[2] nutrient-rich microbial growth medium

[3] An artificial organic compound or sugar derivative used widely as a visual indicator for the Blue-White Screening

2.1.2.1. Blue-white Screening

Another popular method to determine if the cloning was successful or not is the blue-white screening. This method is based on insertional inactivation, i.e. the vector contains a specific gene which can be inactivated by interrupting its sequence with a DNA fragment [32].

Briefly and simplified, for the blue-white screening, the vector contains a gene called *lacZ* and the bacteria a complementary gene. This combination reacts with a compound on the agar plate, X-gal, causing a blue-colored product, i.e. the colonies grow blue. However, if the insert is ligated to the vector, the *lacZ* gene is interrupted. Hence, the combination between the *lacZ* and the bacterial gene do not exist, and in turn, it cannot react with the X-gal. This causes the grow of white colonies [1,32]. A schematic representation of the vector with and without insert as well as a schematic representation of this method are illustrated in Figure 2.2.

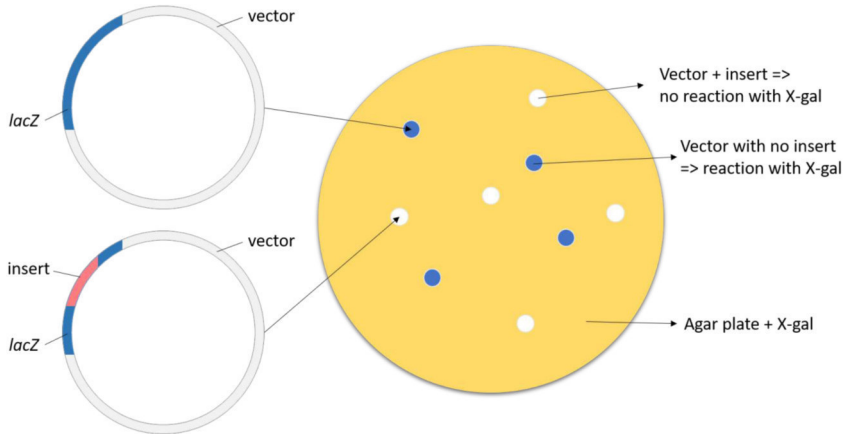

Figure 2.2. Schematic representation of the vector with the *lacZ* gene and with and without the insert as well as a schematic representation of the growing blue and white colonies. The blue colonies have the intact *lacZ* gene, causing a reaction with the X-gal. The white colonies have an interrupted *lacZ* gene, and thus, no reaction can be seen. Illustration based on [32].

This is a widespread method which can be used to discard immediately colonies without inserts. Nonetheless, false positives can occur, i.e. white colonies not containing the inserts. This may occur, for example, if the vector ligates with itself, but its ends are slightly modified. The blue reaction will not happen even if the insert is not present. Also, after the antibiotic is completely used up, colonies without the insert may appear white. Therefore, these must be inspected with another method, normally with gel electrophoresis.

2.1.2.2. Gel Electrophoresis

Gel electrophoresis is an extremely widespread technique to separate molecules depending on their size and electrical charge. In a container filled with a gel, such as agarose, an electrical field is applied to drive DNA molecules through the gel to the positive electrode as the DNA molecules are negatively charged. Smaller and, in case of DNA molecules,

shorter molecules travel faster, as they can slither more easily through the gel pores. Hence, a separation based on the length of the molecules is performed. Usually, the container has different tracks or lane to allow the sample to migrate separately from each other, avoiding cross-contamination. For a proper visualization of the results, the DNA molecules are marked to be fluorescent to ultraviolet (UV) light. Normally, a set of DNA molecules with different but defined lengths is used as reference during the gel electrophoresis [1].

2.2. Microfluidics

Microfluidics involves the study of flows inside spaces with dimension in the microscale. The volumes used in this field range from microliters down to even picoliters. This miniaturization changes nothing regarding the physics of the fluid; however, it changes dramatically its interaction with the channels, other fluids, and the outside world. For example, in the macroworld, the gravitation force plays an important role, whereas in the microfluidics it is negligible [5, 33].

One of the most important characteristics of the microfluidic flow is its laminar nature. Contrary to the macroscales, the flow in the microfluidics is predominantly laminar, as the viscous forces dominate the flow. This is characterized by the Reynolds number, which is defined as the ratio of inertial forces to viscous forces [34, 35]:

$$Re = \frac{Inertial forces}{Viscous Forces} = \frac{\rho u D_h}{\mu} \tag{2.1}$$

hereby is u the velocity of the fluid and D_h the hydraulic diameter of the channel, whereas ρ and μ, density and dynamic viscosity, respectively, are constant fluid properties [34,35]. For a rectangular channel, D_h is defined as:

$$D_h = \frac{4A_c}{P_w} = \frac{4wh}{2(w+h)} \tag{2.2}$$

with A_c as the cross-section area of the channel, P_w as the wetted perimeter of the channel, and w and h as the width and height of the channel, respectively [36].

The $Re_{cr} = 2300$ defines the difference between laminar and turbulent regimes. If $Re > Re_{cr}$, the flow is characterized as turbulent, whereas if $Re < Re_{cr}$, the flow is considered laminar [34]. As $Re \propto D_h$, the smaller the dimensions of the system are, the lower the Reynolds number is, sometimes even with $Re < 1$ [35].

The Navier-Stokes equation of incompressible flow neglecting gravity forces is defined as [37]:

$$\frac{\partial \mathbf{u}}{\partial t} + (\mathbf{u} \cdot \nabla) \cdot \mathbf{u} = -\frac{1}{\rho}\nabla p + \nu \nabla^2 \mathbf{u} \tag{2.3}$$

With the equation for the conservation of mass:

$$\nabla \cdot \mathbf{u} = 0 \tag{2.4}$$

A dimensionless form of Equation 2.3, following the detailed calculation in [37], can be obtained as follows [37]:

$$\frac{\partial u^*}{\partial t^*} + (u^* \cdot \nabla^*) \cdot u^*) = -\nabla^* p^* + \frac{1}{Re} \nabla^{*2} u^* \tag{2.5}$$

In this work, the flow to be analyzed is laminar with very low Reynolds numbers. For these cases, the flow can be simplified and characterized as the Stokes or creeping flow. The Stokes equation, a simplification of the Navier-Stokes equations that neglects the inertial forces because Re $\rightarrow$ 0, defines the flow as follows [37–39]:

$$0 = -\nabla^* p^* + \nabla^{*2} u^* \tag{2.6}$$

2.2.1. Capillary forces

As mentioned before, the physics of the microfluidics is the same as in the macrofluidics, but the interaction with the surroundings is clearly different. One example of this is capillarity. This phenomenon describes "the spontaneous movement of the liquid based on cohesive forces within the liquid or adhesive forces between the liquid and its surroundings." [40]. The capillary effect is normally used for filling the microchannels without external forces. It depends, principally, on the surface tension and the wetting properties of the channel surfaces. The surface tension yields a curvature, i.e. meniscus, at the liquid-air-solid interface. A concave meniscus is found in wettable, i.e. hydrophilic, channels, whereas a convex meniscus is formed in hydrophobic surfaces.

The capillary effect can be described the Young-Laplace equation [40, 41]:

$$\Delta p = \gamma(\frac{1}{R_1} + \frac{1}{R_2}) \tag{2.7}$$

with R_1 and R_2 as the two principal radii of curvature, and Δp_{cap} as the Laplace pressure, i.e. the pressure difference between the two phases.

The Laplace pressure for a round channel Δp_{capR} [42] and for a rectangular channel Δp_{cap} [43] Equation 2.7 are given as follows, respectively:

$$\Delta p_{capR} = 2\gamma \frac{cos\theta}{r} \tag{2.8}$$

$$\Delta p_{cap} = \gamma(\frac{2cos\theta}{h} + \frac{2cos\theta}{w}) \tag{2.9}$$

with γ as the surface tension of the liquid, θ as the contact angle of the liquid and the channel, assumed the same for all walls. Moreover, r_{ch} is the channel radius, and w and h are the width and height of the channel, respectively.

In hydrophobic surfaces, the capillary pressure increases by narrowing the channel. This increment can slow the flow or even stop it. Then, in order to restart the flow, the capillary pressure must be overcome, i.e. external pressure must be given to the fluid.

The burst pressure Δp_{burst} defines the maximum capillary pressure at the liquid-air interface at an abrupt change of geometry required to overcome this geometry. Presuming a gradually expansion of the walls, but a constant channel height, Δp_{burst} is defined as [43]:

$$\Delta p_{burst} = max(-\gamma(\frac{2cos\theta}{h} + \frac{2cos(\theta + \alpha)}{w_\alpha})) \tag{2.10}$$

with α as the angle between the start of the channel expansion and the position of the meniscus, and $w_a = w + 2r - 2r \cdot cos(\alpha)$ as the effective channel width, which depends on α (see Figure 2.3).

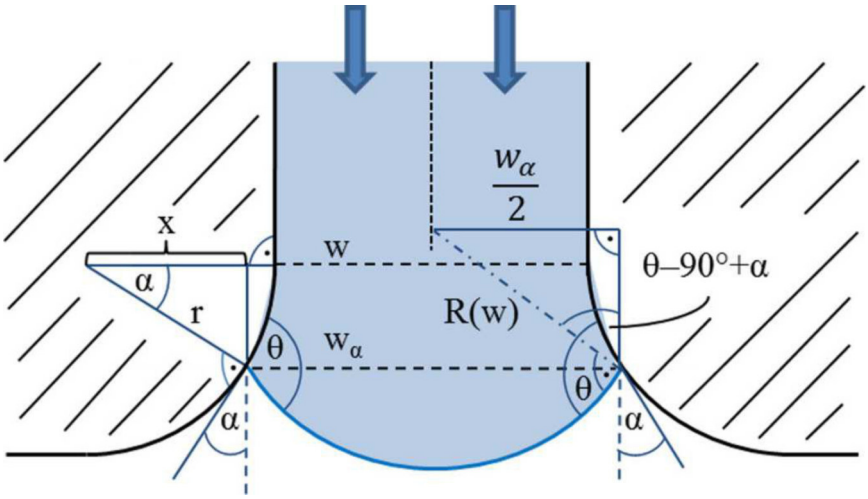

Figure 2.3. Channel with gradually expanding walls and its parameters. With $R(w) = \frac{w_\alpha}{-2cos(\theta+\alpha)}$, w is the channel width, w_α the effective channel width, θ the contact angle, α the opening angle of the channels at the position of the meniscus, r the radius of the expansion, and $x = r \cdot cos(\alpha)$ (Taken from [43]).

2.2.2. Mixing

Mixing involves the transport of species, temperature, and phases to obtain a more homogenous composition. On the macroscale, mixing is principally based on convection effects and eddy diffusion as the flow is defined as turbulent. In microfluidics, on the other hand, the regime of the fluids is basically laminar, due to the extremely low Reynolds number, causing mixing to occur mainly by molecular diffusion, or by advection.

The flux due to diffusion is defined by the Fick's law, which states that the molar flux is proportional to the concentration gradient [44]

$$J_x = -D\frac{\partial C}{\partial x} \tag{2.11}$$

where J_x is the diffusion flux, i.e. the flux of particles, and C their concentration. The negative sign state that the diffusion flux and concentration gradients are in opposite direction. The factor D is known as the *diffusion coefficient* and is a property of each species.

The transport of diluted species is described with the Fick's law and the stationary balance equation:

$$-\nabla \cdot (-D\nabla c + c\mathbf{u}) = 0 \tag{2.12}$$

Molecular diffusion, caused by the random motion of molecules, is a very slow process. Long structures or longer times are required to achieve a high mixing efficiency; therefore, advection, caused by the motion of the fluid, is preferred. It is striven to avoid straight channel, but to implement special microstructures to cause chaotic advection and, thus, enhance the mixing [45–47].

Micromixers are divided in two groups: active and passive mixers. Active mixers require external sources or moving parts to function, whereas passive mixers rely on the energy driving the fluids [45, 47]

Active micromixers

Active micromixers require external sources of energy to enhance the mixing effect. This type of mixers has generally simple structures, simple control systems, and a higher mixing efficiency; however, as they depend on external sources, the integration to microfluidic devices results more difficult as well as more expensive [46]. There are different energy sources used for driving the fluid, such as pressure, electrical forces, ultrasonic actuation, magnetic forces, and thermal power. [45, 48].

Passive micromixers

Passive micromixers do not require external sources for functioning and rely only on the driven forces of the fluids. Presently, passive micromixers can be divided in three-dimensional (3D) and two-dimensional (2D) mixers. The latter consist of planar structures to create chaotic advection. These structures can be grooves or barriers with different dimensions and geometries, Split-and Recombine structures, obstacles in the channels, asymmetric channel structures, zig-zag channels, etc. Split-and-Recombine structures consist on separating the flow streams in two channels and then rejoining them again. This enhances the mixing as the contacts areas of the fluids are enlarged and the flow is disrupted. Obstacles in the channel generate chaotic advection, which enhances the mixing efficiency [45–48]. 3D passive mixers are composed of complex structures in different planes. This type of mixers has a significantly more complex design and, thus, fabrication processes, but a higher mixing efficiency [45]. Mostly, for biological applications, passive mixers are implemented as they are easier to integrate in the devices. Specific examples are described in Chapter 4.1.1.

2.2.3. Microvalves

Valves are a crucial component in the fluidics field. Their fundamental function is to control, regulate, and redirect the fluid transport by opening and closing pathways, partially or totally. This allows the fluid to be stopped for a certain time, separated from another stream, diverted to other channel, among other functions. Common valves are mostly operated electrically or mechanically, and can be divided in pressure vales, flow control valves, stop valves, and directional control valves [49].

Common valves cannot be simply downsized and implemented in microfluidic devices; therefore, microvalves are being developed in the recent years, as they are crucial to develop fully automated and complex, but also highly reliable, microfluidic systems. Presently, microvalves can be divided in two major categories: active and passive valves.

Active microvalves require external power sources to work, whereas passive microvalves rely on pressure changes to function [50, 51]. Moreover, microvalves are also divided regarding their initial state in *normally open*, *normally closed*, and *bistable* [50]. Normally open valves require an energy input to close the flow; otherwise, remain open without any external power supply. Normally closed valves are, on the contrary, closed without energy consumptions and require power to open. Bistable valves have the characteristic of requiring power only for the transition between two positions, remaining stable in either of them without extra power supply [50].

Active microvalves

Active microvalves can consist of mechanical moving parts activated with magnetic, electric, piezoelectric or thermal actuators; non-mechanical moving parts, which are operated with smart materials; and external sources, such as pneumatic systems. Mostly, active microvalves use a flexible membrane coupled to an energy source to activate it. Microvalves with non-mechanical moving parts are gaining more interest because of their simpler structure and disposability. Phase change microvalves, using hydrogel, sol-gel, paraffin, or ice, are based on opening or closing the flow path, or on activating a membrane with plugs formed due to the phase change. Electrochemical and rheological methods have also been applied [50–52]. External activated microvalves work generally with air pressure or vacuum, i.e. pneumatic valves. This type of valves remains sealed even at high pressures; however, its complex structures with external pumping hinder the integration and miniaturization [50]. Active microvalves have several advantages, such as an actual physical barrier to reverse flow, excellent resistance to high back pressure, and highly leak-tight designs. They are very efficient and mostly spread in MEMS [53].

Passive microvalves

Passive microvalves are mostly check valves, i.e. they allow the fluid to flow in only one direction, consist also of mechanical or non-mechanical moving parts. Mechanical moving parts include flaps, membranes, or spherical balls, which are activated. Passive microvalves without mechanical parts use structures, such as nozzles or diffusers, to regulate the flow. Additionally, this type of microvalves use capillary forces to control the flow, exploiting the influence of the microchannel geometry and the surface properties [50]. Burst valves are a great example of this type of valves. They are single-use valves that rely on the flow resistance to work. If the driven pressure is greater than the valve can resist, the valve bursts open irreversibly, letting the fluid flow. Burst valves have different principles [52]. Some are based on the capillary forces, i.e. increasing the capillary pressure or resistance in the channel by abruptly changing the geometry of its cross-section (see Chapter 2.2.1).

Passive microvalve have often simpler designs and can be integrated more easily to the microfluidic devices. This, combined with the fact that they do not require extra power sources, makes them a great option for life-science applications.

2.3. Heat transfer

Heating and cooling are important topics for this work. Therefore, the fundamental principles of heat transfer and some relevant effect are explained in this section.

Heat transfer is the process of transporting thermal energy from a system to another, or even within the system, provided that a temperature gradient exists. The process of transferring heat, from higher temperatures to lower temperatures, continues until both systems, or subsystems, reach an equilibrium, i.e. reach the same temperature. The heat transfer rate $\dot{Q}$ is defined as the amount of heat transferred per unit time [54, 55].

Depending on the literature, the modes of heat transfer are divided in *thermal conduction*, *convection*, and *radiation*. However, heat transfer by convection requires the participation of thermal conduction; hence, the modes of heat transfer are thermal conduction and radiation [54].

Thermal conduction

Thermal conduction occurs in materials that present a temperature gradient. This process is defined by the movement of molecules within the materials. If the heat transfer occurs between solids or static fluids, the process is defined by the law of Fourier. It states that the heat flux $q = \frac{\dot{Q}}{A}$, i.e. the heat flow per unit area perpendicular to the flow is proportional to the negative of the local temperature gradient [56]:

$$q = -\lambda \frac{dT}{dx} \qquad \dot{Q} = \lambda A \frac{dT}{dx} \tag{2.13}$$

with λ as the thermal conductivity (material property), T is the local temperature, and x is the coordinate in the flow direction.

An example of this type of heat transfer is illustrated in Figure 2.4. Based on this, by integrating Equation 2.13 across the wall,

$$\dot{Q} = \frac{\lambda A}{L}(T_i - T_f)\ ,\ T_i > T_f \tag{2.14}$$

Conduction

Regarding calculation methods, there is a difference between heat transfer between solids or static fluids and heat transfer between a solid and a moving fluid, known as **convection**. Hereby, the thermal conductivity of the fluid and the thickness of the boundary layer define the heat transfer [54]. Depending on the flow generation, two differentiation are made: By *free convection*, the flow is generated by density differences, occurring due to the temperature gradient. *Forced convection* occurs when an external pressure difference is generated, e.g. flow in a pipe or air generated by a fan [54, 56].

Radiation

This heat transfer mode occurs without the need of a medium. By radiation, the electromagnetic waves, or photons, transfer the heat from one surface to another. As this mode do not play an important role in this work, it will not be explained in detail [54, 56]. Nonetheless, some electromagnetic effects, important for this work, are considered.

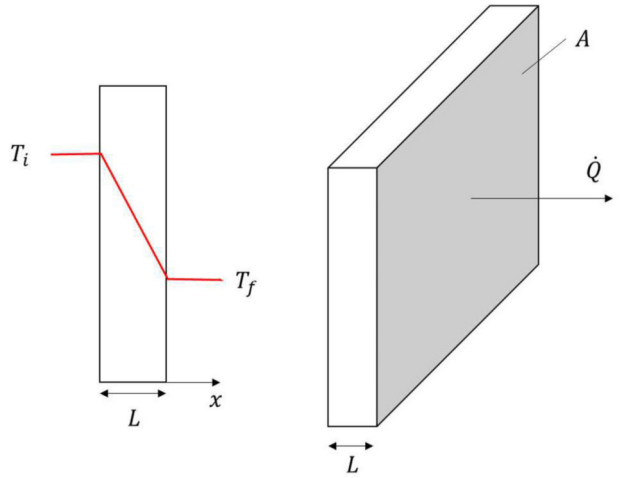

Figure 2.4. Example of heat transfer mode: conduction across a wall, showing the temperature gradient and heat transfer direction.

2.3.1. Electromagnetic Energy Conversion

There are different mechanisms that transform electromagnetic energy into thermal energy, such as the Joule Heating, Seebeck Effect, Peltier Cooling/Heating Effect, and the Thomson Effect. For this work, the Peltier Effect plays an important role and, thus, is explained in detail in the following section. However, for a better understanding of this effect, the Seebeck Effect must be presented before.

Seebeck Effect

The Seebeck effect describes the phenomenon of generating a current flow between the junction of two materials at different temperatures and is the basic principle of thermocouples. As shown in Figure 2.5, if the temperatures at the junctions A and B are different, an open circuit electromotive force[4] (emf), V, is generated between 1 and 2. The emf is proportional to the temperature difference [57].

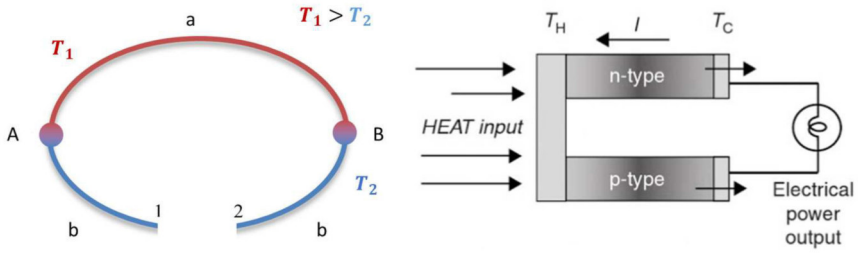

Figure 2.5. Left: Schematically representation of a thermocouple used to explain the Seebeck effect. As two different temperatures are at both junctions A and B, an emf is generated at 1 and 2 (based on [57]). Right: Example of a thermoelectric generator based on the Seebeck effect [57].

[4] electrical intensity developed by a source of electrical energy

Peltier Cooling/Heating Effect
The Peltier Effect is the reverse situation of the effect of the Seebeck effect [55, 57]. By applying an external emf source (at 1 and 2), a current flow is generating, heating one junction and cooling the opposite one. In Figure 2.6 a thermoelectric refrigerator exemplifies this effect [57].

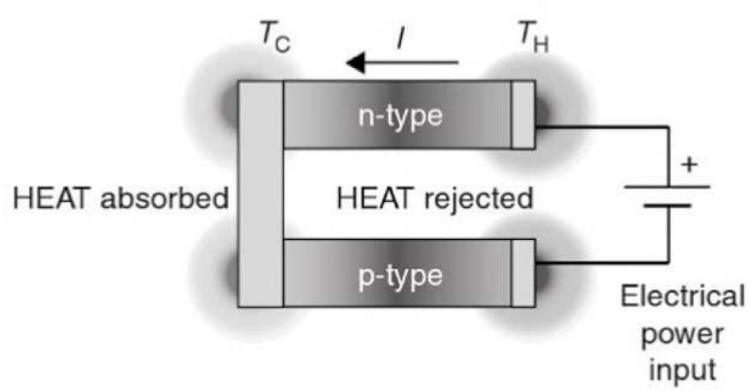

Figure 2.6. Left: Example of a thermoelectric refrigerator based on the Peltier effect. An electrical current flows anticlockwise, causing the left side to heat up, whereas the right side is cooled down. [57].

Thermoelectric cooler (TEC)
The function of a TEC is based on this effect. By applying a current flow, a temperature difference, i.e. a heat flux, is generated, cooling one side as the other is heated. If the polarity is switched, the hot side becomes the cold side and vice versa. A TEC consists of several thermocouples connected in series to each other. At each side, a ceramic plate is placed as an excellent thermal conductor, but electrical isolator.

2.4. PDMS Fabrication

In this work, the entire system was fabricated with the well-widespread material PDMS. It is a low-cost polymer with numerous advantages (see Chapter 3.4) and is an extremely appealing material in the microfluidic field due to its easy handling and its fast fabrication, i.e. replica molding and irreversible bonding. In the following section, both processes are explained in depth.

2.4.1. Replica molding

A standard PDMS fabrication process starts by mixing the liquid PDMS with a curing agent in a specific weight ratio. Both components must be thoroughly stirred to obtain a homogenous mixture [39, 58, 59]. By mixing, air bubbles are trapped in the mixture. Therefore, to avoid undesirable imperfections by structuring the PDMS, the mixture is degassed in a desiccator until it is air bubble free. Afterwards, by taking advantage of its liquid state, PDMS is poured in a mold which has the negative replica of the desired structures (Figure 2.7 (A,B)).

While in the mold, the PDMS is left to cure at room temperature or any other desirable temperature for a certain time (Figure 2.7 (C)). The viscosity of the mixture starts to increase gradually. Afterwards, it begins to thicken, coming to a gel-like consistency, until it finally solidifies into a flexible elastomer [60]. The curing time depends directly on the temperature at which the PDMS is being cured. Each manufacturer specifies this dependence for its specific type of PDMS. Table 2.1 shows the dependency of the temperature on the curing times for two different types of PDMS, namely *Sylgard*® 184 and Elastosil® RT 601 [61,62]. During this step, it is particularly important to examine the surface where the mold is to be placed. Any unevenness is directly structured in the PDMS, producing undesirable changes in the form, e.g. irregular thickness.

	Temperature	**Curing time**
Sylgard® 184	23 °C	~48 h
	100 °C	45 min
	125 °C	20 min
	150 °C	10 min
Elastosil® RT 601	23 °C	~24 h
	70 °C	20 min
	100 °C	10 min

Table 2.1. Depending on the type of PDMS, the temperature influences the curing time differently. Exemplifying this, the temperature with their respecting curing times of two different PDMS, namely *Sylgard* ® 184 and Elastosil® RT 601 are presented [61, 62].

Once cured, the PDMS is peeled off from the mold, obtaining a structured PDMS part with the positive replica of the mold (Figure 2.7 (D)) [39,59,63–65]. Owing to the flexibility and elasticity of the material, casting off the PDMS can be done smoothly and without damaging the structures. The structures are molded with great accuracy in micrometer [63], or even nanometer [64], range. After demolding, the PDMS part can be used immediately without further processing.

This is a significantly low-cost fabrication method as there is no need for special rooms or laboratories, nor special or expensive equipment. Hence, it can be performed under normal environmental conditions. Furthermore, it can be implemented by personnel without prior knowledge after a relative brief introduction.

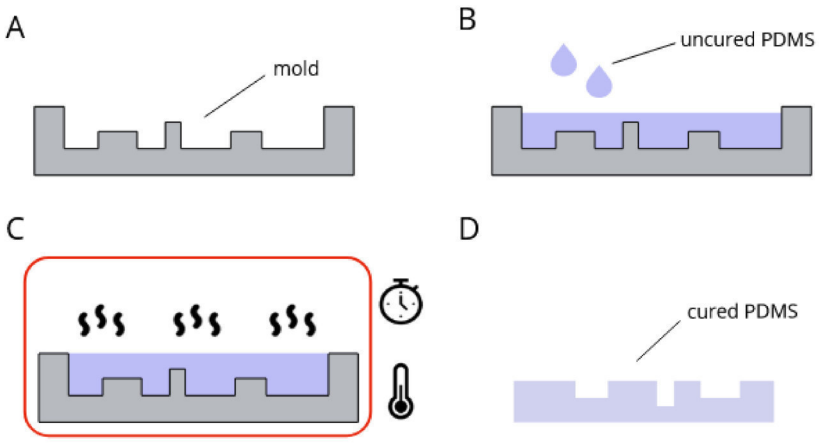

Figure 2.7. PDMS fabrication steps. (A) Mold with the negative structures of the desired ones. (B) Liquid PDMS is poured in the mold. (C) The PDMS is left to cure at a given temperature for given time. (D) A structured PDMS part with the positive replica of the mold is obtained.

2.4.2. Plasma bonding

A drawback from replica molding is its limitation to fabricate enclosed structures that could act as microchannels. By demolding the PDMS part, the structures are open and are in the need of a cover to obtain a functional microchannel. There are different bonding techniques to seal the PDMS devices. These methods can be classified in two groups: reversible and irreversible.

Reversible bonding takes advantage of the flexibility of PDMS. Minor imperfections of a flat surface can be matched up by its elastic deformation. Van der Waals bond are created allowing liquid to be enclosed without leakage. By removing one of the parts, the seal is destroyed; but the parts remain practically intact. Hence, these can be reused several times. This process is done at room temperature and is indeed fast; however, pressures above 0.3 bar are not supported [63–66].

Irreversible bonding can be achieved with different methods: using different PDMS:curing agent ratios to obtain a sticky part [67, 68]; coating a PDMS part with uncured PDMS, curing agent or UV-curable glue [67, 69–71]; partially curing both parts and joined them together as the curing finishes by forming a bond at the contact face [67, 72]; and finally, oxygen plasma treatment. The latter is the most widely used technique [67].

In the framework of this work, oxygen plasma treatment was selected as the bonding method. Therefore, this method is described in detailed. Both PDMS surfaces to be bonded are exposed to oxygen plasma for up to 1 min [64, 65] and brought in contact within seconds to form a strong bond. Chemically, PDMS is composed of repeating –O–$Si(CH_3)_2$– units. By exposing it to plasma, silanol groups (Si–OH) are formed; therefore, by contacting the surfaces to be bonded, these groups react to groups such as OH, COOH and ketone forming an irreversible bond [63–65, 67, 73, 74]. However, the oxidation effect is not permanent. The original groups are brought back again to the surface by exposing them to air; in contact with water, they do remain oxidized [64]. Nonetheless, if both parts do come in contact, the bond is irreversible [63].

As mentioned, it is the most widespread method for bonding PDMS. This is, mainly, because it generates irreversible bonds and PDMS can be used with different materials such as itself, glass, Si, SiO_2, quartz, Polyethylene (PE), Polystyrene (PS), among others [63, 65, 67]. However, it has its disadvantages. First, it is an expensive method since a specialized equipment for the plasma generation in a vacuum chamber is needed. Additionally, even though the part is only exposed to plasma for a few seconds, the whole process is slow because the chamber must be depressurized and then pressurized again. Additionally, the number of parts to be treated simultaneously is limited by the size of the chamber. Lastly, it delivers inconsistent bonding results [67].

Moreover, in practice, after the PDMS parts are exposed to the plasma, they must be brought in contact within seconds; otherwise, the results are not ideal. As the bonding is immediate and irreversible, the surfaces cannot touch any other surface, or two results occur: i) if the contact is with another activated surface, e.g. PDMS or glass, the bond is created, although not where it was desired or ii) if the contact is with another surface, e.g. the bottom of the machine, the bond does not work at all anymore. These are important issues to take into consideration when bonding using plasma oxidation as this complicates, e.g. the exact positioning of the parts.

3. Concept of the Automated Integrated Microfluidic Device (AIMD)

The accurate development of an innovative system entails, first and foremost, an intensive literature research to properly establish the limitations and possible improvements of the existing systems. Therefore, this chapter starts presenting an overview of the existing microfluidic systems which have been developed within the molecular biology field. Afterwards, the biological and technical requirements of the AIMD are presented as they are the most important basis for the design. Subsequently, a roughly description of the modular system and the modules is given. Lastly, the selected material and fabrication methods for the entire system are described.

3.1. State of the art: Microfluidic devices for molecular biology and DNA analysis

In the recent years, the microfluidics have gained more popularity among the research community in biological and medical fields as the microfluidic systems offer great advantages compared to standard procedures. The aim of developing μ-TAS is increasing constantly as these systems allow not only the integration of a biological procedure or analysis in one device, but also its automation. Moreover, these systems provide the possibility to reduce the reagents volumes and to perform high-throughput processes, hereby decreasing research costs.

Therefore, several microfluidic systems have been developed in the molecular biology field. Mostly, these systems have been focused on the PCR, a method used to amplify a DNA segment into millions copies within an extremely short period of time [7–12].

Nonetheless, devices with other applications are also documented. Li et al. (2011) [13] describe a programmable microfluidic system for volumes in the sub-microliter to 100 microliter range. In this device, a commercial mRNA amplification procedure was demonstrated using different protocols for mixing, incubation and bead-based purification steps. The architecture is extremely flexible and can be used for any protocol including the steps mentioned before. This system uses pneumatic valves and pumps as well. It is a multilayer, glass/polymer-PDMS-glass/polymer chip and was fabricated using photolithography. The top layer is the fluidic layer, whereas the bottom layer is the pneumatic layer, responsible for the fluid control. This device has also of a temperature control part, consisting of TECs with their respective heat sink and fan.

Easley et al. (2006) [14] propose a microfluidic device to perform genetic analysis using whole blood as a sample. The device is able to perform in less than 30 minutes: DNA

purification, PCR, size separation by Capillary Electrophoresis (CE), and detection by laser-induced fluorescence to analysis the fragment sizes. The device has three different functional domains, separated from the others by valves, consisting of PDMS membranes, which are also used as pumps. This device is made from glass (borofloat glass slides). This group was able to confirm the presence of two different types of bacteria from whole blood and nasal aspirate.

An integrated microfluidic device for the automatic extraction of Mitochondrial deoxyribonucleic acid (mtDNA)[1] was developed by Chang et al. (2010) [15]. The device has a multilayer structure and consists of micropumps, a micromixer and a temperature module. The dimension of the chip is 30 x 30 mm and 6.5 mm in height. The design supports vertical integration which allows a reduction of the chip size. Furthermore, extra modules can be integrated, if required. In the first module, a pneumatic micropump transports the samples, reagents, and waste solution. It consists of PDMS membranes, activated peristaltically. The second module is a pneumatic micromixer of PDMS channels and a PDMS layer. These are deflected in series, generating a swirl for mixing. The last module consists of microheaters, temperature sensors, and a temperature controller. The extraction and purification of the mtDNA was performed successfully, even with better results than a commercially available kit.

At the IMT, a microfluidic device based on digital microfluidic technology was developed by von der Ecken (2017) [16, 75] to perform a free programable synthesis of TALEN. The digital microfluidic chip was fabricated as well as its control system. Several tests were performed regarding the drop mobility to ensure that all biological substances could be moved. After some slight adaptations, results of a successful ligation were obtained. Therefore, it was proven that an automated TALEN-synthesis can be performed on-chip.

Other devices have been also developed specifically for the molecular cloning process. Each step of the cloning process has been performed in a microfluidic device. In the next section, these devices are presented.

3.1.1. Digestion

Xie et al. (2008) [17] developed a microfluidic device for enzymatic digestion and on-line CE separation. The glass-PDMS device is composed of temperature-controlled microreactors, a CE channel, pneumatic valves and pumps, and microheaters. The latter, and their respective resistance temperature sensors, are located to properly control the temperature. Pneumatic pumps and valves, using a PDMS membrane, manage dosing the product of the digestion into the CE channels and to separate the substance to avoid cross-contamination. The pressure and vacuum for the actuation of the valves was controlled by a self-made device.

An enzymatic digestion was tested on-chip. The temperature was maintained at 37 °C during the reaction, which occur in the microreactors. For these tests, 7 µl of digestion reaction was used. Afterwards, the product was dosed into the CE channel. Hereby, a 0.5% Hydroxypropyl Methyl Cellulose (HPMC), 0.1% Polyvinylpyrrolidone (PVP), 6% mannitol and Tris-Borate-Ethylenediaminetetraacetic acid (EDTA) (TBE) solution was used as

[1] an important subunit of a cell associated with aging degenerative diseases, and cancer [15]

the sieving matrix and fluorescence detection was implemented. The results showed an efficient digestion and CE detection.

Lin et al. (2012) [18] designed also an integrated microfluidic chip for DNA digestion, followed by CE analysis. The device consists of two gel-filled chambers: one for DNA enrichment, the other for DNA purification; a micromixer, a reaction zone, and a CE channel. The DNA sample and the restriction enzymes are mixed electroosmotically, i.e. by switching a DC electric field. Then, the mixture is transported to a serpentine channel, the reaction zone, where the actual digestion occurs. After the digestion, the sample is transported through another gel-filled chamber before flowing to the CE channel. Here, the sample is injected and separated. Finally, almost at the end of the chamber, a time-resolved optical detection occurs. The device consists of two layers: a glass-based layer for the digestion and a PMMA-based layer for the CE separation. The temperature is set using a commercially available TEC. The channel dimensions within the device are 100 µm in width and 40 µm in depth.

For the digestion, 6 µl of the DNA to be digested were used as well as a 14 µl mixture of enzymes and two buffers, previously mixed. The device was then kept at 37 °C with a TEC. For the CE, 1.2% HPMC with TBE was used as buffer. The results showed that a rapid DNA digestion can be performed on-chip and at least 11 fragments can be concentrated and analyzed within 24 min.

Papadopoulos et al. (2014) [19] developed a passive micromixer with a zigzag geometry for mixing the DNA to be digested with restriction enzymes. At 37°C, both mixing and digestion are achieved within 2.5 min. This group focused its research on the design and fabrication method of the micromixer. The channels are 60 µm deep and 400 µm wide, as for the length it was determined after simulations results. The device is fabricated from an imide-based photosensitive dry-film using flexible printed circuit technology.

They successfully digested 7.4 µl DNA without further incubation. The device was placed on a hot plate to maintain it at 37 °C. Using a peristaltic pump, the sample was driven through the microchannels, and the product was collected at the end of the micromixer with an Eppi. Without incubating, the sample was directly analyzed with gel electrophoresis, proving the success of the digestion. They claimed to be the first micromixer, where both the mixing and the digestion occurs. Normally, a micromixer is followed by a reaction zone. Nonetheless, only a few devices for on-chip digestion can be found.

All systems show an efficient performance of the biological protocol. However, the dosing and recovery of the reagents and products, respectively, still occur manually and no integration with the next steps of the process are addressed.

3.1.2. Ligation

There are also some devices reported for the ligation step. Liu et al. (2008) [20] reported an unconventional microfluidic device based on Electrowetting-on-dielectric (EWOD). This system consists of a plate with coplanar electrodes, i.e. the ground and activation electrode are positioned on the same plane, and a hydrophobic shelter.

The insert, 5 µl, the vector, 5 µl, and a buffer solution, 1.5 µl, which included the ligase, were dispensed with a pipette in individual reservoirs. Then, a droplet of DNA and a

droplet of vector, each 0.3 µl, were generated and mixed on the electrodes. This mixture was then transported to the ligation buffer reservoir and it was incubated for ~5 min. Afterwards, the mixture was collected in an Eppi and was transformed off-chip. They demonstrated that a ligation with a total volume of 2.1 µl, without waste, can be performed on-chip.

Ko et al. (2011) [21] describe a glass-PDMS microfluidic device for DNA ligation. It consists of a micromixer with nozzles and pillars and a microreactor with a serpentine channel as it does not generate bubbles. The dimensions of the micromixer are 10.33 mm, 400 µm, and 100 µm in length, width, and height, respectively. The microreactor is 20 mm in length and the same width and height as the micromixer.

The biological results were performed as follows: the micromixer was filled with 10 µl ligase buffer. One micropipette tip was placed on each of the two inlets. One tip was filled with 4 µl ligase and 4 µl of the insert; the other, depending on the experiment, with 4 µl ligase, 1-3 µl vectors, and 1-3 µm deionized water. Thus, the total volume was for all experiments 8 µl. After mixing, the reagents were pumped into the microreactor and were kept there for 1-5 minutes at room temperature. After the time elapsed, the product was taken from the chip with a micropipette. A manual transformation was performed afterwards to determine the success of the ligation. They concluded that the ligation process can be successfully performed on-chip with a clear reduction of the ligation time. The best results were achieved with 8 µl ligase, 4 µl insert, and 3 µl vector, thus, the volumes could not be reduced, compared with other ligation microfluidic devices.

These systems show excellent ligation results as well. However, their fabrication is complex and, in case of the device based on digital microfluidics, a high setup investment is required. Moreover, the dosing and recovery of the substances occur manually. Neither the digestion nor the transformation steps were performed on-chip, leaving these systems as standalone devices for only one step.

3.1.3. Transformation with heat shock

Nagamine et al. (2005) [22] propose an on-chip transformation of bacteria. Different plasmid can be transformed simultaneously as it is a microbial array chip, i.e. each transformation area is separated from each other. The device is made of PDMS channels 5 mm, 500 µm, and 25 µm in length, width, and height, respectively, with a silicon substrate, where the plasmids were immobilized. The substrate has pyramid-shaped chambers with an area of 400 x 400 μm^2 at the top and 100 x 100 μm^2 at the bottom.

0.2 µl plasmid was dosed in each well and then, the competent bacteria, *E. coli*, were injected into the channels with a syringe pump. The chip was incubated at 4 °C for 1 h. Afterwards, the bacteria was exposed to a heat shock at 42 °C for 90 s. The PDMS was then peeled off, the bacteria were exposed to Super Optimal Broth (SOC)[2] medium, and then incubated at 37 °C for 1 h. The medium was replaced with another one and the chip was further incubated at 37 °C for 16 h. After a colorimetric detection, it was concluded that a simultaneous on-chip transformation of different plasmids can be achieved.

[2] nutrient-rich bacterial growth medium

Another device for transformation was proposed by Li et al. (2007) [23]. They present a microfluidic device with built-in platinum heaters for the heat shock. The microchannels as well as the microchamber (1200 x 1480 x 50 μm^3 in length, width, and depth, respectively), where the transformation takes place, are made of PDMS. The 200 nm-thick platinum microheaters were deposited on a Pyrex substrate with a 10 nm chromium adhesion layer. An insulation layer was then deposited as well.

A volume of 0.3 µl of the competent cells, *E. coli*, with the ligation products were injected in the iced device, but only 0.1 µl entered the microchamber. Using resistive Joule heating, the microchamber was heated from 0 to 50 °C within 5 s and the temperature was stable for 90 s. Afterwards, the device was left on ice for 2 minutes before washing the sample with LB[3] medium. The device showed a comparable or even better transformation efficiency compared to conventional methods.

Sha et al. (2011) [24] present a microfluidic device for heat shock transformation consisting of a PDMS device with a micromixer and a commercially available quartz capillary. The reagents are loaded, mixed, transformed, and recovered automatically. The heat shock mechanism consists of placing the capillary in two hollow chambers, i.e. plastic syringes. The first one, water at 42 °C flows continuously to expose the bacteria to a local heat shock, whereas in the other, cold water at 0 °C flows continuously.

The microfluidic device was placed on ice before the transformation. Then, 1 µl of competent cells, *E. coli* and 0.5 µl plasmid DNA were loaded directly into the micromixer with a syringe pump. After the micromixer, the product was pumped further into the capillary, where the heat shock occurred. At the end, the transformed bacteria were collected in an Eppi. It was concluded that a reasonable transformation efficiency can be achieved with this device.

The transformation devices, although efficient, are not suitable for automation. Mostly, the heat shock is performed manually by placing the chip on ice and on a hot plate or TEC. In Sha et al. (2011) [24], the process runs automatically; however, by using flowing water to realize the heat shock extra heating and cooling devices are needed, which are not mentioned in the publication. Moreover, the actual water temperature that reaches the hollow chamber is not known, probably causing reproducibility issues.

3.1.4. Integrated Systems

Digestion-Ligation

Wang et al. (2011) [25] present a gel-based microfluidic device that can perform DNA digestion, gel electrophoresis, DNA extraction, and DNA ligation on-chip and within 1 h. This device is made of PMMA and consists of two DNA separation channels. Each channel is comprised as follows: it starts with a buffer zone, then a gel zone followed by an extraction well and another gel zone, and finally another buffer zone. The DNA is loaded in the first gel zone and the digestion occurs there. Underneath this section, two TEC are positioned to control the temperature during the digestion process. The platinum electrodes for the gel electrophoresis are submerged in each buffer zone, as they are filled with the electrophoresis solution. A channel connected directly to the extraction well is

[3] nutrient-rich microbial growth medium

intended for the ligase to reach the digested products. This channel is equipped with a valve to divide it from the extraction well. They concluded that successful digestion and ligation procedures could be performed on-chip faster and with less DNA loss than with conventional procedures.

Yang et al. (2014) [26] propose a functionalized microfluidic device for digestion and ligation. A silicon-PDMS microfluidic chip with a serpentine channel for dosing the reagents was developed. It includes a microheater and a temperature sensor to control the temperature accurately. The silicon surface was functionalized accordingly to allow the digestion and ligation of DNA. Both the digestion procedure as well as the ligation procedure were tested separately and, then, sequentially. It was concluded that a rapid DNA digestion and ligation can be performed on-chip.

Ligation-Transformation with heat shock

Hong et al. (2006) [27] developed a microfluidic chip for gene ligation and gene transformation with a parallel architecture. These devices use micromechanical valves and were fabricated with multilayer soft lithography. The ligation chip required 12 fluid channels, 30 valves, and 9 actuation channels, whereas the transformation chip, 8 fluid channels, 47 valves and 11 actuation channels. The fluidic channels are 100 µm wide and 10 µm deep and the actuation channels had 200 µm and 15 µm in width and depth, respectively. An integrated chip for both processes together was also developed. This has 16 fluid channels, 91 valves, and 23 actuation channels. The sample volumes are in nano-scale, being 60 nl the maximum volume. Each actuation line is connected to an external solenoid valve. Rotatory mixers are implemented to mix all the reagents by opening and closing valves sequentially.

The ligation tests were performed with a total volume of 6 nl. To evaluate the ligation efficiency, the ligation was performed on-chip, but the transformation was performed in conventionally, i.e. off-chip. Their results show that the device can achieve an efficient ligation process on-chip. The transformation process was also tested, using heat shock as the transformation method. For this purpose, a thermal stage or heat block are used. The results delivered are also positive, concluding that both ligation and transformation processes can be achieved on-chip with a mechanically operated valve system.

Ligation-Transformation with electroporation

Shih et al. (2015) [28] present a microfluidic chip which involves the DNA ligation and transformation. It consists of two parts based on two different microfluidic techniques: digital and droplet microfluidics for ligation and transformation, respectively. The DNA ligation section comprises a digital microfluidic device with 76 electrodes: 12 reservoir electrodes, 8 mixing electrodes, 3 digital-to-channel electrodes, and 41 actuation electrodes. The reservoirs have a total volume of 1.5 µl, whereas the droplets dosed 0.2 µl. The next part of the devices is intended for incubation, consisting of a serpentine channel 1.5 mm wide with two inlets for the oil phase and one for vacuum. Moreover, 4 valves control the exit of the digital microfluidic part, the oil inlets, and the entrance to the serpentine channel. This section can store up to 16 droplets without volume loss. At the end of the incubation zone, two electrodes are positioned to pulse and electroporate the cells, i.e. for the transformation. Three different ligation protocols were performed on-chip. All

experiments delivered successful results, showing that the device works perfectly with less volume and an integration of two steps.

These integrated devices delivered promising results. Just as the single-function devices, the structures and fabrication methods are complex and investment costs are high. However, these systems provide clear basis for further developments. They established the basics: the steps of the molecular cloning process can indeed be carried out on-chip; however, for a fully automation and integration new design must be implemented. The microfluidic systems previously discussed are summarized in Table 3.1. Their characteristics are presented for a better understanding of the state of the art.

Several microfluidic devices for molecular biology and genetic analysis have been developed. Most of the analytical steps, and in case of the molecular cloning process all steps, have been performed on-chip with results at least as efficient as conventional processes. However, these devices do not leave the academic research as no fully automated system exist yet [53]. Hence, the development of such a system would be a great option to spread the systems to more end users.

Group	Digestion	Electrophoresis	Ligation	Transformation	Device	Heating/cooling mechanism	Dosing	Integration	Special features
Xie et al. (2008) [17]	○	HPMC	x	x	glass - PDMS	Ti/Pt microheaters	manually	x	
Lin et al. (2012) [18]	○	HPMC	x	x	glass - PMMA	TEC	manually	x	
Papadopoulos et al. (2014) [19]	○	x	x	x	photosensitive dry-film	hot plate	manually	x	only mixer
Liu et al. (2008) [20]	x	x	○	x	digital microfluidics	x	droplets	x	digital microfluidics
Ko et al. (2011) [21]	x	x	○	x	glass - PDMS	x	manually	x	
Nagamine et al. (2005) [22]	x	x	x	heat shock	silicon substrate - PDMS	not specified	manually	x	
Li et al. (2007) [76]	x	x	x	heat shock	Pyrex substrate - PDMS	platinum heaters	manually	x	
Sha et al. (2011) [24]	x	x	x	heat shock	PMDS and quartz capillary	hollow chambers with flowing water	automatic with syringe pump	x	automated, simple
Wang et al. (2011) [25]	○	gel	x	x	PMMA	TEC	manually	2 steps	gel-based
Yang et al (2014) [26]	○	x	○	x	silicon substrate - PDMS	x	manually	2 steps	functionalized surface
Hong et al. (2006) [27]	x	x	○	heat shock	silicone	thermal stage	manually	2 steps	parallel architecture with pneumatic valves
Shih et al. (2015) [28]	x	x	○	electroporation	digital microfluidics	x	droplets	2 steps	

Table 3.1. Overview of the existing microfluidic devices in the molecular cloning field. ○ - present; x - not present.

3.2. Requirements

After the intensive literature research summarized in Chapter 3.1, it was concluded that no microfluidic system existed to completely automate a molecular cloning process. Therefore, the development of an AIMD that would cover this technology gap started. As it is known, the first step to design any system is to define its technical requirements. Moreover, if the system has a specific application such as medical or biological, specific requirements must also be determined.

Liu et al. (2009) [53] states that there are four critical factors to consider when developing fully integrated microfluidic systems for biomedical purposes: i) device material, as its properties define the characteristics of the surface in contact with the reagents, ii) temperature control because generally biological processes require different, but accurate temperatures, iii) valves to separate individual steps and avoid cross-contamination, iv) sample transport throughout the device. Based on these four factors and in collaboration with the biologists of the ITG, the requirements for the AIMD were defined as follows:

Modular design and integration: Each step of the molecular cloning process must be performed on an independent microfluidic device, i.e. a module. However, each one of the modules must be straightforwardly connectable with the others to obtain a fully integrated device. Therefore, the AIMD must have a modular design. Additionally, to achieve a functional integration of all modules, each one must have the same overall dimensions and similar dimensions regarding channels, mixers and other components.

Efficiency: A crucial characteristic of the AIMD is its potential to perform a molecular cloning process at least as efficiently as the standard procedure. This requirement is essential for the device's future favorable reception among the biological community.

High-throughput cloning: The process time of one molecular cloning process depends completely on the biological reactions occurring and cannot be accelerated by using a microfluidic device. Thus, to achieve a clear advantage over the standard procedure, the AIMD must be able to parallelize at least four different molecular cloning processes, i.e. at least four different DNA fragments can be cloned at the same time. In this way, the cloning time can be speeded up by performing more than one process simultaneously, i.e. the AIMD must enable high-throughput cloning.

Automation: Furthermore, even if the cloning time cannot be directly reduced, the time needed for an entire procedure can be decreased by automating the process. Hence, the biologists' workload is reduced and can use their time more efficiently. To this purpose, the dosing of the reagents, the fluid transport within a module and between the other ones, and specific processes, such as the heat shock (see Chapter 2.1.1.3), must be automated.

Bio-compatibility and Re-usability: The chosen material for each module must be bio-compatible and easily sterilized. If the complete sterilization of the AIMD can be ensured, it could be reusable. The parts of the AIMD, which are not in direct contact with the biological reagents, should be as possible reusable. Moreover, a successful bacterial recovery should be ensured.

Low complexity: The entire AIMD must have a simple structure and setup to facilitate its handling and operation by non-technical personal, i.e. biologists in their labs. Thus,

as few machines such as pumps or valves as possible should be used, and a user-friendly control should be ensured.

Flexibility: Not all ligation nor transformation protocols are the same, though they are similar. Essentially, the difference lays in the time each step lasts or the desired temperature. Thus, the user must be able to enter the desired parameters for temperature, time, flow rate, etc.

Reduced volumes: A standard molecular cloning process uses a total volume of 10 µl. The AIMD should not exceed this total volume. Reducing the volume of the reagents should be striven for to try to reduce costs.

Zero dead volume: The biological reagents are very costly. Therefore, no volume should be lost in any module nor in any microfluidic component to take fully advantage of the AIMD.

Dosing and Metering: To achieve a full automation of the process, the AIMD must be able to dose and exactly meter the reagents directly from the commonly used Eppi. A dosing system must be implemented in each module and it must be flexible to dose and meter volumes in range of 0.5 µl up to 32 µl.

Mixing: A mixing system must also be implemented in each module where the mixing of substances occurs. The efficiency of the mixing must be at least as good as a manual mixing. Passive or active mixing can be implemented (see Chapter 2.2.2). However, passive mixing is preferred to avoid increasing the complexity of the AIMD.

Flexible flow stop: Some reactions within the molecular cloning process take more than just a few seconds to occur. The AIMD must be able to allow the fluid to stop for a certain time for the different reactions to take place before being transported to the next microfluidic component or next module. These certain times also vary from protocol to protocol; therefore, they must be controlled as parameters that can be entered by the user.

Temperature: Some reactions of the molecular cloning process must occur at specific temperatures. The bacteria must be kept at ice temperature up to 30 minutes, depending on the protocol, before the heat shock takes place (see Chapter 2.1.1.3). Additionally, during the heat shock, the bacteria must be heated rapidly to 42 °C for up to 90 s. Therefore, the AIMD must be able to control this temperature.

Simple and low-cost fabrication: Another important aspect to take into consideration is the fabrication method. It must be simple, reproducible and cost-efficient. Undoubtedly, the material selection must be closely related with the fabrication method.

3.3. Modular system

The general concept of the system is to have a microfluidic device, which enables the automation of the molecular cloning process, i.e. an AIMD [77]. Originally, three steps of the molecular cloning process, namely, digestion, ligation, and transformation, as well as bacterial recovery and growth should be performed on-chip. Thus, following the requirements listed in Chapter 3.2, a rough draft of the system was developed. It consists of a multi-layered device with four different modules. Figure 3.1 shows an overview of the modules of the AIMD with their principal features as well as their reagents and products. Each module has different components such as mixers, dosing and distribution

systems and heating and cooling systems, depending on their specific purpose within the system. Within a module, these components are assembled in different layers to ensure a design simplicity as well as a miniaturization.

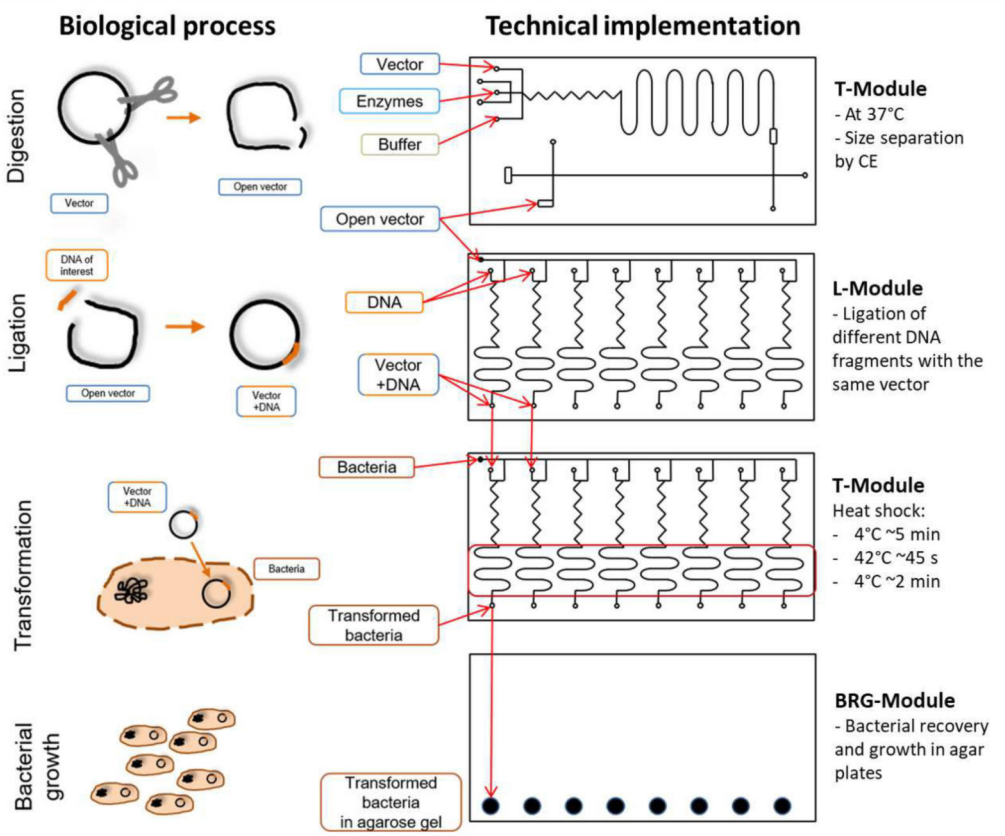

Figure 3.1. Schematic representation of the overall structure of the AIMD. It consists of four different modules, each one for one step of the molecular cloning process. The first module (D-Module) is where the digestion takes places. The product of this reaction is then transported to the ligation module (L-Module), i.e. the module where the ligation reaction occurs. After the ligation, in the transformation module (T-Module), the recombinant DNA is inserted in the component bacteria. Finally, in the bacterial recovery and growth module (BRG-Module) the transformed bacteria are left to grow and multiply.

Module Digestion (D-Module)

As it can be derived from the molecular cloning process (see Chapter 2.1.1), the first module is the D-Module. The D-Module is intended, firstly, to digest the cloning vectors; then separate the required cut parts from the shorter ones; and finally, redirect the open vectors to the next module.

For the digestion to occur, the cloning vectors are mixed with an enzyme and this mixture is left at a certain temperature for a certain time, depending on the protocol. The digested vector is then separated using CE with Capacitively Coupled Contactless Conductivity Detection (C^4D). The components of this module are, thus, a passive mixer, a reaction zone at a constant temperature, namely 37 °C, a separation, and a redirection

channel. At the end of the redirection channel is an outlet, which is the connection with the next module. The D-Module is schematically shown in Figure 3.2.

One important issue to consider by the development of this module is the volume of the digested vector. CE with C^4D works efficiently with volumes in a pico- or nanoliter range; however, the volume of digested vector required for the next step is much larger. Thus, it is important that an automated analysis can be done several times consecutively. Moreover, although CE is normally performed with optical detection, C^4D was chosen because the samples do not need to be marked or labeled and it has a simpler, compacter, and low-cost setup.

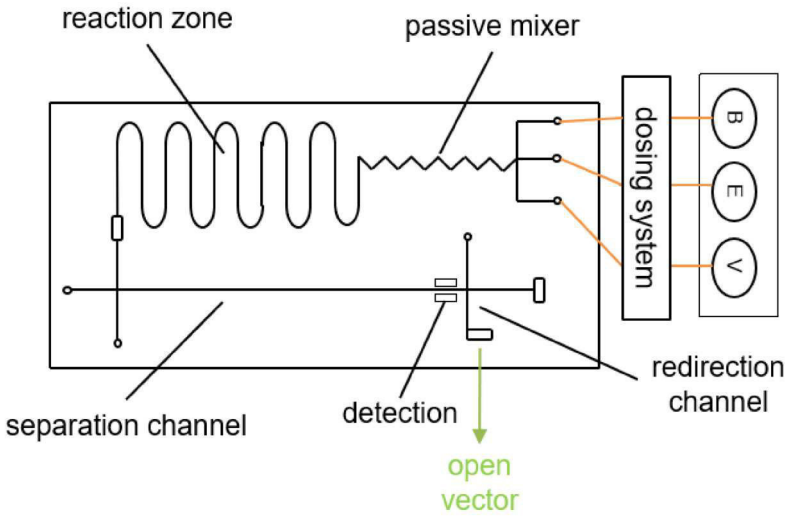

Figure 3.2. Schematic representation of the D-Module. This module consists of a passive mixer, a reaction zone, a separation channel for CE, C^4D detection, and a redirection channel. The reagents are the vector (V), enzymes (E), and buffer (B).

Module Ligation (L-Module)

The second module enables the simultaneous ligation of different inserts with the same vector. For a high-throughput ligation, the same vector, mixed with a buffer solution and the ligase, is mixed with the different inserts. Therefore, the L-Module consists of a dosing system for the vector, in case the D-Module is not connected, the ligase, and the buffer. Also, it comprises a passive mixer to combine these three reagents to obtain a Vector-Ligase-Buffer Mixture (VLB). As this mixture is the same for all parallel processes, a distribution system divides it equally. The module has also extra identical dosing units for the different inserts. The VLB and the inserts are mixed in different, but identical, passive mixers to obtain the recombinant DNA, from now on referred as Ligation Mixture (LM). Finally, each mixer is followed by its respective reaction zone, where the LM remains as the ligation takes place. These components can be seen schematically illustrated in Figure 3.3. To simplify the design, the L-Module is composed of three-layers. Each layer and their functionality are described in detail in Chapter 5.2.

An important aspect of the L-Module is controlling and transporting the fluid control. Using only one micropump and a directional control valve, the reagents are exactly

dosed and equally distributed without any volume loss or bubble generation. The flow is stopped without losing any volume as well as without external contamination. See Chapter 4 for detailed explanations.

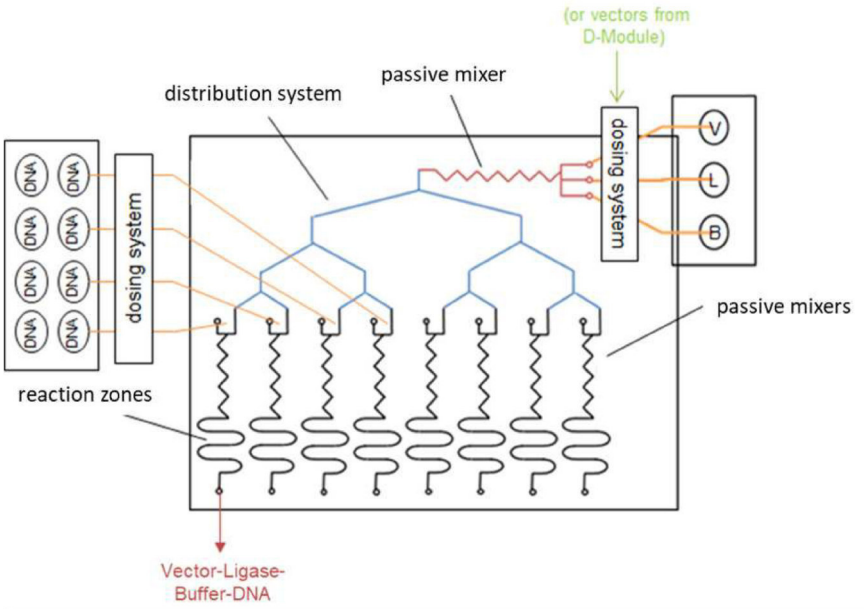

Figure 3.3. Schematic representation of the L-Module. It consists of a dosing system for vector (V), ligase (L), and buffer (B); a passive mixer to combine them to a VLB; a distribution system to divide the VLB equally; identical passive mixers to mix the VLB with the inserts; and their respective reaction zone, where the actual ligation takes place.

Module Transformation (T-Module)

In the next module, the T-Module, the transformation occurs. First, the LM from the L-Module is mixed with competent bacteria and the actual transformation happens by exposing this to a heat shock. The competent bacteria are the same for all parallel processes; hence, this module is composed of a dosing and distribution system for the bacteria, followed by identical passive mixers, where the bacteria are mixed with the LM. If the module acts independently, a dosing system for the LM is also integrated. After the mixing, the Bacterial Mixture (BM) reaches the zone where the actual transformation takes place, i.e. zones for the heat shock with heating and cooling units. Figure 3.4 shows a schematic representation of the T-Module. The detailed structure description of the T-Module is found in Chapter 5.3.

Controlling and transporting the fluids is also an important issue in this module; specially during and after the heat shock. During the transformation, an abrupt change in temperature is expected, preferably without disturbing the bacteria. Moreover, after the heat shock, the Transformed Bacteria (TB) are very sensitive and must be treated delicately. Comparable to the L-Module, this module also works with one micropump and a directional control valve. If both modules are combined, the same micropump and the same control valve can be used at the same time.

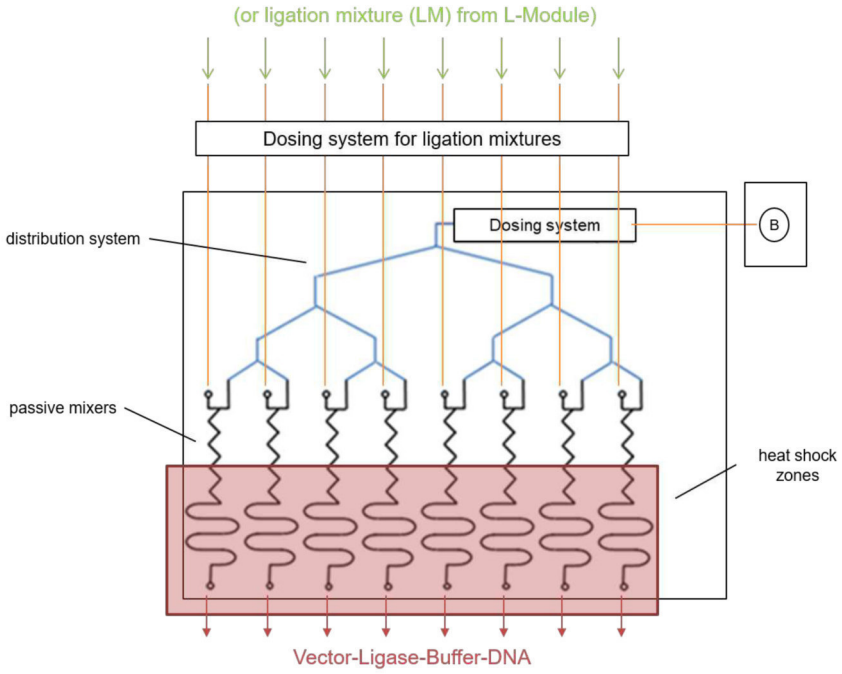

Figure 3.4. Schematic representation of the T-Module. It consists of a dosing and distribution system for the competent bacteria (B); passive mixers to combine the LM with the competent bacteria; and transformation zones, where the actual transformation takes place. As these zones require an abrupt change in temperatures, heating and cooling units are required.

Module Bacterial Recovery and Growth (BRG-Module)

The last module is intended to allow the TB to recover after the heat shock and start to multiply. The Culture Medium (CM) is incorporated to the TB and then incubated at 37 °C. Hence, this module consists of identical simple passive mixers, where the TB is mixed with the CM and reaction zones, with enough oxygen to ensure the bacterial growth. At the end, small agar plates or spots are placed to culture the bacteria. As the amount of CM is not particularly important, there is no dosing system in this module. The flow of the CM stops after a certain amount of time to obtain an approximate volume. In Figure 3.5 the schematically representation of the BRG-Module is shown.

Integration

Even though the modules can act independently, they are also fluidically connected with each other to perform as an integrated system. Each module has several inlets for the reagents and outlets for the products, depending on their functionality. The outlets from a previous module are linked to the inlets of the next one, creating an integrated system. The connection between the modules as well as its multilayered nature is shown in Figure 3.6.

In this work, the L-Module and the T-Module were developed from the first idea to prototype, i.e. design, fabrication, characterization, and application (see Chapter 5); whereas the D-Module and the BRG-Module remained in the design planning phase.

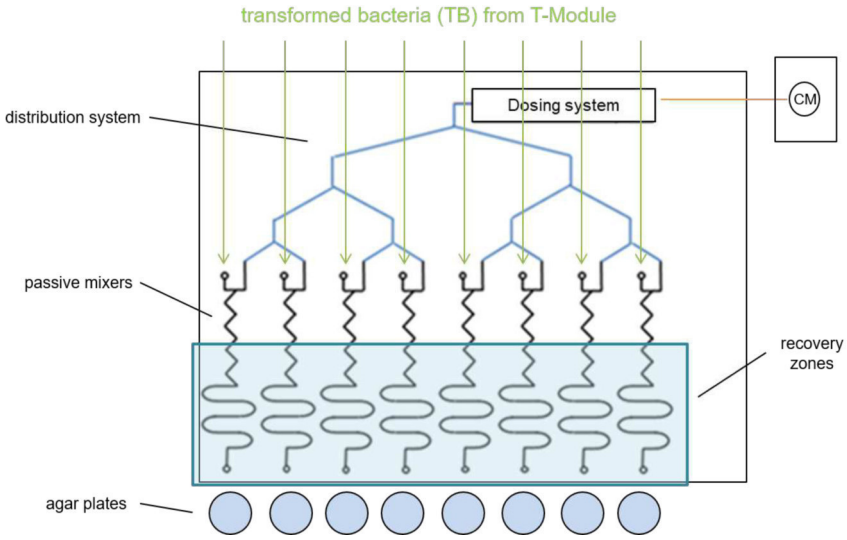

Figure 3.5. Schematic representation of the BRG-Module. It consists of simple, passive mixers for the TB and the CM, followed by recovery zones, where the bacteria can grow with enough oxygen and without disturb.

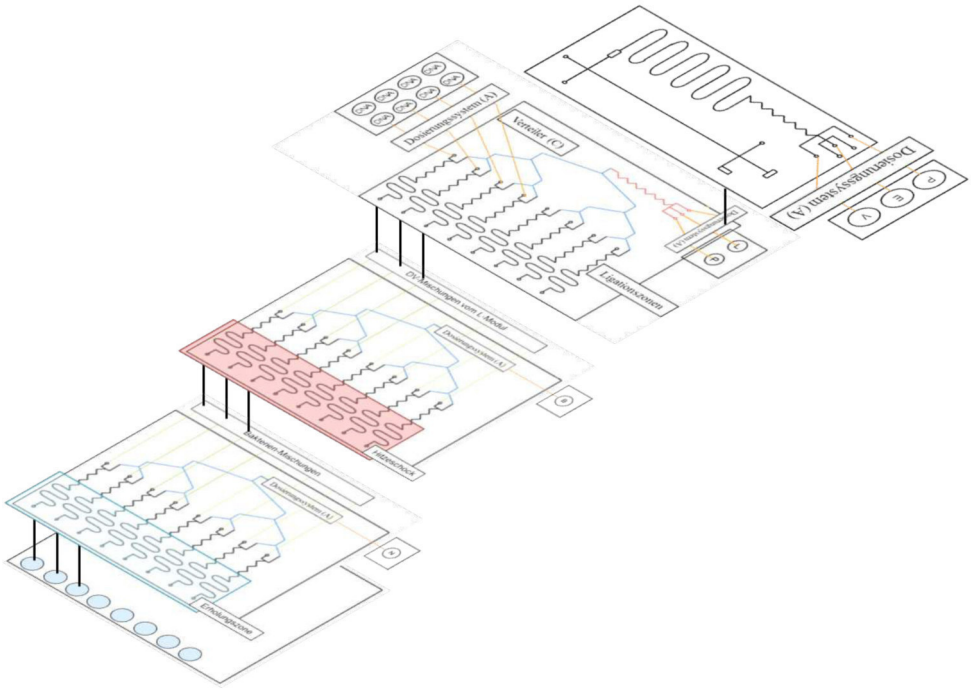

Figure 3.6. Schematic representation of the fluidic connection between the different modules of the AIMD. The outlets from a previous module are linked with the inlets of the next one, as the products of a module are the reagents of the next.

3.4. Materials

Selecting the proper material is a decisive aspect of the development of a microfluidic device. As mentioned on Chapter 2.2, though the physical properties of the fluids in

the microfluidic world are the same as in the macroworld, their interaction is extremely different. Hence, the material defines basic features of the device, such as hydrophobicity or hydrophily.

There are several demands that the chosen material must fulfill to ensure the functionality of a system. In biomedical applications, as is this case, the material must be bio-compatible. In other words, exposing the biological substances to the material does not jeopardize their composition or properties. If the substances react by any means to the material, their performance and effectivity could be affected, causing a lower efficiency of the AIMD. As the molecular cloning process operates at different temperatures, the AIMD must also be fabricated with a material resistant to a specific temperature range. Fortunately, this process covers a relative minor temperature range, namely, from 0 °C to 42 °C. This range is not a problem with the most widespread materials. Moreover, the molecular cloning process involves a heat shock; thus, the material must enable abrupt changes of temperature. Furthermore, an easy handling is expected.

The fabrication method plays a major role in the material selection. Within the framework of this work, several microfluidic components had to be designed, tested and characterized. To this purpose, a great quantity of samples had to be fabricated throughout the entire development. Therefore, a material which allowed a low-cost fabrication as fast and simple as possible without neglecting structure precision was essential.

In recent years, the material selection for developing microfluidics systems with biomedical applications have been continuously expanding. Conventional materials such as glass and silicon are not the only option anymore and are being gradually replaced with different polymers [63, 64, 70, 78–84]. This is occurring, mainly, because polymers have a large list of advantages that make them extremely appealing to both industrial applications as well as academic research, i.e. mass production and rapid prototyping, respectively [63, 65, 78, 79]. Polymers are low-cost, robust, transparent, bio-compatible, and, most importantly, have rapid fabrication techniques, such as injection molding, hot embossing, and thermoforming [65, 78–80, 85]. Moreover, the structured material can be sealed using simple techniques, such as adhesives or thermal bonding [63].

Polymers have also some disadvantages regarding surface chemistry, compared with silicon and glass, e.g. they react negatively to organic solvents. Besides there are not enough methods to modify their surfaces [53]. Other weak points are their relative low resistance to high temperatures as they have low glass-transition temperatures [53, 63]; their inherent fluorescence, and lastly, exiting methods for metal microfabrication cannot be employed [53]. Nevertheless, the advantages overweigh these drawbacks. Some of the most widespread polymers used in biomedical microfluidics devices are PDMS, PMMA, Polycarbonate (PC), Cyclic olefin copolymer (COC), PS and more recently, Polyethylene terephthalate (PET) [13, 15, 17, 21, 22, 65, 70, 82–84, 86–90].

3.4.1. Polydimethylsiloxane (PDMS)

After careful consideration, PDMS was selected as the material for the AIMD. There are a great variety of reasons that support this decision and will be presented in the following section. PDMS $[(CH_3)_2SiO]_n$ is an organic polymer, namely, a silicone elastomer [59, 91]. It is an inexpensive material, widely used in the microfluidic systems for biomedical

research as well as other fields such as the food industry, cosmetics, clinical applications, etc. [58, 59, 92].

If PDMS is not cross-linked, i.e. if it has a low-molecular weight, it is in a liquid state with high viscoelasticity [59]. By mixing this liquid PDMS with a curing agent, cross-links start to form, bonding the polymer chains together, i.e. the molecular weight increases. This process is not immediate; at room temperature, the process takes up to 48 hours to finish. However, it can be accelerated by exposing the mixture to higher temperatures. When the PDMS is totally cured, it becomes a transparent, rubber-like material [61].

As a cured elastomer, PDMS has numerous advantages for microfluidic devices. It is, as mentioned, optically transparent, an excellent characteristic for optical detection [63, 64]. It is also flexible; therefore, it can be elastically deformed and demolded from the finest structures without damage [58,63,93]. Another extremely decisive characteristic of PDMS is its biocompatibility. It is non-toxic for biological organisms and compatible with blood [63, 64, 93]. In addition, it is permeable to gas, enabling cell culture [59]. Other important properties are that it is chemically inert, impermeable to water, and hydrophobic, because of its CH_3 groups [58, 64, 87]. The latter can be both an advantage as well as a disadvantage as the poor wettability produces a higher risk of generating air bubbles and undesirable adsorption of molecules [64]. However, hydrophily can be achieved with plasma treatment oxidation or surface coating, at least for a certain time [58, 63, 64].

Possibly, the most important characteristics of PDMS and the decisive reasons to select this material are its easy handling and its fast fabrication. Within a few hours, a structured PDMS part is obtained by curing the liquid PDMS in a mold and then sealed by treating the surface with plasma. (For a detailed explanation see Chapter 2.4).

In this work, *Sylgard*® 184 Silicone was used. Its properties are summarized in Appendix A.1. As this is the most widely used type of the PDMS, there is plenty literature and research available. Hence, some difficulties presented throughout the development could be overcome more easily.

3.4.2. Polymethyl methacrylate (PMMA)

After PDMS, the second most important material for this work is PMMA. As explained in Chapter 2.4, to produce PDMS parts, a mold with the negative desired structures is required. In this work, all molds were fabricated from PMMA using micro-milling machines. Advantages and disadvantages to select this material follow.

PMMA, commonly known as Plexiglas®[4], is a colorless, amorphous thermoplastic polymer highly rated, primarily due to its high transparency. Its light transmission of 92%, shatter resistance and the fact that it is inexpensive makes it a great lightweight alternative to glass [94–97]. Therefore, it is widely used in numerous sectors, such as the automotive, building, and optical industry [96], and recently in the BioMEMS field and microfabrication, e.g. as a photoresist in lithographical processes [85]. Hence, commercially speaking, it is the most important polymer of its class [95].

PMMA has medium strength, high stiffness and hardness as well as a very high impact resistance compared to glass; although it is to some extent relative brittle. With an

[4] other trade names: Altuglas®, Degalan®, Acrylite®, BarloCast®, Perspex® [94]

adequate surface treatment, it becomes extremely scratch resistant and obtains a high-gloss finish. Moreover, it has acceptable electrical and dielectric properties and high weatherability and aging resistance. It is chemically resistant solely to weak acids. Its glass-transition temperature T_g depends on the manufacturing processes and is relatively low, ranging between 105 °C-115 °C [94, 96]. Depending on its composition, it can be employed in a range temperature of 40 °C-75 °C continuously, and up to 100 °C on short-term exposures [94]. Furthermore, PMMA is highly machinable and its suitable for different fabrication techniques including laser cutting [96, 97].

Despite all its positive properties, PMMA has its drawbacks. It has a poor chemical resistance to strong acids and bases as well as polar solvents. As mentioned, its continuous temperature is relatively low for numerous purposes. Also, it has a low fatigue resistance, is notch sensitive and highly prone to crack under stress. Moreover, due to its high electrostatic chargeability, it tends to attract dust particles [94].

Normally, PMMA parts and semi-finished products are fabricated with two different methods, namely, by casting or extruding. PMMA casting consists of mixing in molds the required elements for the polymerization. As this process develops in the mold, the material forms homogenously and has the same characteristics in all directions. Whereas by extruding, the molding compound is pushed through a mold while the polymerization takes place. This extrusion occurs in a specific direction; hence, it influences the properties of the material heterogeneously, i.e. they vary depending on the direction of the extrusion. Manufacturers ensure that cast PMMA has better optical qualities such as a higher transparency and light transmission as well as less internal stress [94, 96, 98].

In the recent years, PMMA has become an excellent option to fabricate micro elements such as micro-optical components [99] or microfluidic devices [78, 100, 101]. In the field of the latter, PMMA is being increasingly used as an alternative to directly produce the microchannels. However, it is also a great alternative to fabricate the molds for PDMS replication, which are mostly fabricated by means of photolithography [102]. PMMA molds are low-cost and can be easily produced by means of micro-milling. As PDMS is hydrophobic, it peels off from a PMMA mold relative effortlessly.

A transparent PMMA of cast quality was chosen as the material for the molds for PDMS replication. In Appendix A.2 a table summarizing its properties is found.

3.5. AIMD Fabrication

The complete AIMD device as well as all the different microfluidic elements that were developed and tested in this work were fabricated with the same method. After the design of the modules or components was developed, the fabrication process consisted of four basic steps:

1. Micro-milling the PMMA molds of the different layers
2. PDMS casting of the layers
3. Bonding the layers
4. Attaching the fluidic connections

The AIMD was miniaturized to minimize the reagent volumes and to take up the minimum space as possible. It has a nearly square form being 42.3 mm in length and 38.8 mm in width. All the functional layers expect the one where the heat shock occurs (see Chapter 4.5.3.1) are 1 mm thick. The heat shock layer is 0.72 mm thick and the covers vary between 2 mm and 4 mm. For a better handling, the molds were made of PMMA blocks with an overall dimension of 47.3x43.8x5 mm (Figure 3.7 (left)). The dimensions of the microchannels and other structures vary within the different modules. The microchannels are 0.4 mm and 0.8 mm wide, whereas the height range between 0.2 mm and 0.5 mm. Figure 3.7 (right) shows an example of a final PMMA mold.

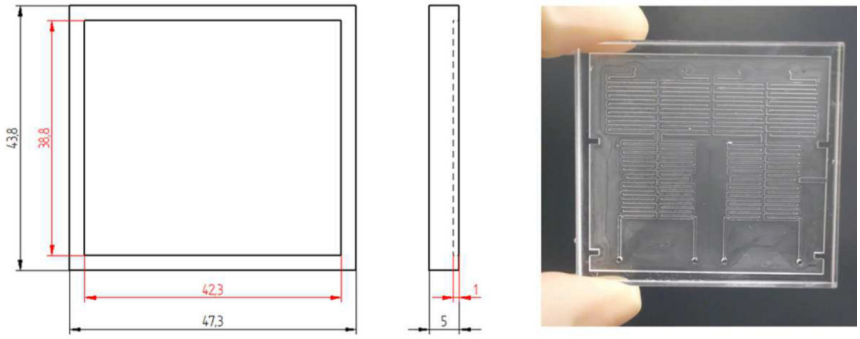

Figure 3.7. Left: Overall dimensions of the PMMA molds shown in black and the PDMS layers shown in red. Right: Example of a final PMMA mold.

3.5.1. Mold fabrication

All molds were fabricated by micro-milling using two different machines at the IMT. Most of the molds used for testing were milled with the KOSY[5] micro-milling machine. The final molds were milled at the IMT mechanical workshop with an MMC 600 2Z[6] machine for fly-cutting and ultra-precision milling. Milling cutters with different diameters, namely, 0.1 mm, 0.3 mm, 0.6 mm and 0.8 mm were used depending on the smallest distance between the structures. Mostly, all molds were milled with a rotation speed of 50 000 rpm and a feed speed of 50 mm/s. The cutting depth of the three smallest tools, 0.3 mm, 0.5 mm, and 0.6 mm was 0.05 mm, whereas for the 0.6 mm was 0.2 mm. The parameters for each tool are summarized in Table 3.2.

Tool diameter [mm]	**0.1**	**0.3**	**0.6**	**0.8**
Speed [rpm]	50 000	35 000-50 000	50 000	50 000
$Feed_{xy}$ [mm/s]	30	30-50	30	30
Infeed [mm]	0.05	0.05	0.05	0.2

Table 3.2. Milling parameters for 3 different cutting tools, namely, 0.1 mm, 0.3 mm, 0.6 mm, and 0.8 mm.

[5]MAXcomputer GmbH
[6]LT-Ultra-Precision Technology GmbH

To evaluate the milling processing and the surface quality, the molds were analyzed using a Scanning Electron Microscope (SEM) in the clean room of the IMT. For a second discernment, a White Light Interferometry (WLI)-microscope was used to inspect the surface quality as well as the height of the structures. The SEM and WLI-microscope images show the negative structure of the microchannels with a relative smooth surface, even though the milling patterns can be seen on the surface (see Figure 3.8 and Figure 3.9).

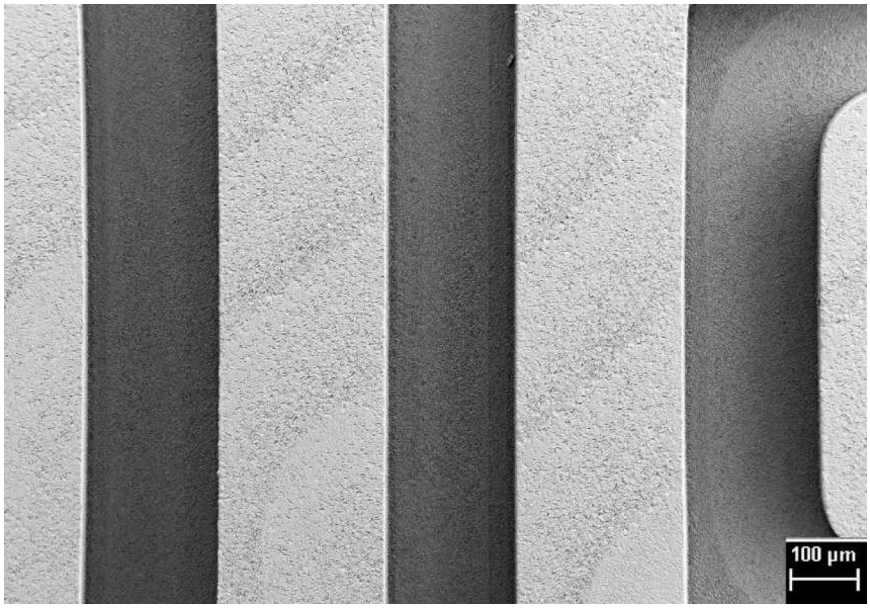

Figure 3.8. SEM image with a 50x magnification shows a relative smooth surface of the negative structures of the microchannel as well as the milling patterns.

Moreover, a mean structure height of ~197 µm for a 200 µm-microchannel was measured with the WLI-microscope. These results can be seen in the graph below in Figure 3.9. Hence, the accuracy expected by micro-milling was achieved. Furthermore, formation of burr on the surface of the mold was detected as well. However, as seen in Figure 3.10, the burr is not on the microchannels nor the inlets. As the burr does not affect the functionality of the microfluidic structures, the surface quality was evaluated as adequate.

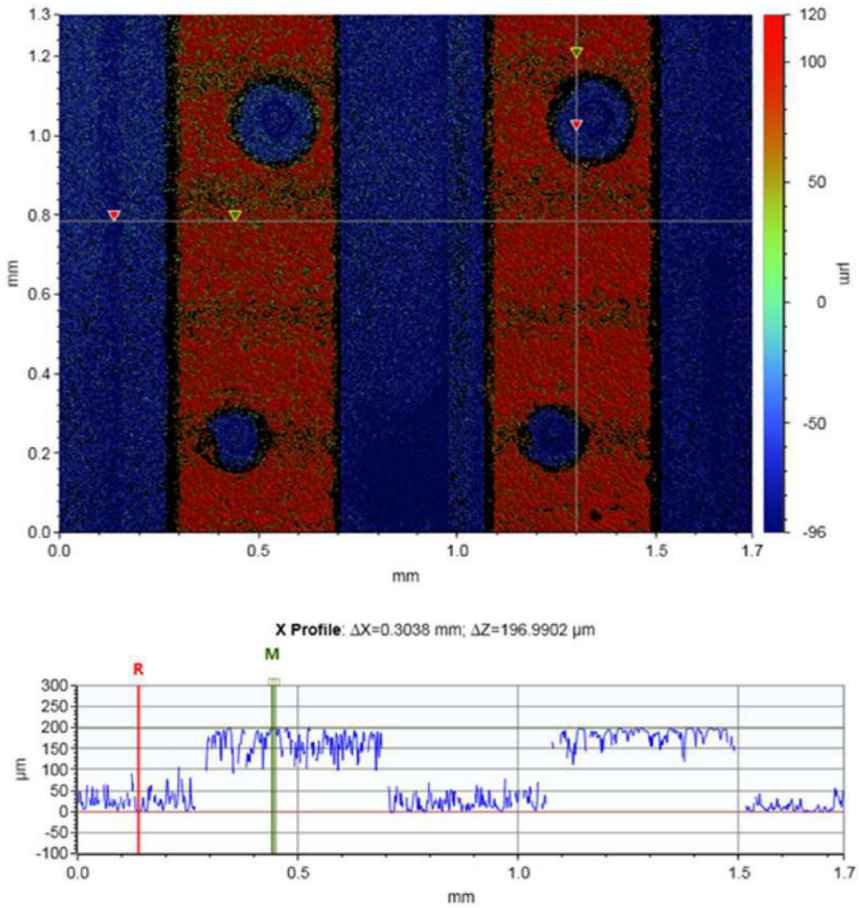

Figure 3.9. WLI-microscope image showing the milling patterns as well as the height of the milled negative structure of a microchannel with micropillars, i.e. round-shaped hollows on the mold.

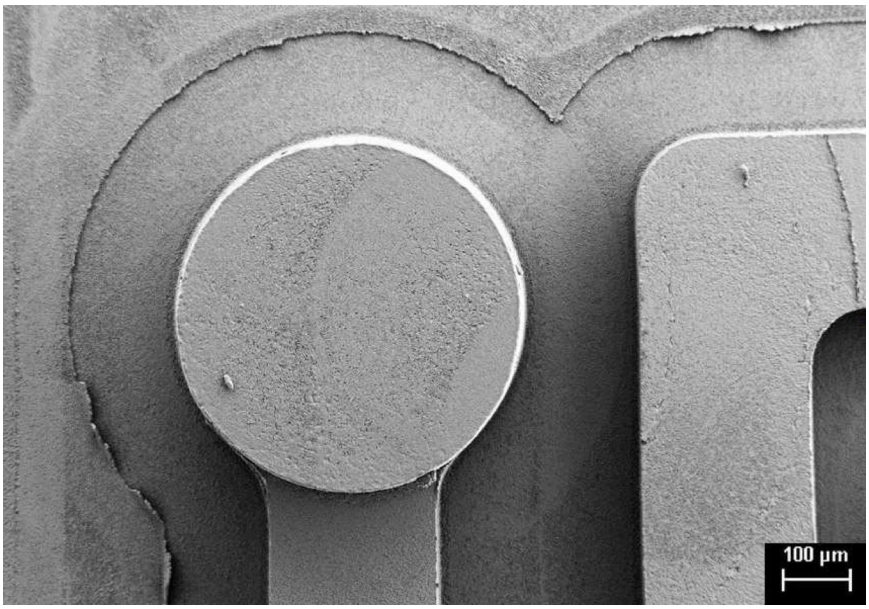

Figure 3.10. SEM image of the PMMA with a 50x magnification showing the negative structure of an inlet.

3.5.2. PDMS casting

Once a mold is fabricated, it can be used to cast PDMS (see Chapter 2.4.1). For all tests and final parts, *Sylgard*® 184 Silicone was mixed with a curing agent in the standard ratio 10:1. After thoroughly mixing, the mixture was placed in an exicator, under vacuum, for 5-10 minutes to release the air trapped inside it. During this process, the mold was rinsed with isopropanol and compressed air or nitrogen to avoid dust particles on the mold, and as a result, on the PDMS part. Once the mixture was air bubble free, the liquid PDMS was slowly poured into the cleaned mold, trying to avoid generating new air bubbles. However, even by pouring the PDMS in the mold as carefully and slowly as possible, pouring without air bubbles was not possible. Air was invariably trapped, particularly, in the holes corresponding to the obstacles of the mixers (see Chapter 4.1.3). Figure 3.11 shows an example of this situation. As might be expected, the air prevents a correct functionality of the mixer, in addition to becoming a weak point within the PDMS part. Hence, the mold was placed again inside the exicator for 15-20 minutes until all air was released. This time depends on the curing: as the viscosity of the PDMS increases, it takes longer to release the air.

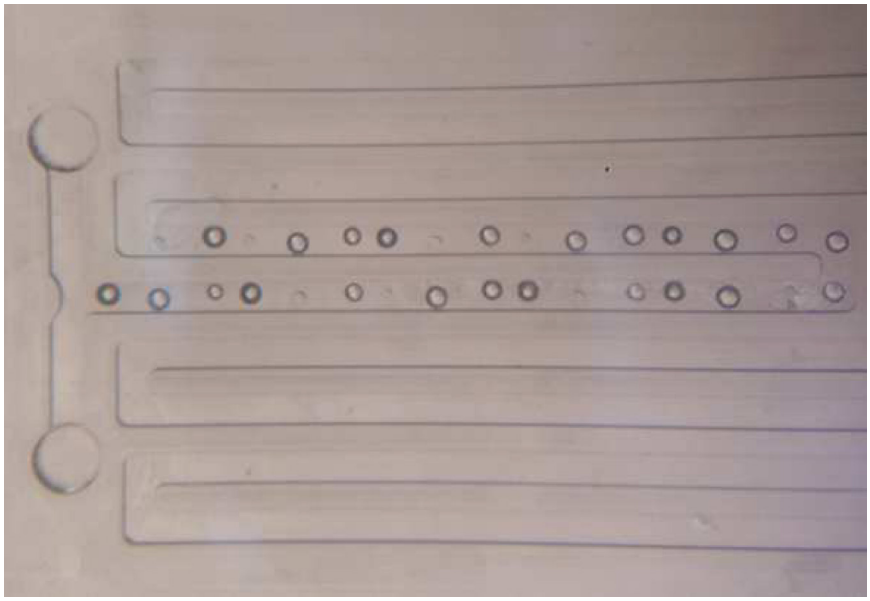

Figure 3.11. Air bubbles generation by PDMS casting even by carefully and slowly pouring of the liquid PDMS in the mold.

Lastly, the PDMS was cured at 65 °C for 90 minutes. After cooling for a few minutes, each PDMS part was demolded with the following procedure: the PDMS was slightly peeled off at one corner of a mold. Then, isopropanol was injected through the small gap, forming a thin layer between the mold and the PDMS. This layer facilitates the demolding of the PDMS without damage. The PDMS was then peeled slowly off, continuously injecting more isopropanol if required. Principally, the mixers require careful attention as they have crucial structures such as the pins. Demolding hastily or too abruptly caused a rupture of these small pins (see Figure 3.12). This caused not only damage to the PDMS part, but to the mold as well as the PDMS was trapped inside the holes and was nearly

impossible to remove it. Therefore, peeling off the PDMS extremely slowly with abundant isopropanol was crucial.

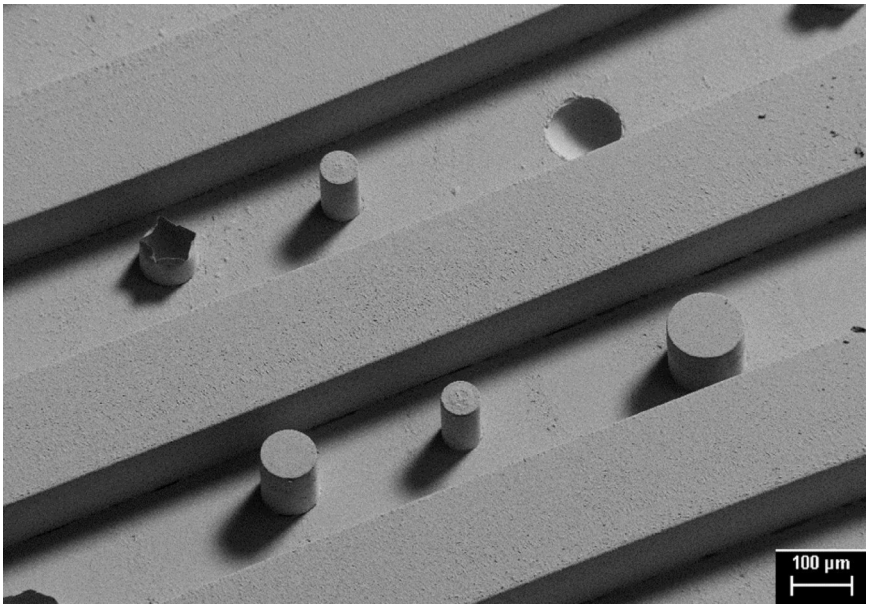

Figure 3.12. SEM images with a 50x magnitude of damaged pins of a mixer after an abrupt demolding. In the first row, the first pin from the left is half broken and the third one was completely torn. The row below has three intact pins.

3.5.3. Plasma bonding

The next step to fabricate the AIMD is to bond the different PDMS layers. Plasma bonding is the selected bonding method and is thoroughly described in Chapter 2.4.2. Briefly, both surfaces to be bonded are activated by exposing them to plasma and then immediately pressed together, forming an irreversible bond.

After the plasma exposure, the PDMS parts are to be aligned properly to each other at the first attempt. Once the activated surfaces come in contact with each other, they cannot be repositioned. Hence, as the outlets of one layer must match the inlets of the next one, an exact alignment of the layers is required. To achieve this, PMMA alignment holders were developed. The difference between the holders was the height as this varied depending on how many layers were already bonded.

The fabrication steps of an alignment holder are shown in Figure 3.13. Both a top (green) and a bottom part (red), 60 mm in width and length, were milled to fit each other (A). Then, an opening with the dimensions of the AIMD, namely, 42.3 mm x 38.8 mm, was milled, while both parts of the holder were bonded together, reversibly, with green tape (B). This was required to ensure the correct alignment of the PDMS parts because even if the milling process is exact, an offset can always occur. This was avoided by milling both parts together. On the top part, 1 mm was left as support for the PDMS during the plasma exposure. Finally, a PMMA piece was glued with UV curing adhesive to the bottom part (C). The height of the top part was selected to be thinner as the PDMS part (or PDMS bonded parts) to ensure contact between both PDMS parts (D).

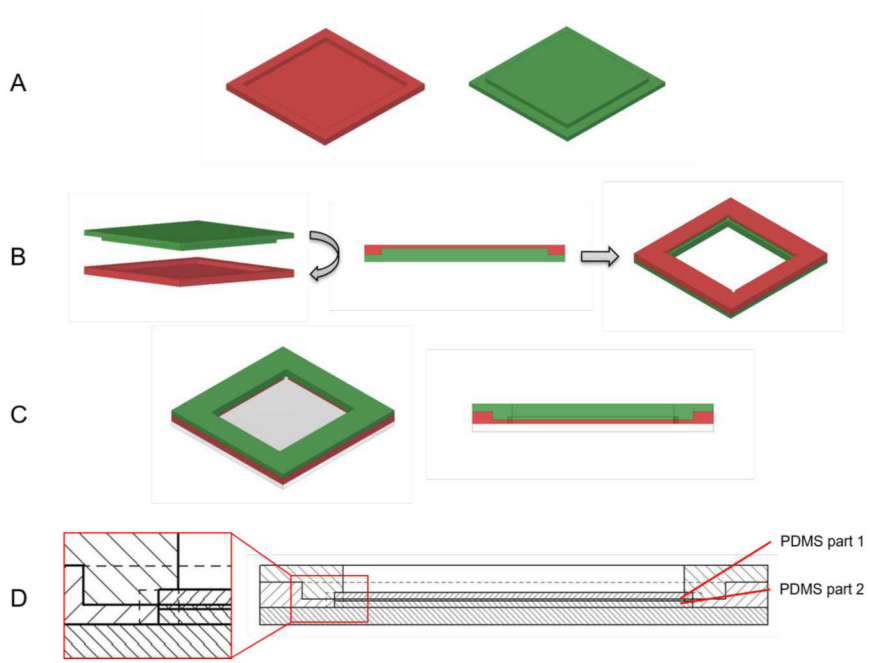

Figure 3.13. PMMA alignment holder fabrication steps. (A) Both a top (green) and a bottom (red) part were milled to fit each other. (B) An opening with the dimension of the AIMD was milled while both parts were bonded together, reversibly, with green tape. (C) A piece of PMMA was glued to the bottom part with UV curing adhesive. (D) A small area was left on the top part to support the PDMS part during the plasma exposure.

In this work, the 4-TEC[7] located in the cleanroom of the IMT was used. The PDMS parts were exposed to plasma for 5 s with an O_2-flow of ~0.06 SLM, 100 W power, and ~0.595 mbar during the process.

The PDMS parts were positioned in the holder and inside the vacuum chamber. The chamber was evacuated until the pressure was < 0.01 mbar and then filled with oxygen. After reaching ~0.595 mbar, the plasma was turned on (Figure 3.14 (B)). After 5 s, the plasma was turned off, the oxygen flow stopped, and the chamber evacuated. Then, the chamber was opened and as soon as the parts could be reached inside the chamber, the top part of the holder was aligned with the bottom part (C). Finally, the top PDMS part was pressed manually to the other through the gap (D).

The bond quality was inspected manually immediately after bonding. Due to the low-pressure values (< 1 bar) generated in the AIMD, trying to peel apart both PDMS parts manually is enough for a first evaluation of the bond. Normally, if the bond is working, both parts cannot be separated anymore. Throughout the entire work, a successful bonding rate was estimated to be 80%. Reasons for the failed attempts are yet to be determined. However, as mentioned in Chapter 2.4.2, this bonding technique is widely used despite its inconsistent results. Furthermore, the bond quality was analyzed with the SEM. In Figure 3.15 two bonds are shown. The left image with a 200x magnitude is a perfect bond as it cannot be distinguished where one PDMS parts ends and where the other one starts. In the right one with 200x magnitude as well, a hardly recognizable boding line can be

[7]Vakuum-Anlagenbau GmbH (Vierkirchen, Deutschland)

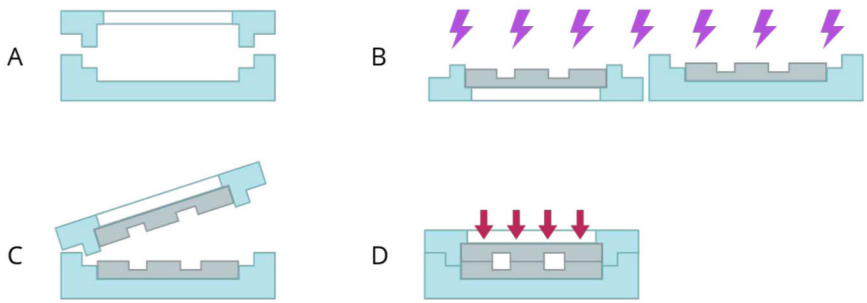

Figure 3.14. Schematically representation of plasma bonding of the different PDMS layers. (A) PMMA alignment holder. (B) Plasma exposure of the PDMS for 5 s. (C) Alignment of the top part of the holder with the bottom part. (D) Pressing of the top PDMS part through the gap.

seen. In a zoom image with 1000x magnitude, air trapped between the two PDMS parts can be seen. However, these defects are so small that they can be neglected.

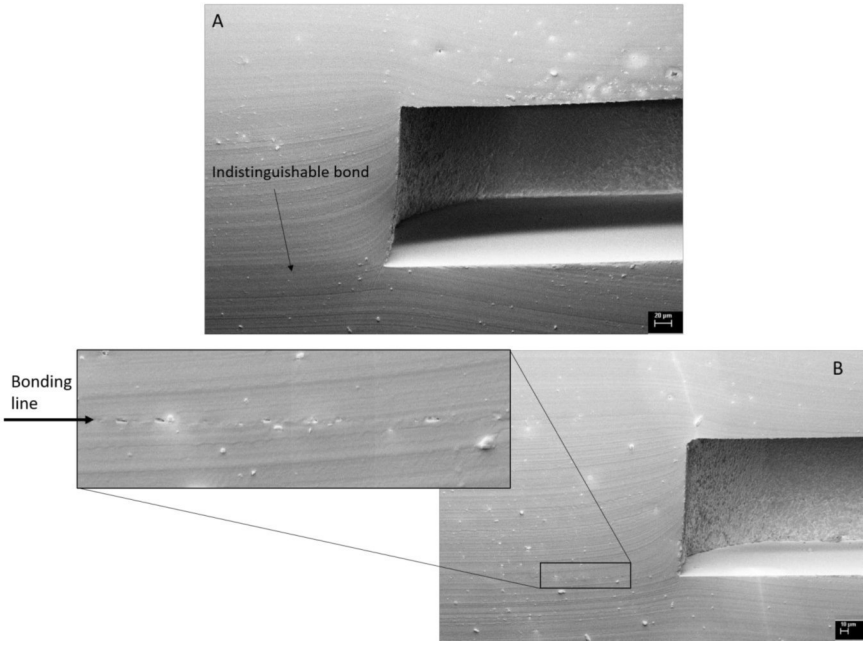

Figure 3.15. A) Bond indistinguishable (200x magnitude). B) Bond less perfect as air can be seen trapped between the PDMS part (200x magnitude). The bonding line with small holes is shown in the zoomed in image (1000x magnitude).

The first attempts to bond the PDMS layers were without an alignment holder. As Figure 3.16 (top) shows, the alignment of both layers was not exact. These defaults could be seen with the naked eye. Hence, the alignment holder previously described was designed. With this device, the positioning improved considerably. Errors could not be seen easily; hence, the crucial spots were evaluated with the SEM. Figure 3.16 (bottom) shows with a 100x magnitude the outlet of the bottom layer matching the channel of the bottom one. The offset is of only ~20 µm (Figure 3.16 (bottom) with 500x magnitude). All the outlets were designed to be 0.1 mm larger in diameter than the inlets to compensate any

offset occurring during bonding. The offset seen during the examination of the bonding is under this limit. Thus, the layers were bonded using the appropriate holder.

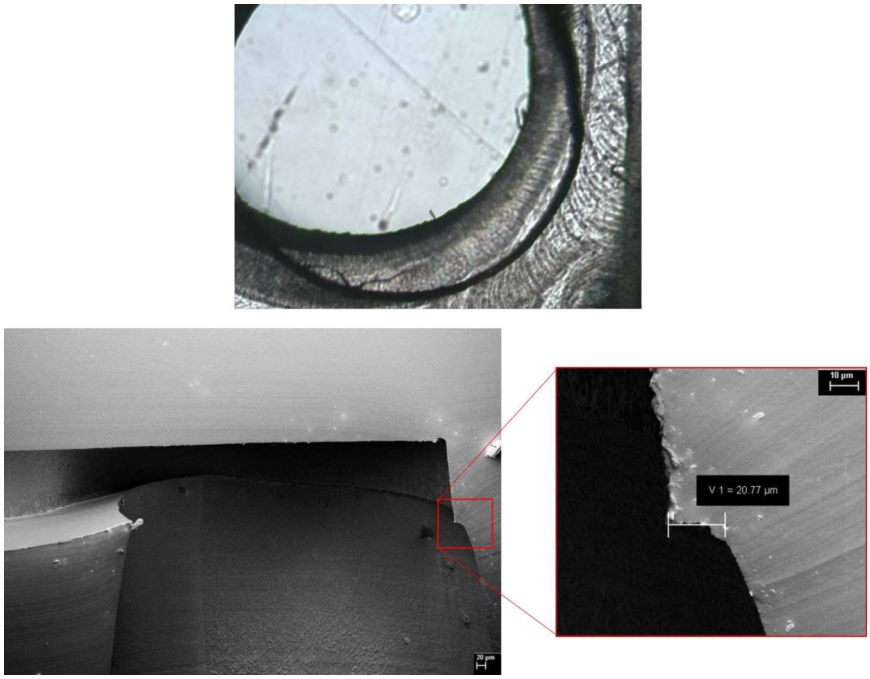

Figure 3.16. Evaluation of the layers alignment through SEM images. Top: Displaced inlets of two layers after bonding without an alignment holder. Bottom: SEM image of an outlet in the bottom layer aligned with the channel of the top layer (100x magnitude). The zoom in image with a 500x magnitude shows an offset of only ~20 µm.

4. Microfluidic Components of the AIMD

Every module of the AIMD consists of different microfluidic subsystems, or components, to perform the basic functions required. The first component introduced is for mixing, as this is a crucial procedure in the cloning process. A summary of the existing mixing methods is provided, and then the course of the development until the final mixer is outlined. Afterwards, the other components, responsible for the control and transport of the substances through the modules, are presented: an on-chip blocking valve, developed to stop the flow, is introduced. The distribution component, responsible for ensuring that the substances are dispensed equally for each parallel process, is described. The principles of these components are the same for each module; their specific characteristics, dimensions and positioning in each module are described in Chapter 5. Lastly, the development of the heating and cooling systems, relevant for the heat shock, is presented.

4.1. Mixing system

As mentioned in Chapter 2.2.2, most biological or biomedical processes are the product of a reaction after two or more substances are brought in contact. Mainly, as most biological reagents are dissolved in a buffer, the procedure to bring them together is by mixing. Hence, one of the most important functions of a microfluidic device in this field is its ability to mix, and the AIMD is no exception.

In the L-Module, the vectors are mixed with the ligase and the inserts, whereas in the T-Module the ligation product is mixed with the bacteria. Finally, the transformed bacteria are mixed with the culture medium. Although mixing occurs in every step, it is most important for the ligation. Therefore, the micromixer was designed principally for this application and it was accordingly modified for the other modules. In this work, a passive micromixer was selected to reduce the external energy sources. Different micromixers were developed to achieve the optimal mixture. The first idea was to use the split-and-recombine concept combined with a non-straight channel. After first results, a new concept was developed, changing to a straight channel, but with asymmetrical obstacles. In this section, both ideas for the micromixers with their characterization are presented. This is proceeded by a brief overview of the mixing technologies in the microfluidics.

4.1.1. State of the art: Mixing in microfluidics

Micromixers are one of the most important components in the microfluidic devices. As mentioned in Chapter 2.2.2, passive micromixers are preferred in the microfluidic field due to its easier integration. The mixing efficiency is not perfect; therefore, numerous groups

have developed and optimized passive micromixers and have used them for biomedical microfluidic devices [19, 21, 48, 51, 103–113]:

[27] describe a microfluidic chip, fabricated by multilayer soft lithography, with active micromixers that use pneumatic forces to work. Chang et al. (2010) [15] also present a PDMS pneumatic micromixer for extraction of mitochondrial DNA. Through four air chambers, compressed air flows to deflect a PDMS membrane, causing a swirling flow. Shih et al. (2015) [28] and von der Ecken (2017) [75] propose mixing with an alternative technology, namely digital microfluidics. All these systems are very efficient and show promising results; however, their fabrication and control are cumbersome and difficult to integrate with other microfluidic components.

Other groups have implemented passive micromixers for biological application, specifically for some steps of the molecular cloning process. Ko et al. (2011) [21] propose a micromixer with micropillars and micronozzles, based on the Tesla-mixer and an obstruction mixer. Through the micronozzles, the streams are divided and then collide again. Micropillars with a diameter of 180 µm, positioned asymmetrically along the channel, were used as obstacles to disrupt the fluid. They affirmed that positioning the obstacles asymmetrically enhance the mixing. This micromixer is 10.33 mm in length, 400 µm in width, and 100 µm in height. The micromixer was fabricated in PDMS and was bonded to a glass substrate. This group used the micromixer to perform ligation processes on-chip, successfully. Moreover, Papadopoulos et al. (2014) [19] describe a micromixer with a zigzag geometry. The V-shaped zigzag structures are 800 µm wide, 60 µm deep, and the channels are 400 µm wide. The results showed that ca. 150 zigzags delivered the best mixing efficiency. This micromixer was fabricated using a photo imageable dry film by means of flexible printed circuit technology. It was applied for a conventional DNA digestion procedure. Furthermore, Lin et al. (2012) [18] presents a T-form active micromixer for DNA digestion. Hereby, the substances are mixed by switching the DC electric flow. This microchannels were etched in a glass substrate and these were closed with a glass cover by means of thermal fusion bonding. The microchannels were 40 µm deep and 100 µm wide.

As the aim of this work was not to develop an innovative micromixer, the best qualities of different micromixers were analyzed to select the best one that suited the application. The mixing efficiency as well as the simple design and fabrication were taken into consideration. Based on the results of these existing works, it was decided to implement a passive micromixer as their advantage outweigh the disadvantages. Split-and-Recombine structures as well as obstacles along the channel were chosen.

4.1.2. Split-and-Recombine Micromixer with Zigzag-Channels

For the first concepts, split-and-recombine structures and zigzag-channels, the latter based on a previous work from this group [70], were combined differently to obtain different micromixers. As described in Chapter 2.2.2, split-and-recombine structures enhance mixing when the flow streams, previously separated, collide again and zigzag-structures increase the mixing efficiency by bringing a relative chaotic flow in the channels.

The width of the channels was 400 µm, whereas the height was either 100 µm, 150 µm or 200 µm. The micromixers were designed for a total capacity of 10 µl. Figure 4.1 shows

three examples of these. The first two have three and four split-and-recombine structures, respectively, whereas the third one has one split-and-recombine structure as well as a reaction zone at the end. All micromixers were fabricated following the method described in Chapter 3.5.

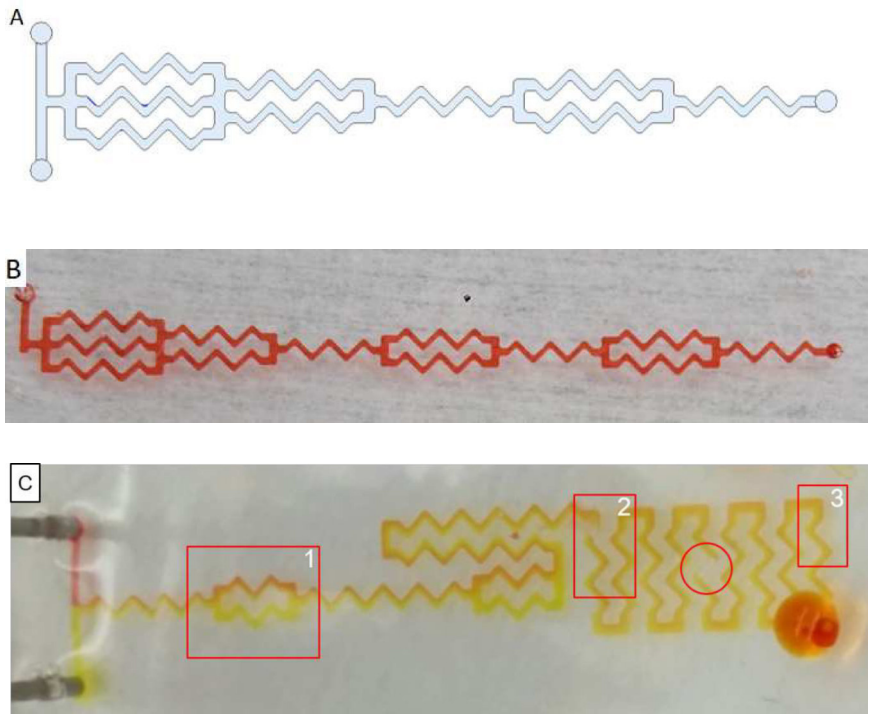

Figure 4.1. Two examples of the first concepts of the micromixer with split-and-recombine structures. A) Sketch of a micromixer with three split-and-recombine and zigzag-channels. B) PDMS micromixer with four split-and-recombine structures and zigzag-channels as well. C) PDMS micromixer with a split-and-recombine structure and a reaction zone: At position (1), both colors are still distinguishable; at the beginning of the reaction zone the contact front between the colors starts to fade (2); finally, at the end of the reaction zone is not distinguishable anymore (3). One drawback: air trapped inside the channels, shown circled in red.

The pretests were performed by mixing colored distilled water. Using a high-accurate, two-channel syringe pump[1], red and yellow distilled water was pumped with a flow rate of 2 ml/min in each inlet of the micromixer. Firstly, the results showed that the height was not influencing the mixing results significantly; therefore, 200 µm was chosen as this dimension allowed more volume in shorter channels. Moreover, purely optically, the mixing accuracy was analyzed. In Figure 4.1 (bottom), an orangish reaction zone, the mixture between red and yellow, can be appreciated. The micromixer consisting of two split-and-recombine structures showed the best results. At the first split-and-recombine structure (1), both colors are still clearly noticeable. At the beginning of the reaction zone, the contact front between the colors is faded (2), whereas at the end of the reaction zone (3) is not distinguishable anymore. Although, at the end of the reaction zone a high

[1]PHD ULTRA™ Harvard Apparatus

mixing accuracy can be assumed, at the end of the micromixer, the mixing is not quite complete.

4.1.2.1. Biological tests

Ligation tests were performed with these micromixers to trace the correct optimization path. The pGEM®-T Easy Vector System I was used for these tests. The pGEM®-T Easy Vector (50 ng/µl), 3015 base pairs (bp) in length, was used as plasmid. The Control Insert DNA (4 ng/µl), 542 bp in length, was used as the DNA of interest to be cloned. The T4 DNA Ligase and the 2X Rapid Ligation Buffer were the other two components used [114]. All components are ready to use, although they must be thawed at room temperature before use. In Appendix A.3, more information about the Vector System is listed.

Three different experiments, with a total of 10 µl each one, were performed, namely, a standard procedure (C1), one without control insert (C2), and one without vector (C3). An overview of the experiments can be found in Table 4.1. For the first experiment (C1), the standard protocol was followed: 2 µl DNA, 1 µl Ligase, 5 µl buffer und 1 µl distilled water were mixed on-chip. For experiment C2, DNA was replaced with distilled water, whereas for experiment C3, the vector was replaced with distilled water. For all experiments, the substances were left in the reaction zone for 1 hour for the ligation to take place. Afterwards, the product was pumped out and put in an Eppi [115].

	Insert	**Vector**	**Ligase**	**Buffer**	**Water**	**Total**	
C1	2	1	1	5	1	10	
C2	-	1	1	5	3	10	[µl]
C3	2	-	1	5	2	10	

Table 4.1. Summary of the first ligation test using the first micromixers.

To analyze the ligation efficiency, a manually transformation was performed. *E. coli* were used as competent cells and the heat shock was the selected method for the transformation. Then, transformed bacteria were placed on agar plates with an appropriate antibiotic and were cultivated over night at 37 °C. Bacterial colonies grew exclusively in agar plates of experiments C1 and C2. The vector contains the gen resistant to the antibiotics; therefore, without vector, no bacterial growth can take place. This is the case for experiment C3 and as expected, no colonies were seen on the corresponding agar plates. The blue-white screening method explained in Chapter 2.1.2.1 can be used with the pGEM®-T Easy Vector System. Thus, as expected, on the C1-agar plates, white and blue colonies grew, whereas in the C2-agar plates, only blue colonies were seen. Two C1 white colonies and two C2 blue colonies were picked and cultured again over night. Subsequently, the vector was isolated and cut with standard methods to release the insert. To verify if the insert was indeed contained in the white colonies, gel electrophoresis (see Chapter 2.1.2.2) was used. In lane 2 of Figure 4.2, the vector and insert of C1 can be seen. On lane 3, the vector without insert is seen as well. The other two colonies, namely lane 1 and 4, were probably impurities as they do not show vectors nor inserts.

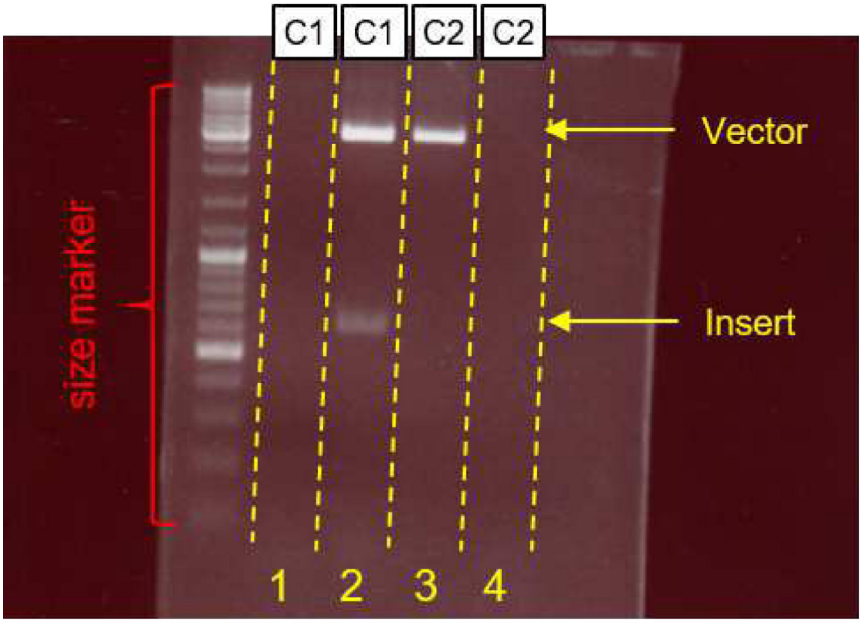

Figure 4.2. Ligation results using gel electrophoresis: size marker on the left lane, C1 experiments in lanes 1-2, and C2 experiments lanes 3-4.

Even though the results achieved were to some extent favorable, these micromixers showed some disadvantages. The first one, as mentioned above, was that the mixing was not finished inside the micromixer, but at the end of the reaction zone. This meant, the micromixer had to be longer to achieve a complete mixing. The other main drawback was the bubble generation. During the tests with distilled water, and even with the biological tests, it was extremely difficult to fill the micromixers without air being trapped in the channels (see Figure 4.1). Possibly, the changes in direction of the zigzag structures were to abrupt, causing the flow to avoid the corners. Therefore, a micromixer with a new design was developed.

4.1.3. Micromixer with cylindrical obstacles

As mentioned in the section above, the mixing efficiency of the first micromixers was not ideal. The main problem was the air trapping inside the channels. However, this was not the only situation in need of being changed. As different components and modules of the AIMD were being developed simultaneously, all components had to be adapted accordingly during the project. In this case, to minimize the reagents of the cloning process, it was decided to reduce 60% of the ligation total volume, i.e. form 10 µl to 4 µl (see Chapter 5.2 for the volumes of each ligation component). Therefore, the micromixer had not only to be optimized, but downsized as well.

The best course of action to avoid the air trapping is to return to straight channels. However, this sinks the mixing efficiency drastically (see Chapter 2.2.2). Therefore, to maintain a chaotic flow a micromixer with obstacles was designed. This solution was also simple to dimension for the new total volume.

4.1.3.1. Design

The new design was also based on the idea of bringing chaos to an otherwise extremely laminar flow. In this case, instead of relying on the walls of the channels, obstacles were to be positioned throughout the channel to divert the flow, i.e. to create a chaotic flow. The design was based on the micromixer developed by Ko et al. (2011) [21] (see Chapter 4.1.1).

Different forms for the obstacles were worth considering; however, cylindrical obstacles, i.e. micropillars, were chosen for a simpler fabrication (details in Chapter 4.1.3.3). These, with three different diameters, namely, 100 µm, 150 µm, and 200 µm, were positioned asymmetrically in the channel. The first micropillar with 100 µm is located 20 µm to the left of the center line of the channel. The next micropillar, with 200 µm in diameter, is placed 700 µm after the first one and 50 µm to the right of the centerline. After 800 µm, the 150 µm micropillar is positioned, 50 µm to the left from the centerline. The pattern of the three micropillars repeats itself along the channel. This configuration can be seen in Figure 4.3 (left). The channels are 400 µm in width, 400 µm in height, and ~20 mm in length. This final design has a capacity of ~2 µl, as it was enough for the mixing, and was selected after simulating different configurations (explained below). A reaction zone is connected to the micromixer to contain the 4 µl. The micromixer (blue) and the reaction zone (cyan) as a unit are shown in Figure 4.3 (right). These dimensions correspond to the micromixers used in the L-Module.

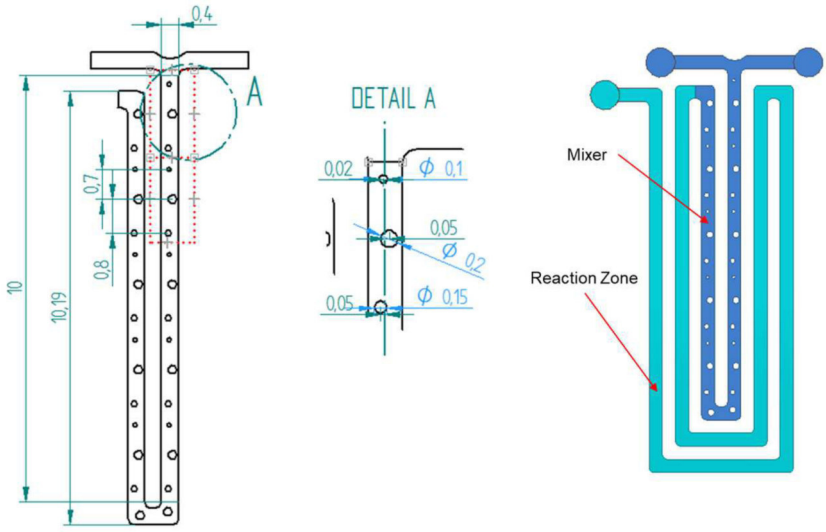

Figure 4.3. Left: Dimensions of the 4 µl-micromixer and its obstacles. Three micropillars with different diameters, namely, 100 µm, 150 µm, and 200 µm, were positioned asymmetrically in the channel. It is 400 µm in width, 200 µm in height, and ~20 mm in length. Right: Micromixer, shown in blue, connected to the reaction zone, shown in cyan, for a total volume of 4 µl.

The competent bacteria are highly sensitive. In a microfluidic device, it should be avoided for it to flow through narrow spaces such as the ones in the micromixer previously described. Therefore, a wider micromixer was developed exclusively for the bacteria. The principle idea of the previous micromixer is the same for the new one, but the dimensions are larger. These changes were backed by the results of the simulations (see

Chapter 4.1.3.2). The principal adjustment was made to the width of the channel: it was doubled to 800 µm. The pattern of the three micropillars with different dimensions is also further employed. However, in this case, the diameters of the micropillars were also doubled to 200 µm, 300 µm, and 400 µm, respectively. The obstacles had to be enlarged because the smaller ones did not influence the flow enough to cause the required chaos. The spaces between the micropillars and the channels walls are still larger than the smaller micromixer. The obstacles are positioned asymmetrically along the channel. The smallest one, namely 200 µm, is 50 µm to the left of the centerline. The largest one, 400 µm, is located 90 µm to the right of the center of the channel. Lastly, the 300 µm-micropillar is 100 µm to the left. The length of the micromixer is also ~20 mm. This micromixer can contain ~3.5 µl and has a reaction zone at the end for the rest of the volume. The micromixer with its dimensions is shown in Figure 4.4.

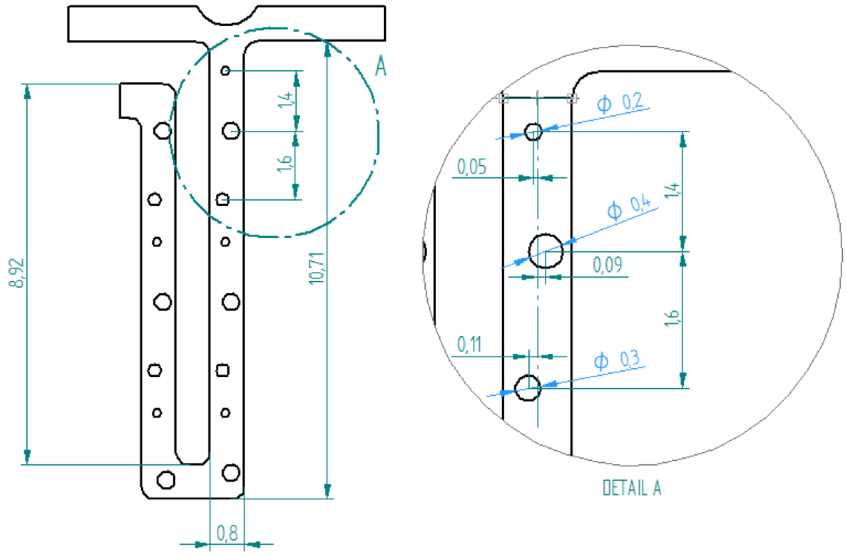

Figure 4.4. Dimensions of the larger micromixer and its obstacles. Three micropillars with different diameters, namely, 200 µm, 300 µm, and 400 µm, are positioned asymmetrically in the channel. The channel is 800 µm wide, 200 µm deep, and ~20 mm in length.

4.1.3.2. Simulation

The designs of the micromixers were tested theoretically by simulations. The mixing efficiency along the channel was quantified by analyzing the final concentration of the flow at the end of the micromixer. One inlet was presumed to have a 0% concentration, whereas the second one a 100%. Hence, a perfect mixing at the end of the micromixer would correspond to a 50% concentration. The simulation was performed with COMSOL Multiphysics[2].

The Reynolds number *Re* is crucial for the characterization of the flow and, therefore, for the correct selection of the simulation interface. As the biological substances

[2]version 5.3

are mostly dissolved in buffers, the fluidic properties of water can be used as starting parameters. According to Equation 2.1, the Reynolds number Re_M for this case is

$$Re_M = \frac{\rho_w u_1 D_{hM}}{\mu_w} = 0.91 \tag{4.1}$$

with ρ_w as water density, u_1 as the velocity at the inlets, D_{hM} as the hydraulic diameter of the micromixer for a squared microchannel, and μ_w as water dynamic viscosity. All parameters are summarized in Table 4.2.

Water properties		**Micromixer parameter**	
ρ_w	1000 kg/m3	u_1	3 mm/s
μ_w	$8.9{\cdot}10^{-4}$ Pa s	D_{hM}	0.27 mm

Table 4.2. Water properties and micromixer parameters required for the Reynolds number calculation.

COMSOL offers the *Creeping Flow* interface, specially defined for significantly low Reynolds numbers. It applies the Stokes equation for the flow (Equation 2.6), as the inertia forces can be neglected in the Navier-Stokes equation, and the Fick's law (Equation 2.11) for the diffusive transport (see Chapter 2.2).

For the diffusion, the diffusion coefficient of the DNA in water is required. In the literature, there is no specific value that can be used. However, Lukacs et al. (2000) [116] correlated empirically the diffusion coefficient of DNA in water D_w with the number of bp as follows:

$$D_w = 4.9 \cdot 10^{-6} n_{bp}^{-0.72} \tag{4.2}$$

In this work, the DNA to be ligated has a length of ~2000 bp. Hence, using Equation 4.2, the diffusion coefficient D_{2000} is $2.058{\cdot}10^{-8}$. Furthermore, the diffusion coefficient D can be roughly calculated with the Stokes-Einstein equation [117]

$$D = \frac{k_b T_M}{6\pi\eta r_H} \tag{4.3}$$

with $k_b = 1.38{\cdot}10^{-23}$ (Boltzmann constant), T_M is the medium temperature, η is the medium viscosity and r_H is the Stokes radius.

The Stokes radius of DNA molecules depend on its bp size and its form. Heinzmann et al. (2007) [118] measured the radii of three different forms of DNA, namely closed coil, open coil, and linear, r_c = 62.8 nm, r_o = 77.9 nm, and r_l = 86.8 nm, respectively. Substituting these values in Equation 4.3, the diffusion coefficients D_c, D_o, and D_l for closed coil, open coil, and linear DNA, respectively, were calculated and are summarized in Table 4.3.

These values can be compared with the diffusion coefficient calculated with Equation 4.2. Therefore, the four values were used for the simulation to analyze the influence of the bp size by mixing.

The fluid domain for the simulation (Figure 4.5 (center)) was derived from the 3D-model of the micromixer (Figure 4.5 (left)). Both models were created in Solid Edge ST8[3]

[3]Siemens PLM Software

DNA form	Stokes radius [nm]	Diffusion coefficient [m^2/s]
closed coil	r_c = 62.8	$D_c = 2.9582 \cdot 10^{-12}$
open coil	r_o = 77.9	$D_o = 2.3848 \cdot 10^{-12}$
linear	r_l = 86.8	$D_l = 2.1402 \cdot 10^{-12}$

Table 4.3. Stokes radii and diffusion coefficients of closed coil, open coil, and linear DNA.

and imported into COMSOL, whereas the mesh was compiled directly in COMSOL. The height of fluid domain was set to 100 µm for reducing computation time as a symmetry plane was presumed at half the height of the channel. Different mesh sizes were tested to find the optimal size; however, only the element sizes were modified as the tetrahedral form stayed unchanged. The optimal mesh (Figure 4.5 (right)) was selected considering the best results with the minimal computation time, ~37 min, and had a minimum element size of $8.01 \cdot 10^{-3}$ mm.

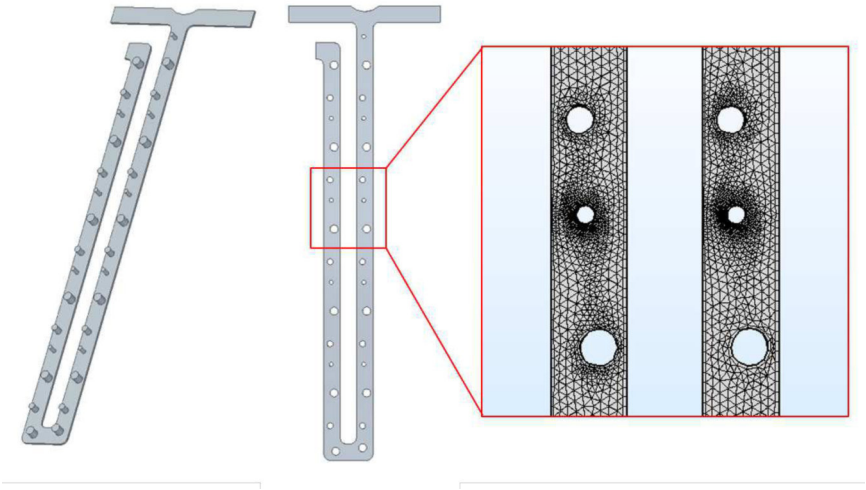

Figure 4.5. Left: 3D-model of the micromixer. Center: Fluid domain of the micromixer for simulation. Right: Optimal mesh for simulation with tetrahedral elements.

In Figure 4.6, the simulation results for the concentration are shown for the closed coil (1), open coil (2), linear 3, and ~2000 bp-DNA (4). The results show a nearly perfect mixing at the end of the micromixer, with a negligible variation between the different diffusion coefficients, more specifically, between the size or form of the DNA. The mean value of the final concentration yields 0.5035 with a standard deviation of $9.33 \cdot 10^{-6}$, which represents an excellent mixing efficiency. An overview of the concentration results is found in Table 4.4.

DNA	Final concentration [mol/m^3]	
	Water	Water/Glycerin
closed coil	0.5035146309	0.49298
open coil	0.5035222188	0.49296
linear	0.5035336669	0.49294
~2000 bp	0.5035336705	-
mean	0.5035	0.49296

Table 4.4. Simulation results. Concentration at the end of the micromixer for different forms of DNA and for water and a water/glycerin 50% (w/w) mixture.

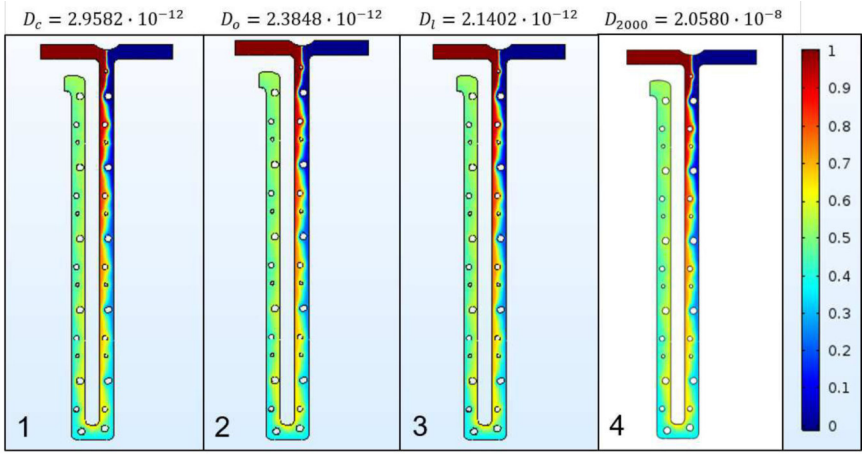

Figure 4.6. Simulation results of the final concentration for different DNA forms. (1) closed coil DNA; (2) open coil DNA; (3) lineal DNA; and (4) Final concentration for ~2000 bp-DNA. Red represents a 100% concentration, whereas blue 0%. The results show a high mixing efficiency at the end of the micromixer, with a negligible variation between the different size or form of the DNA.

For the ligation, a ligase to bind the insert with the vector is required (see Chapter 2.1.1). This enzyme is normally in a solution that is 49.2% glycerin and 50% water. Therefore, after obtaining accurate results with water, another simulation was performed with the properties of a water-glycerin 50% (w/w) solution at room temperature (see Table 4.5), but the same velocity. The mixing was analyzed for the closed coil, open coil, and linear DNA, but not for the ~2000 bp-DNA as the previous results showed that they were almost identical to the linear DNA. The mixing efficiency was extremely accurate, as well as it can be seen in the results of linear DNA (Figure 4.7). These results are also summarized in Table 4.4.

Water/Glycerin 50% (w/w)	
ρ_g	1139.1 kg/m^3
μ_g	6.97·10^{-3} Pa s

Table 4.5. Water/Glycerin 50% (w/w) at room temperature

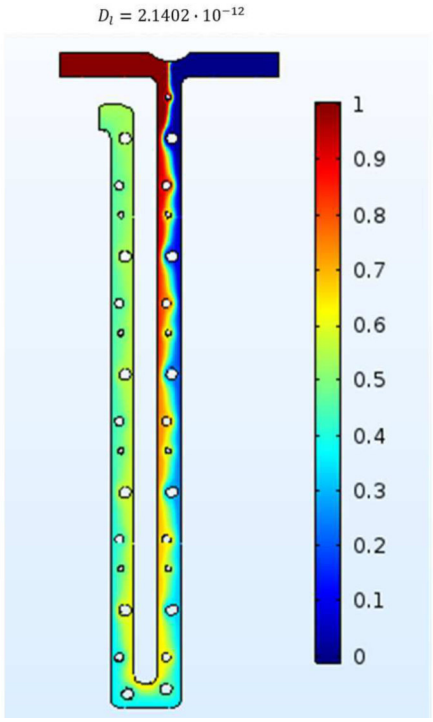

Figure 4.7. Simulation results for linear DNA in a water/glycerin 50% (w/w) solution. Red represents a 100% concentration, whereas blue 0%. The results show a high mixing efficiency as well.

Both the simulation with water as well as with water/glycerin delivered a high mixing efficiency. Therefore, this design was selected for the development to follow. As mentioned before, a larger micromixer for the T-Module was developed as well. To corroborate the efficiency of the micromixer, even after an alteration of its dimensions, a simulation with water was performed. The results do not vary significantly from the smaller micromixer. The same forms of DNA were analyzed, delivering the following results: closed coil: 0.504548495; open coil: 0.504543240; and linear: 504541440 (Figure 4.8). Hence, this micromixer is used in the modules that required a wider micromixer.

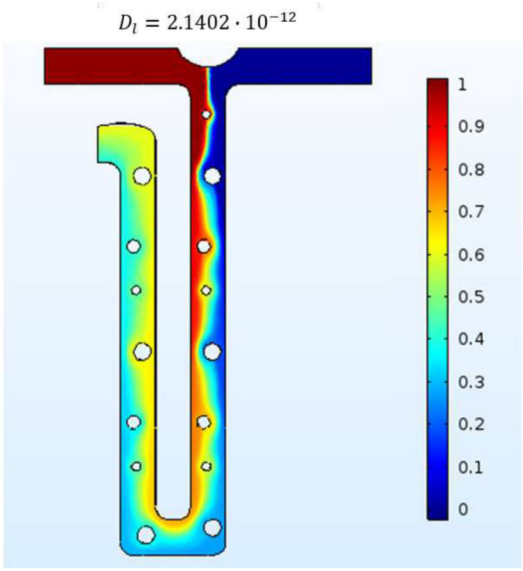

Figure 4.8. Simulation results for linear DNA in the larger micromixer. Red represents a 100% concentration, whereas blue 0%. The results show a high mixing efficiency even after modifying the dimensions.

4.1.3.3. Fabrication and Characterization

The micromixers were fabricated with the same method as the rest of the components (see Chapter 3.5). Therefore, a mold with the negative structures was required. As mentioned before, cylinders selected as obstacle form because its simple fabrication. To obtain micropillars in PDMS parts, bores are needed as negative form. Drilling is a standard procedure in the micromachining field; therefore, it is extremely reliable and has minimum difficulties. Bores were drilled in the PMMA mold with the corresponding tools. They have a nominal dimension for the depth of 200 µm, but with a lower deviation. This is to prevent the obstacles being taller than the channel height as this would have as consequence a failure by bonding. Figure 4.9 (top) shows a SEM image with 50x magnification of the bores of a PMMA mold of a 4 µl-micromixer. The bores for both micromixers were fabricated with great accuracy with a maximum deviation of 9 µm (Figure 4.9 (bottom)).

The main problems by the fabrication of the micromixer were the air bubbles in the holes and the rupture of the micropillars by peeling off the PDMS from the mold. The issue with the air bubbles was resolved with the desiccator. The isopropanol film and a slow demolding were enough to maintain the scrap rate to almost zero. See Chapter 3.5 for a detailed explanation. In Figure 4.10, a SEM image with a 100x magnification shows a PDMS channel with two working micropillars.

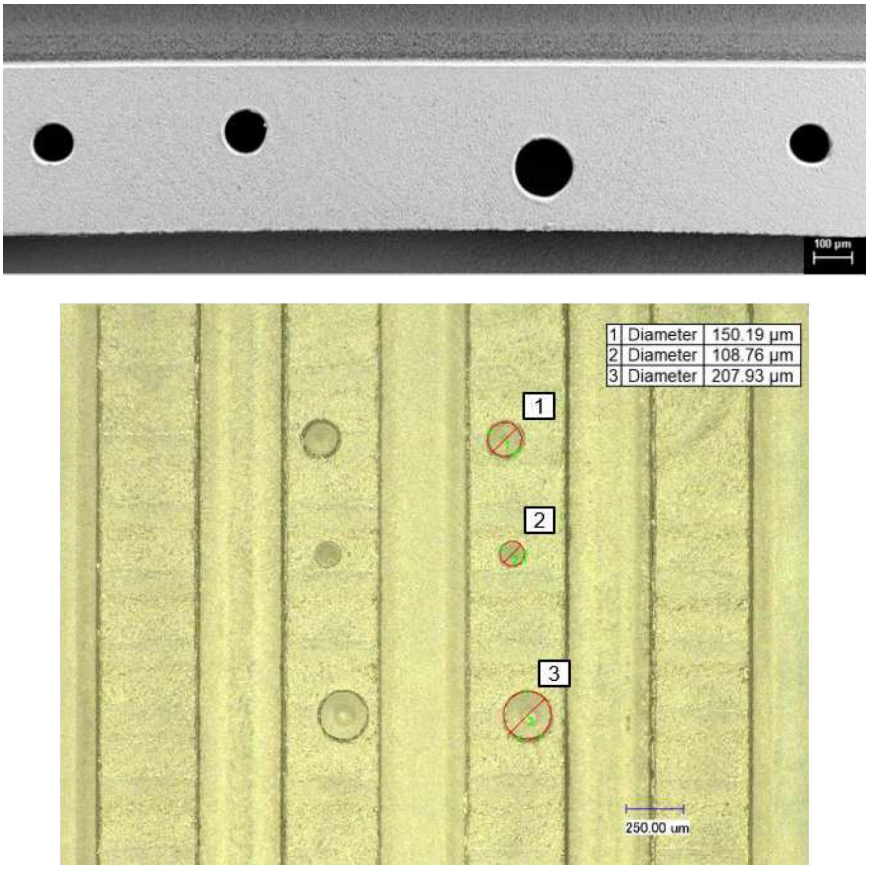

Figure 4.9. Top: SEM image with 50x magnification of the negative structures for the cylindrical obstacles of a PMMA mold. Bottom: on the left, bores of the mold of the 4 µl-micromixer with their dimensions, whereas on the right, the mold of the larger micromixer is shown.

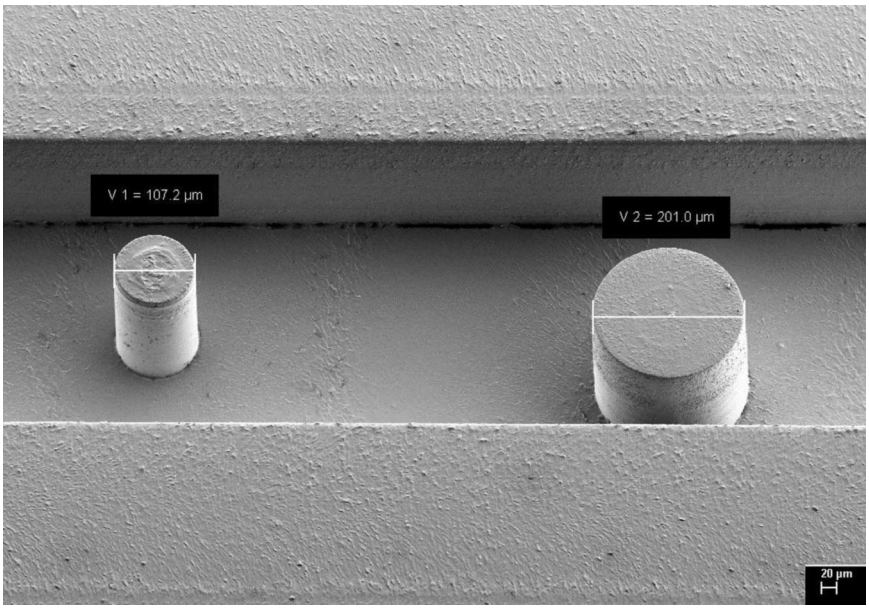

Figure 4.10. SEM image with 100x magnification of two cylindrical obstacles of a PDMS micromixer.

As the first micromixers, the 4 µl-micromixer was tested with red and yellow distilled water, using the same method described in Chapter 4.1.2. In this case, no air trapping was detected by filling the channels. In addition, a high mixing efficiency was observed at the end of the micromixer (Figure 4.11 (left)) as an orangish fluid was distinguishable with the naked eye. For a better optical analysis, a comparison between both original colors was made (Figure 4.11). Firstly, both channels were filled with red-colored water and a picture was taken at the end of the micromixer (right-top). The same procedure was conducted, but with yellow-colored water (right-bottom). Finally, the mixing was performed. At the end of the mixer, an orange-colored water can be seen at the end of the micromixer, a clear mixture between both flows (right-center).

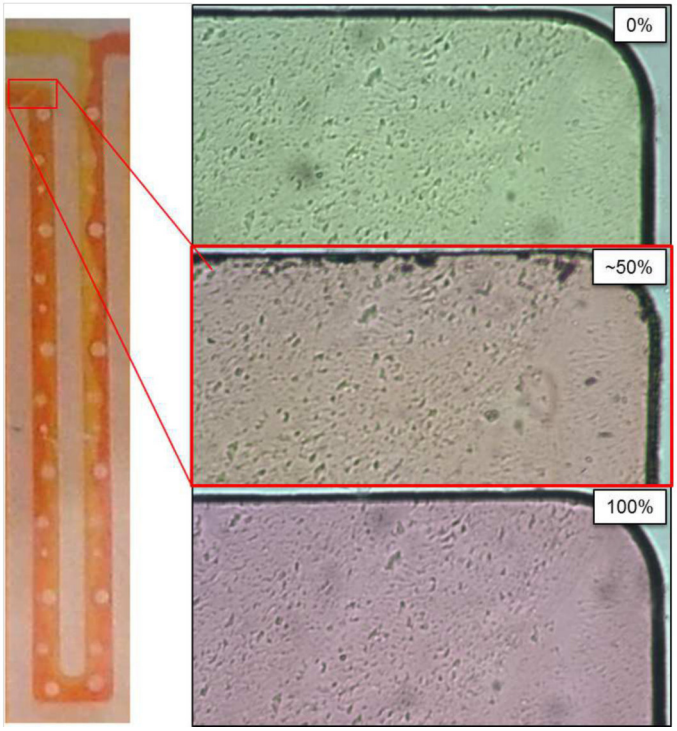

Figure 4.11. Results of micromixer characterization. Comparison between pure red, pure yellow, and the mixing of both at the end of the micromixer. Left: Each inlet of PDMS was filled with red- and yellow-colored water, respectively. An orangish fluid can be seen at the end of the micromixer. End of the micromixer: filled with yellow-colored water (top), filled with the mixture with an orangish color (center), and filled with red-colored water (bottom).

4.2. Blocking valve

As mentioned in Chapter 3.2, one the most important aspects to consider during the development of a microfluidic device is the use of valves to set apart process steps and avoid cross contamination. In this work, valves are required for metering (see Chapter 4.3.2) and to stop the fluid for a given time to allow the biological reactions to happen. After a brief review of the existing valves used for microfluidics, the requirements of the valve needed for this work are listed. A design description and its characterization follow.

4.2.1. State of the art: Valves in microfluidics

The first idea to control the fluid of the system was to use commercially available valve. However, using external standard valves found in the market had several disadvantages. Principally, they have large dead volumes: >5 µl, an extremely high number for a system planned for 4 µl up to 16 µl. Besides, even though several valves are considered *microvalves*, the dimensions are relatively large. For example, the WhisperValve[4] is considered a microvalve with an extremely compact design, with 7 mm as the smallest width and an internal volume, including the connections, of 5 µl [119]. Although this valve is perfect for small systems, for a microfluidic system is still too large. Moreover, external valves are also rather expensive.

Thus, on-chip valves were considered, specifically passive valves, as the external power sources were also to be avoided. Additionally, normally closed valves were required, as their main function in the system is to stop the fluids. Several groups have developed on-chip valves for life-science applications as well as other applications [50]. Zhang et al. (2007) [51] gave an excellent overview of the microvalves used in PCR, whereas Au et al. (2011) [52] reviewed different valves for different uses, such as cell seeding, culture media recirculation, protein separation, cell sorting, RNA amplification, protein crystallization screening, PCR and digital PCR, etc.

Hagmeyer et al. (2014) [43] developed a capillary stop valve, supported by numerical simulations, for a bubble free filling of channels in a microfluidic chip. As all capillary valves, it is based on an abrupt change of geometry of the cross-section of the channels. This abrupt change leads to the pinning of the meniscus of the fluid at the channel walls, causing the flow to stop. If the burst pressure is surpassed, the flow will continue as the valve is overcome. Based on this structure, the blocking valve was developed, as this has a very simple structure and its activation can be integrated with the rest of the system.

4.2.2. Requirements

Several aspects must be considered by choosing the optimal valve for a system. First, the valve initial state is a basic issue to define before selecting a valve. Moreover, the power consumption as well as the actuation source and the maximal pressure to be withdrawn must match the requirements of the system. Specially in life-science applications, the volumes are minimal, and the contamination problems are crucial; therefore, the defined dead volume, contamination resistance, and reusability of a valve are extremely important [53].

As the aim of the AIMD is to parallelize at least four different molecular cloning processes, the total number of required valves is considerably high. For the L-Module, at least four valves are needed at the end of the reaction zone. Furthermore, considering the best-case scenario where only one valve would be required for dosing each reagent, the minimum number of valves for the L-Module would be 8. For the T-Module, the situation is similar. Although the involved reagents are less, namely the LM and the competent bacteria, the heat shock stands in need of stopping the flow as well. In this case, more than 8 valves would be also needed. These numbers are only the optimal number, but as

[4] Christian Bürkert GmbH & Co. KG

explained in Chapter 4.3.2 more than one valve is needed for dosing, and for other functions, such as the distribution (see Chapter 4.4.1), even more valves must be employed.

In this case, the valve size is crucial. It must enable the arrangement of all valves without considerably enlarging the entire system. The valve size goes hand in hand with the potential integration of all valves as well as its form or geometry. Another important issue is the rinsing capability. On one hand, presuming an external use, the valves must have an excellent rinsing capability, as the risk for cross contamination is extremely high, and disposing them after each application is not even considerable. On the other hand, integrated valves with parts difficult to rinse or with a complex fabrication process are unsuitable. Furthermore, considering the number of valves needed, expensive external valves are not feasible, as the costs of the system rise exceedingly. Finally, since the valves are primarily used to stop the flow, normally closed valves must be implemented.

4.2.3. Concept and Design

Standard valves have several drawbacks (see Chapter 4.2.1) that difficult to overcome. Therefore, integrated valves were considered. In the framework of this work, different valves were developed to find the one that best fulfills the requirements. The first valve developed was based on phase change as the working principle [120], and the other one was based on capillary forces [121]. Nevertheless, as acceptable as both ideas were, the fabrication and actuation were complex.

The best option was, however, to *keep it simple*. Therefore, a blocking valve also based on capillary forces, but with a much simpler design, was developed. This valve uses abrupt changes of the channel cross-section to control the flow. As explained in Chapter 2.2.1, the meniscus at the liquid-solid-gas interface influences the capillary pressure that sets in motion the liquid in a microchannel. By changing the dimension of cross-section of the channel, the meniscus varies, and thus the capillary pressure, causing the liquid to slow down or even stop completely.

The blocking valve was developed contemplating its fitting at different points of the device. Therefore, as the channels width vary between 0.4 mm and 0.8 mm, two different valves with different dimensions, but the same principle, were developed. To be able to stop the flow on a surface with a contact angle θ>90°, as is the case of PDMS, the cross-section channel must be narrower. However, for other materials with hydrophilic surfaces (θ<90°), such as PC and PET, the channel must be wider. As a further goal of this work is to switch from PDMS to materials more suitable for mass production (see Chapter 6), the valve was developed considering both types of surfaces. The channel was at first narrowed, and then widened again. Hence, in PDMS, the fluid stops at the narrowing channel, whereas in a hydrophilic surface, the fluid lows slightly further and stops at the widening.

The channels before and after the valves either remained with the original dimension from 0.8 mm to 0.8 mm; changed to a narrower channel, from 0.8 mm to 0.4 mm; or to a wider channel, from 0.4 mm to 0.8 mm. The last two being the same but flipped 180°. In Figure 4.12 both blocking valves with their respective dimensions are displayed.

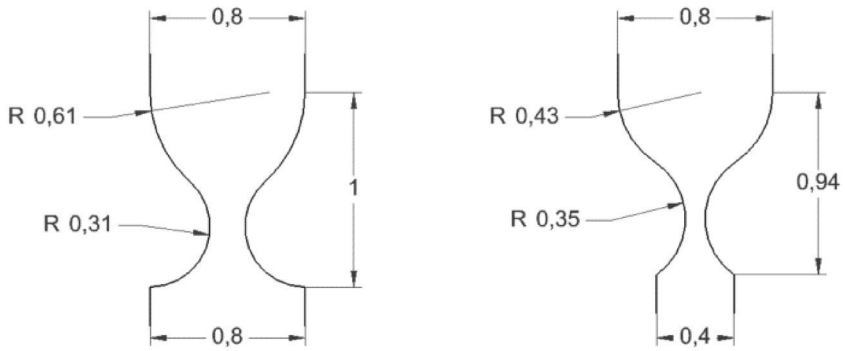

Figure 4.12. Dimensions of the two blocking valves. Left: Valve at the end of a 0.8 mm-wide channel connecting a channel with the same dimensions. Right: Vale at the end of a 0.8 mm channel connecting a channel with 0.4 mm in width.

Developing a valve by itself was not the aim of this work, thus, the functionality of the valve was not tested independently, but together with the dosing and the distribution system. It was modified and adapted until the optimal results, by dosing as well as by distribution, were achieved.

4.3. Dosing system

For a complete automation of the process, all reagents must be extracted from their container and then metered without any user participation. Therefore, in this work, a dosing system consisting of two parts, namely extracting and dosing, was developed with the support of a student thesis [122]. In this chapter, the widespread systems for extracting and dosing fluids are briefly elucidated. Subsequently, the dosing system is described, whereby existing principles or available technology on which the system is based as well as their design is introduced. Lastly, the characterizations results are presented.

4.3.1. State of the art: Dosing in microfluidics

The most widespread solution for automated dosing in microscale is the use of pipetting robots. Nowadays, these robots can exactly dose on a microliter-, or even nanoliter-scale. Nevertheless, these systems are cumbersome, expensive, and not suited for miniaturization. Therefore, other options are being researched. Tsai et al. (2007) [123] summarized different systems used for dosing for drug delivery systems; however, most of them are based on complex micropumps. The non-contact dispensing platform, described in Haeberle et al. (2007) [124], is an interesting solution. It delivers the liquid, in a milliliter-down to picoliter-scale, as free flying droplets on any planar target. A single unit of the dispensing platform consists of a reservoir for the liquid to be dispensed, a nozzle chamber with its respective nozzle to dispense the liquid, and a capillary chamber, which connects the reservoir with the chamber. By placing several units together, the platform allows the dispensing of an extremely high number of reagents. The three different actuation

principles of the platform rely on pneumatic pressure or a piezo actuator. Although these solutions deliver promising results, their structure is still slightly complex. Furthermore, the substance must be in the specific reservoirs, i.e. the reagents must be transferred from the original package.

Trying to simplify the system, the aim was then to dose the reagents directly from the delivered package. In most cases, this is the Eppi. The idea of pumping out the liquid from the Eppi arose and some existent technologies were found. Everflow® offers an adapter for the Eppis which enables the use of these as reservoirs and is commercially available. This adapter functions as a cover for the tube as well as a pumping unit. A pressure source is connected to the adapter, as the pressure inside the tube increases, the liquid flows through the tubing out of the Eppi. The adapter is very robust, infinitely reusable, as it is autoclavable, and can be easily installed. In Figure 4.13 the principle of the adapter is illustrated as well as a 3D-model [125].

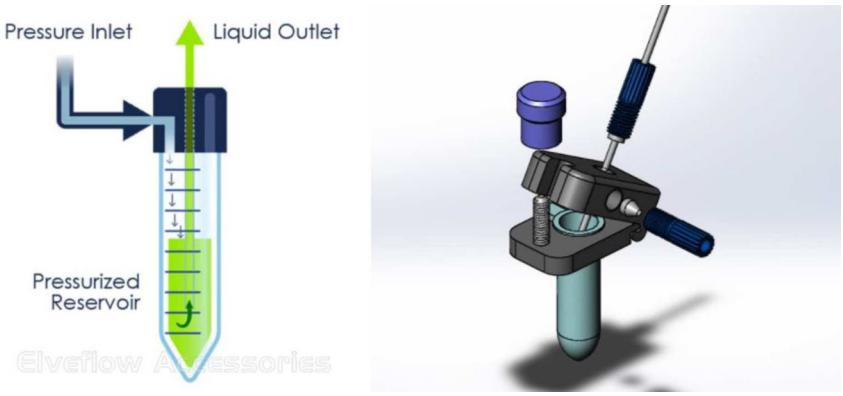

Figure 4.13. Left: Principle of adapter from Everflow® to use Eppis as reservoirs. Right: 3D-model. [125]

4.3.2. Concept

Eppis are the starting point for the dosing, as most of the biological substances are stored in this type of containers. Therefore, the fluids must be directly extracted from these. The simplest method to extract the liquid from the Eppis, without contamination, is the following: by pumping air into the Eppi through a small tube, the pressure increases, obliging the liquid to exit the Eppi through another small tube (Figure 4.14 (left)). This principle was previously commercialized by Everflow® (see Chapter 4.3.1). A cover based on this principle was designed and fabricated. For this purpose, a Luer-Lock tip cap was attached to the cover with screw threads of an Eppis. Two holes were drilled on the cap (Figure 4.14 (right)): i) for a light green Luer-Lock dispense tip with a 0.69 mm inner diameter and a 1.09 mm outer diameter for pumping air with a micropump inside the Eppi; ii) for a flexible tube with dispense needles attached to each of its end; one end should be at the bottom of the Eppi, whereas the other is to be connected with an inlet. Only one micropump is required for this system and it is only in contact with air, eliminating all contamination problems.

Once the liquid was pumped out of the Eppi, it must be exactly metered for a precise process. For this purpose, the principle of the CE microfluidic chip described by Guber et

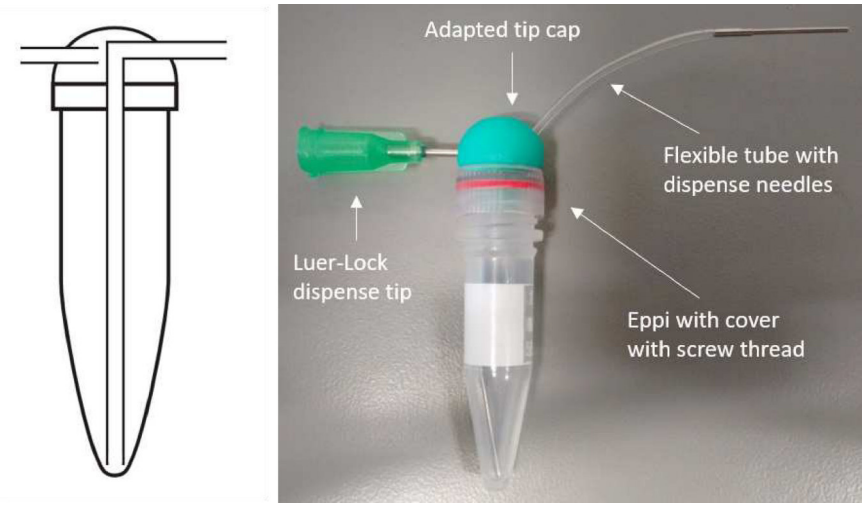

Figure 4.14. Concept and implementation of the dosing system to extract the fluid from the Eppendorf tube. Left: Principle of the extraction. Air is pumped through the left. As the pressure increases inside the Eppi, the fluid is pumped through the open at the top. Right: Adapted cap to implement the extraction of the liquid. The dispense tip to the left is connected to a micropump to pump the air in the Eppi. The flexible tube with dispense needles attached to each of its ends is responsible for pumping out the fluids.

al. (2004) [126] was employed. In this case, a long microchannel with a displaced perpendicular channel (Figure 4.15 (left)) formed two intersections. The distance between both intersections defined the sample volume to be used in the analysis (Figure 4.15 (right)).

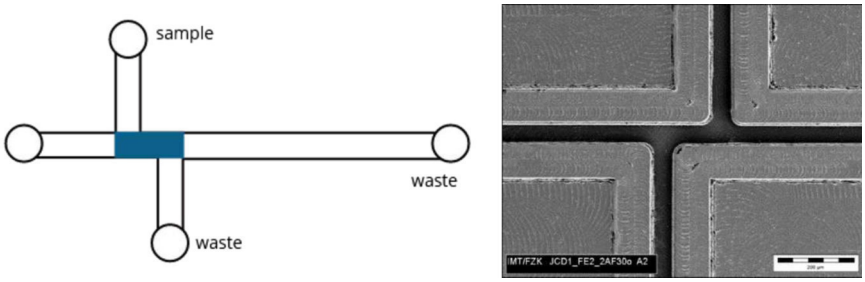

Figure 4.15. CE microfluidic chip. Left: Schematically representation of the microfluidic chip. The section shown in blue represents the sample volume to be used in the analysis. Right: SEM image of the intersection [126].

The first idea for the dosing system was a structure similar to the CE microfluidic chip, i.e. a channel with two different perpendicular channels, as illustrated in Figure 4.16. The dosing volume V_D is determined by the distance L between channel 2 and 3, as the cross-section of the channel does not vary. Therefore,

$$V_D = hwL \tag{4.4}$$

with h as the channel height and w the channel width. Before dosing, channels 1 and 4 are closed with an external valve. The liquid flows through channel 2 into the dosing section (a) and then into channel 3 (b). Subsequently, channels 2 and 3 are closed also externally and air is pumped into channel 1, causing the exact volume between both

channel 2 and 3 to flow (c). Finally, the fluid flows out of the dosing system into the next structure (d).

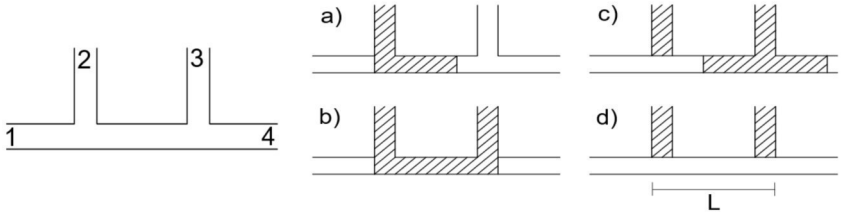

Figure 4.16. First idea for the dosing system: (a-b) As channels 1 and 4 are closed, the liquid flows into channel 2 and then 3. (c) Channels 2 and 3 are closed and air is pumped into channel 1, causing the volume in the dosing section to flow. (d) Dosing section is empty after the liquid flows out of the dosing system.

This principle showed promising results; however, it consisted of several valves, hindering the integration not only of more than one dosing system, but with other required microfluidic components. To overcome this drawback, channel 3 and the valve at the end of channel 4 were replaced with a blocking valve integrated to the channels. The basic principle of this valve is explained in Chapter 4.2. Furthermore, another blocking valve was placed at the beginning of the cross channel to avoid the fluid flowing into it. This will be clarified later as the working principle is explained. The new design is shown in Figure 4.17, marked as L is the dosing section. The dosing volume can be calculated from Equation 4.4.

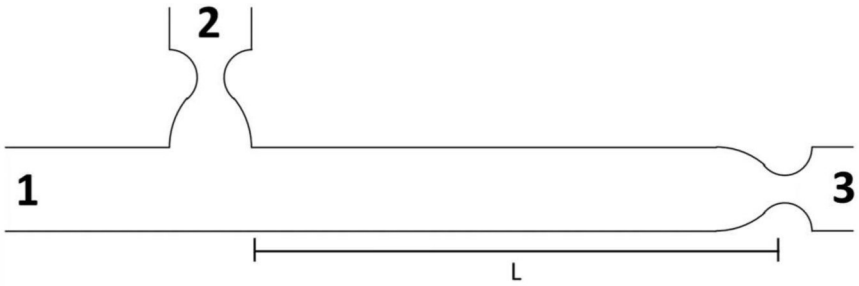

Figure 4.17. Dosing system with blocking valves at the beginning of the cross channel and at the end of the principal channel.

The dosing process, tested with blue-colored distilled water as reagent for a better representation, is illustrated in Figure 4.18. The fluid is pumped in the principal channel (1). The cross channel is not filled because the blocking valve, as the name suggests, blocks the flow, forcing the liquid to remain in the principal channel (2). The blocking valve was placed as near as possible to the principal channel to minimize the flow going in that direction. Once the dosing section is completely filled, the pumping of the reagent stops, and air starts being pumped through channel 2 (3). Through this pumping, the liquid in the principal channel that is not part of the dosing section is pumped back to the Eppi. As consequence of the pressure increasing in the Eppi and in the channel, the blocking valve is overpowered, and the liquid can flow to the rest of the channel (4).

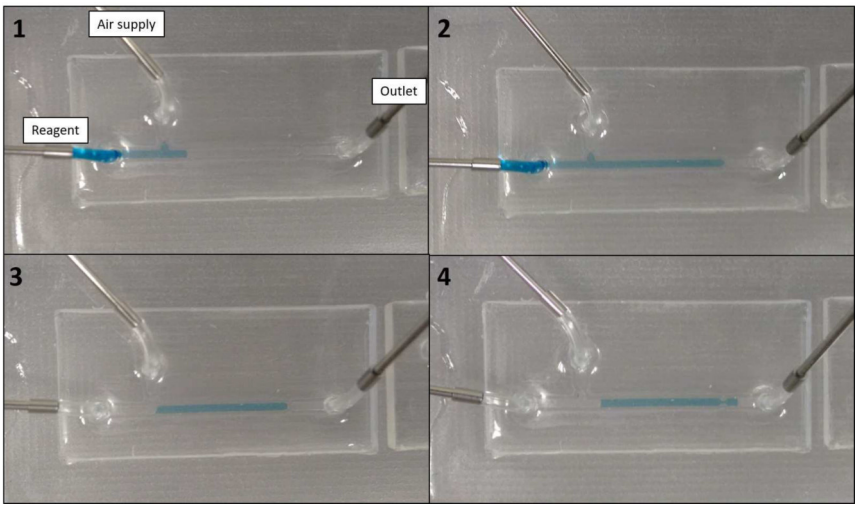

Figure 4.18. Dosing progress tested with blue-colored distilled water. (1) Fluid is pumped in the principal channel. (2) The cross channel does not fill up as a result of the blocking valve at the beginning of it. (3) The pumping of the fluid stops as the air supply is opened. Air begins to enter the cross channel. (4) The rest of the fluid that is not in the dosing section is forced back to the Eppi. Due to the increased pressure in the Eppi and in the channel, the blocking valve is overpowered, and the fluid can flow to the rest of the channel.

4.3.3. Design

For the L-Module, vector, ligase, DNA, and buffer must be extracted and dosed to the channels, whereas for the T-Module, competent cells and culture medium must be withdrawn and metered for its further use. The volumes to be dosed vary from 1 µl up to 32 µl. Therefore, dosing units for the smallest volumes, as these are the most crucial, were designed and developed independently, and then integrated with the rest of the AIMD. The larger dosing units were integrated directly to the modules because the basic principle and functionality had been tested.

Three dosing units for 1 µl, 2 µl, and 4 µl were developed with a channel height of 200 µm and a channel width of 800 µm. Evidently, the dosing section differ from each other. Due to space issues, only the 1 µl dosing unit was designed with a linear dosing section; the rest have a meandering shape. They were designed taking into consideration a dosing area $A_D = hL$, varying only the dosing length L. In Figure 4.19 the designs and dimensions of the 1 µl, 2 µl, and 4 µl are shown, the dosing areas are pictured in turquoise. The dosing areas corresponding to the dosing volumes can be found in Table 4.6.

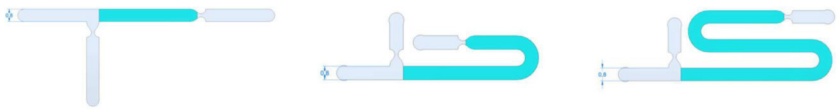

Figure 4.19. Design and dimensions of the dosing units for 1 µl, 2 µl, and 4 µl, from left to right.

Dosing unit	Dosing area [mm^2]	Dosing volume [µl]
1 µl	5.12	1.02
2 µl	10	2
4 µl	20.07	4.01

Table 4.6. Dosing units, 1 µl, 2 µl, and 4 µl, with their corresponding dosing areas and volumes.

4.3.4. Characterization

The fabrication of the dosing units was analogous to the fabrication of the rest of the components and the AIMD (see Chapter 3.5). The functionality of the dosing units was tested together with the extracting system described before. The test setup consists of the micropump mp6[5] to pump air into the Eppi as well as in the cross channel to push the liquid out of the dosing unit. To switch between *extracting* mode and *pumping out* mode, a 3/2-way directional, solenoid control valve[6] was used. The pneumatic circuit diagram of the test set up is illustrated in Figure 4.20.

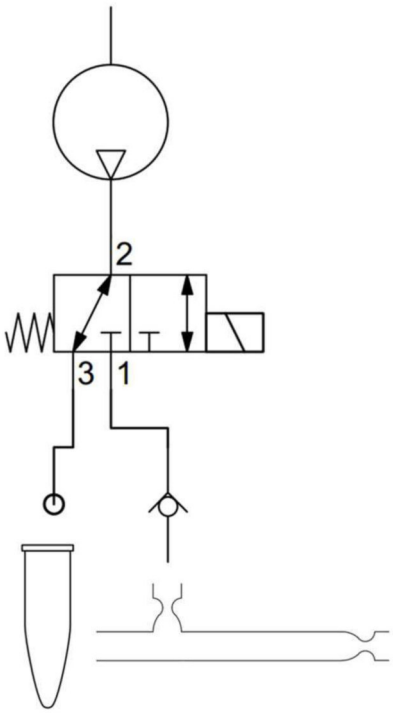

Figure 4.20. Pneumatic circuit diagram of the test setup for the dosing unit. The micropump is connected to a 3/2-way directional valve. One connection goes to the Eppi, whereas the other to the cross channel of the dosing unit.

An Eppi was filled with distilled water to act as the volume to be extracted and metered. The volume dosed V_t was determined by an analytical balance[7] with 0.1 mg resolution:

[5]Bartels Mikrotechnik
[6]Christian Bürkert GmbH & Co. KG - Type 6604T06
[7]Sartorius AG - Type 1801

$$V_t = \frac{m_a - m_b}{\rho} \tag{4.5}$$

The test procedure was as follows: the empty dosing unit was weighted with the precision scale (m_b). Then the dosing unit was connected to the valve ports, and the micropump was switched on, controlled with 50 Hz and 200 V, until the dosing section was filled. Once filled, the valve was triggered, and air was pumped into the dosing unit until the extra volume was returned to the Eppi, but the dosed volume was still on the channel (Figure 4.18 (3)). The dosing unit was then disengaged from the test setup and measured with the precision scale once more (m_a). Finally, the dosed volume was calculated using Equation 4.5 with $\rho = \rho_w$. For water applies: 1 µl $\widehat{=}$ 0.001 g.

Four dosing units of each type, i.e. 4x1 µl, 4x2 µl, and 4x4 µl, were fabricated. Each dosing unit was measured twice. The mean dosing volume of the 1 µl dosing unit is 1.0913 µl with a Mean Average Deviation (MAD) of 0.0988 µl. The 2 µl showed also great accuracy as well as great precision as the mean dosing volume was 2.0188 µl with a MAD = 0.0734 µl. The last dosing unit was the one for 4 µl. With a mean volume of 4.01 µl (MAD = 0.05 µl), this dosing unit proved also to be exact and precise. Hence, with these results, it was determined that the dosing units and the extracting system function accurately when dosing water. An overview of the results can be found in Table 4.7.

Dosing unit	**1 µl**		**2 µl**		**4 µl**		**2 µl G**	
Measurement	**1**	**2**	**1**	**2**	**1**	**2**	**1**	**2**
Dosing volume [ul]	1.32	0.90	2.13	1.96	4.09	3.93	1.9622	1.9799
	1.12	1.04	1.96	2.14	4.03	4.06	1.9622	1.9089
	1.11	1.05	2.08	1.93	3.98	4.06	2.0154	2.0421
	0.98	1.21	1.94	2.01	3.99	3.94	1.9089	1.9811
mean	1.0913		2.0188		4.01		1.9588	
MAD	0.0988		0.0734		0.05		0.0419	

Table 4.7. Overview of the dosing results for 1 µl, 2 µl, and 4 µl dosing units. The experiments were performed with water (first three columns) and a water/glycerin 50% (w/w) solution (last column: 2 µl G). The dosing volume for each dosing unit with the corresponding mean and mean absolute deviation are summarized.

As mentioned before, the ligase solution for ligation is normally 49.2% glycerin and 50% water. As the viscosity of this solution is slightly different to water, the same series of tests were performed, but with a water:glycerin 50% (w/w) solution. The micropump was also with 50 Hz and 200 V controlled. It was observed that this solution flowed slower than water; however, the difference was negligible. In this case, only the 2 µl dosing unit was tested as this is the ligase volume needed in further applications. Analogous to the water tests, Equation 4.5 was used with $\rho = \rho_g$ = 1.12630 g/ml at 20 °C, i.e. 1 µl $\widehat{=}$ 0.00112630 g. The results show a mean dosing volume of 1.9588 µl and a MAD of 0.0419 µl, also included in Table 4.7 (2 µl G).

The competent bacteria must be also extracted from an Eppi. Therefore, it was also tested if the extracting system was able to work with bacteria. As the competent bacteria

is expensive, the tests were performed with *E. coli* OP50. The bacteria were grown first in agar plates. Then, the following protocol for inoculating an overnight culture of liquid LB with bacteria was followed:

5 ml liquid LB were added to a test tube. Then, a colony was picked from the agar plate using a sterile pipette tip and the tip was dropped into the liquid. The tube was covered with a sterile aluminum foil and incubated at 37 °C for 24 h. The growth was checked as the fluid turns turbid.

To approach the flow conditions of the competent bacteria as much as possible, a solution with a similar cell density, i.e. ratio of cell number per volume unit, as the competent cells was striven. The cell density is normally measured optically with a photometer. The light transmitted through a sample is measured. A higher cell density causes an increased turbidity of the sample, which, in turn, causes the light beam to scatter more. Hence, the optical density (OD) is proportional to cell concentration [127]. Normally, the OD of competent bacteria varies between 0.4 and 0.9 (OD_{600}[8]) [128, 129].

Therefore, the OD of the broth was measured at the ITG. For the measurement, 100 µl of the bacteria was added to 900 µl liquid LB. The measured OD was 0.83 (0.083 x 10, considering a 10x dilution factor). As the OD was in the same range as the competent cells, it was used for further tests.

The bacteria flowed out of the Eppi practically as water, without a significant difference. The dosing system was not tested because calculating the density of the bacteria solution was not accurate enough to perform the same tests as with water and the water/glycerin solution. However, based on the flow conditions, it can be assumed that an exact metering of the bacteria can be achieved.

After the tests, it was determined that for all test fluids, namely water, water:glycerin solution, and bacteria, the extracting system and the dosing units work accurately and deliver excellent results. The main problem identified was at the fabrication of the mold and not with the dosing principle itself.

4.4. Distribution system

A mechanism to control the reagents identical in all processes was needed to fully automate the simultaneous run of various processes. There were two options to control these: 1) to dose the reagents for each process individually; 2) to dose the reagents for all the processes at once and then distribute them on-chip.

Treating each process individually meant having a dosing unit for each reagent multiplied by the number of processes to parallelize. In addition, the number of containers off-chip was evidently higher. Therefore, it was not suitable due to space problems not only on-chip, but also off-chip. Distributing the reagents on-chip was a more feasible solution.

In this section, the concept and design of the distribution system, as well as its characterization, is presented.

[8] optical density at 600 nm

4.4.1. Concept and Design

The simplest solution to distribute fluids on-chip is a channel with a T-junction. Presuming identical channels and flow conditions, the volume would be distributed equally after the T-junction. However, in practice this is not the case due to minimal fabrication flaws. Although these flaws can be ignored for the normal flow, for distributing identical volumes even the slightest defect in the channels produce an uneven distribution.

A distribution system based on a T-junction with some modification and different levels was developed. The two main characteristic of this system are the use of the blocking valves and a T-junction with *delay* function. This system can be seen in Figure 4.21. In this case, the test system consists of three distribution levels: Level 1 marked in red, Level 2 in green and Level 3 in orange. The blocking valve was implemented at the end of the channels of each distribution level to overcome the drawback originated by the imperfect channels. By blocking the flow after each channel, the flow is forced to go into an empty channel of the same level, as the resistance is lower. After the entire level is filled, the blocking valves are overcome, and the next channels begin to fill, enabling an even distribution of the volume.

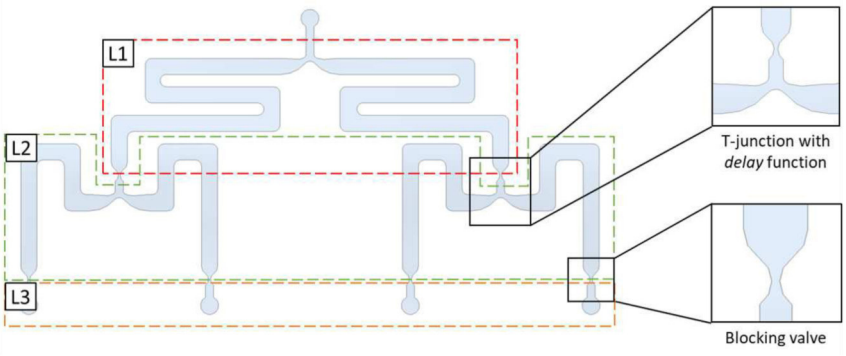

Figure 4.21. Test distribution system with blocking valves and T-junctions with delay functions. This test system consists of three distribution levels: Level 1 marked in red, Level 2 in green and Level 3 in orange. The blocking valves are located at the end of each channel, whereas the T-junctions with delay function are at the beginning of a new distribution level.

Furthermore, to have a better control of the flow, the normal T-junction was replaced with a structure to delay the flow. This is based on the trigger valve developed by Hagmeyer et al. (2014) [43]. However, it was not used to unite flows, but to separate them. By stopping the flow directly at the T-junction, the fluid flows into one channel without even starting to fill the other one. The direction selected by the flow, whether left or right, is random and depends principally on the minimal fabrication flaws. Hence, this cannot be controlled. However, this structure ensures an orderly distribution of the flow, i.e. other channels are not filled at all before the others are filled completely. Figure 4.22 illustrates the unwanted flow avoided by delaying the filling of the channels. The T-junctions with delay function are located at the beginning of each new distribution level (Figure 4.21).

In Figure 4.23 a distribution procedure is shown for a better understanding. After the T-junction, one random channel begins to fill. As expected, it is filled first, whereas the other one remains empty (1). When the fluid arrives at the blocking valve, it stops there (2), and

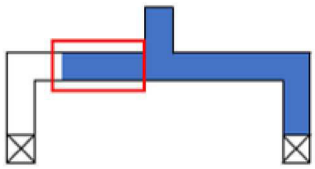

Figure 4.22. Unwanted flow by distributing the fluid shown in schematic form.

the other channel begins to fill (3). Then, as both channels are filled, the blocking pressure is overcome, and the fluid begins to flow into the next distribution level. On this level, the same course of action takes place. One channel of one of both sides is filled first (4), as it is filled completely, the fluid starts flowing in the next one (5). When both channels are filled, the other side begins to fill (6). This can continue until the last levels in the distribution system.

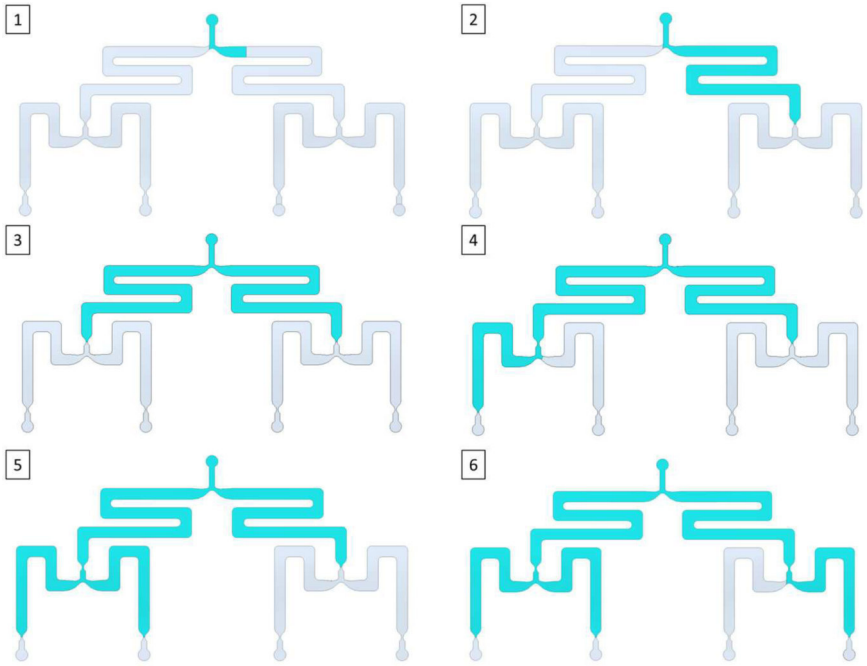

Figure 4.23. Distribution procedure in a test system. (1) One channel begins to fill randomly as the other remains empty. (2) At the blocking valve, the fluid stops, and (3) the other channel begins to fill. (4) Then, as both channels are filled, the blocking pressure is overcome, and the fluid begins to flow into one channel of the next distribution level. (5) As it is filled completely, the fluid starts flowing in the next one. (6) When both channels are filled, the other side begins to fill.

4.4.2. Characterization

This system was fabricated as the rest of the AIMD. For more details see Chapter 3.5. Before casting the PDMS parts, the mold was inspected optically to ensure all structures

were fabricated correctly and rule out any source of error related to the mold fabrication. Figure 4.24 shows the negative structure of a T-junction with delay valve in PMMA.

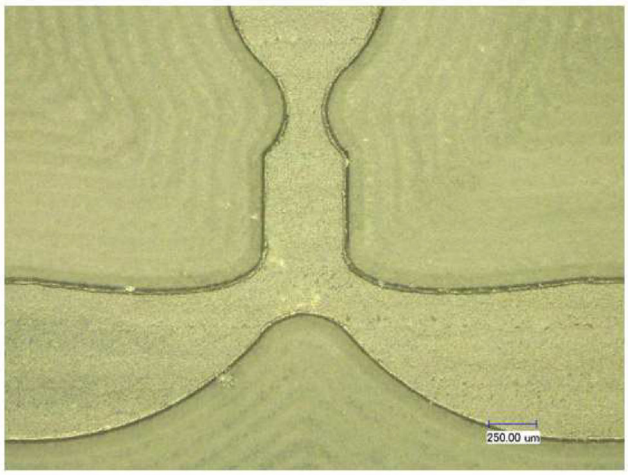

Figure 4.24. Negative structure of a T-junction with delay valve in PMMA

.

To test the functionality of the distribution system, distilled water colored in blue was used. It was pumped out of an Eppi with the extracting system described in Chapter 4.3. The parameter for the micropump were the same used for testing the dosing, namely, 50 Hz and 200 V. The tests showed an adequate distribution of the liquid within the channels. The channels of each distribution level were filled one at a time before starting with the next level. Some of the steps of this test are shown in Figure 4.25.

To ensure the functionality of the distribution system in the entire AIMD, the same test was performed with a solution of water/glycerin 50% (w/w) and bacteria. Bacteria with the same cultivation procedure as for the dosing tests were used (see Chapter 4.3.4). Using the same parameters of the micropump, the water/glycerin solution flowed slower, but correctly, and no significant difference was noted between the results with water and those with bacteria solution. Hence, the distribution system was used in the further development of the AIMD.

Compared with the results of the dosing system, it was determined that the fabrication influences strongly the success of the system. If there are defects in e.g. a blocking valve, the flow does not stop and, thus, the rest of the channels do not fill. Therefore, it is crucial to inspect thoroughly the mold before fabricating PDMS parts.

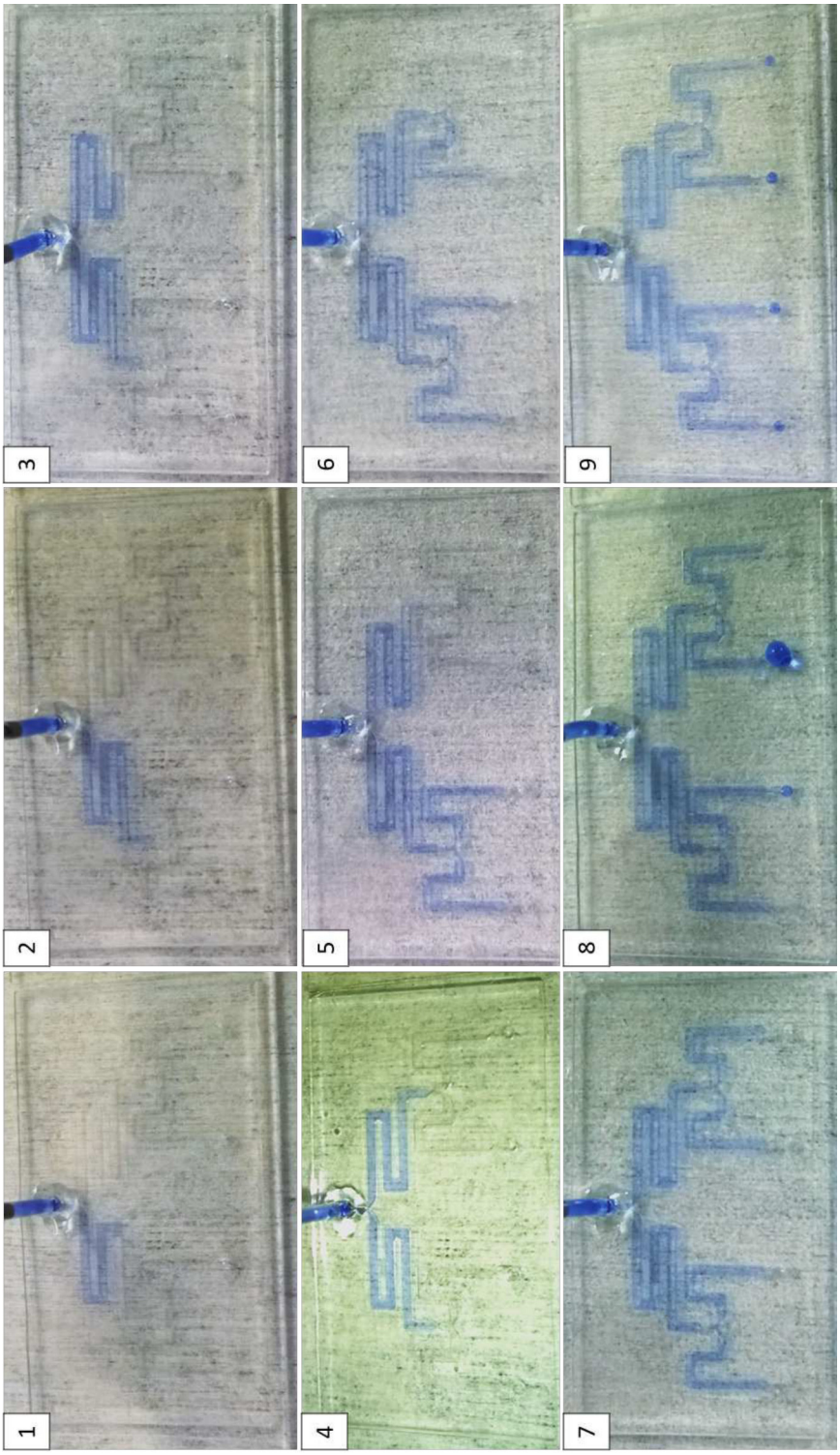

Figure 4.25. Distribution test with distilled water colored in blue. Using the extracting system, the water was pumped into the channel with the micropump parameters: 50 Hz and 200 V. The channels of each distribution level were filled one at a time before starting with the next level.

4.5. Heating and Cooling System

A fundamental function of the AIMD is its ability to expose the bacteria to a heat shock. Therefore, a heating as well as cooling system were developed to achieve this. In this section, its development is described. First, the requirements for the system are listed, followed by an overview of the existing technology used for heating and cooling. Afterwards, its concept and design are introduced. Finally, the characterization results are shown.

4.5.1. Requirements

Briefly, in a standard transformation procedure, the LM is added to competent bacteria in an Eppi and incubated for a certain period. Afterwards, the Eppi is exposed to a high temperature, normally 42 °C, for 45-90 s. Then, it is placed on ice for about 2 minutes before continuing to the next step. For a more detailed explanation see Chapter 2.1.1.3. The transformation protocol used in this work is the same used at the ITG: 42 °C for 45 s and then, 2 minutes at ~0 °C. Therefore, the heating and cooling mechanisms must fulfill the following requirements in order to successfully transform bacteria on-chip:

- First and foremost, the device must be able to heat the fluid inside the channel up to 42 °C at least as fast as the procedure done manually, and then cool it down to ~0 °C.
- The microfluidic channels must be designed for 16 µl. The competent cells are extremely fragile during and after the heat shock; therefore, the design must be simple to avoid forcing the bacteria flow into complex structures.
- The temperature as well as the time for the heating and the cooling must be flexible.
- The heating and cooling mechanisms, and any component not in contact with biological substances, must be reusable.

4.5.2. State of the art: Heating and Cooling in microfluidics

There are several methods for heating and cooling in microfluidic devices. Using a Joule heating resistor is the most common use for increasing the temperature of a system. Generally, a heating resistor made of gold or platinum is deposited or sputtered on a plane surface [17, 76, 130]. Other groups have used external heaters such as hot plates, thermal stages or TEC [18, 19, 25, 27, 53]. Some groups have also implemented non-contact heating methods such as infrared irradiation [53].

There are also different methods for decreasing the temperature within a microfluidic device. Some groups use TEC as they are extremely fast and simple to control; however, their major drawback is their need for a proper heat dissipation mechanism [131]. Other mechanisms consist on placing cooling channels between the fluidic channels. Through the cooling channels water or compressed air is pumped in order to decrease the temperature of the fluidic channels [24, 132, 133]. These last mechanisms, however, need external air or water pumps, making the systems more complex.

4.5.3. Design

In this work, two different concepts for heating and two for cooling were considered. One for each process was selected. The development of the microchannels and the heating and cooling mechanisms was an iterative process. The three involved parts were designed simultaneously and were changed and adapted depending on the test results.

4.5.3.1. Microchannels

As mentioned before, the microchannels must have a relatively simple design to protect the competent bacteria before and after the heat shock. To improve the heat transfer, greater surfaces are preferred, e.g. an elliptical, shallow chamber. However, for the microfluidics, this option is not the best, as it has several drawbacks. Firstly, closing larger chamber is difficult due to the large area without support required as a lid. Additionally, it is to be expected that a greater air bubble problem occurs as the liquid can flow from inlet to outlet without covering the entire chamber. Hence, to maintain a relatively high contact area for the heat transfer, a design with meandering channels was chosen for both heating and cooling. The channels for both processes are 0.4 mm wide and 0.32 mm deep. The thickness of both the cover and the bottom of the device is 0.4 mm to obtain a symmetrical heat transfer. In Figure 4.26 the microchannels for testing with their respective dimensions are shown. The length of the heating channels was set to contain 16 µl, whereas the ones for cooling were designed slightly longer. Moreover, the cooling zone was designed narrower to better fit the TEC (see Chapter 5.3.2).

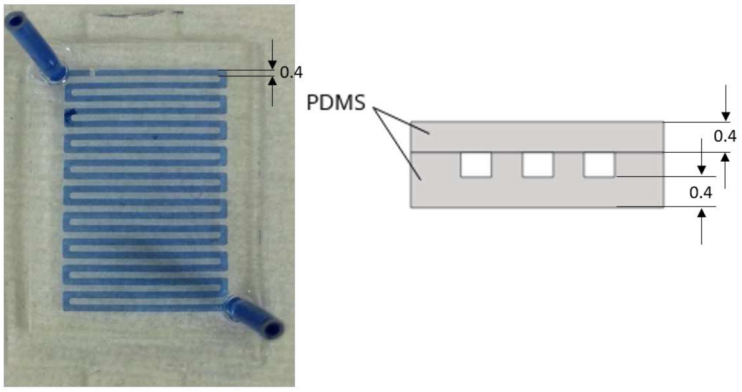

Figure 4.26. Microchannels for testing the heating and cooling mechanisms. Left: PDMS channels for cooling filled with blue distilled water for a better visualization. Right: Sketch of the channels. For a symmetrical heat transfer, the cover as well as the bottom of the channels are 0.4 mm thick.

4.5.3.2. Heating and Cooling

Microheater

The first proposal for heating was to use a gold Joule heating resistor. This is a standard solution, well widespread in the MEMS technology. The main idea was to sputter a gold microheater on a glass slide and bond it to the bottom of the PDMS device. The

microheater had the same meandering structure and dimensions as the channels. Gold was selected because its electrical conductivity and its simple fabrication. As gold has poor adhesion to glass, a titanium layer, ~10 nm-thick was first sputtered, then the ~150 nm-thick gold layer was sputtered. This method is widely used to improve the adhesion of gold to glass.

Water-heating and -cooling

A proposal for both heating and cooling was to use hot water or cold water to heat and to cool, respectively. From a container, hot water or cold water is pumped into a chamber surrounding the PDMS device. The heat transfer takes place between the channels and the chamber. The water is continuously pumped into the container and recirculating as needed. A schematic representation of this system, exemplified for cooling, can be found in Figure 4.27. This is, on one side, a simple mechanism, as only water is required for the actual heat transfer. However, on the other side, it has several drawbacks. It consists of at least two containers and a pump, which would enlarge the whole system and add complexity to it. Moreover, to obtain hot and cold water, a heating and cooling system must be implemented, otherwise the water temperature at the container would not be stable and cannot be controlled. This mechanism was, thus, discarded.

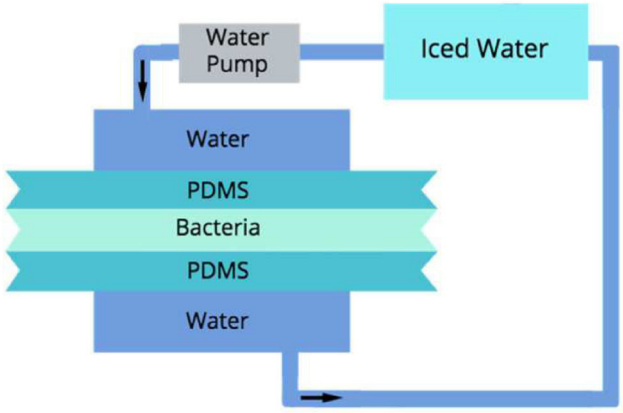

Figure 4.27. Schematic representation of the concept of water cooling. For cooling (or for heating), cold (or hot) water is pumped into a chamber surrounding the PDMS device. Then, it is pumped further to the container. The water circulates through the system as long as needed, whilst the water is kept cold (or hot).

Thermoelectric cooler (TEC) cooling

Another solution for cooling is to use the cold side of a TEC. Its working principle is explained in Chapter 2.3.1. The main idea of this concept is to have at the bottom of a PDMS device the cold side of a TEC. Both surfaces are in direct contact with each other. By applying an electric current, the TEC starts cooling down, i.e. begins absorbing the heat from the surface to which it is in contact, causing it to cool down. This concept is illustrated in Figure 4.28.

Using a TEC has several advantages. First, it can be found in small sizes, suiting well to a microsystem. Additionally, it reaches the desired temperature within seconds, and it can be easily controlled, as it depends on the electric current applied. Presuming a proper dissipation of the heat, temperatures of 0 °C or below can be maintained for extended periods of time. Nonetheless, there are some drawbacks when using a TEC for cooling. The heat absorbed by the cold side of the TEC must be dissipated through the hot side. For this purpose, an adequate dissipation mechanism must be implemented. Normally, heat sinks are placed on the surface of the TEC. However, if the amount of heat to dissipate is greater, more complex systems, such as water-cooling systems or fans, are required.

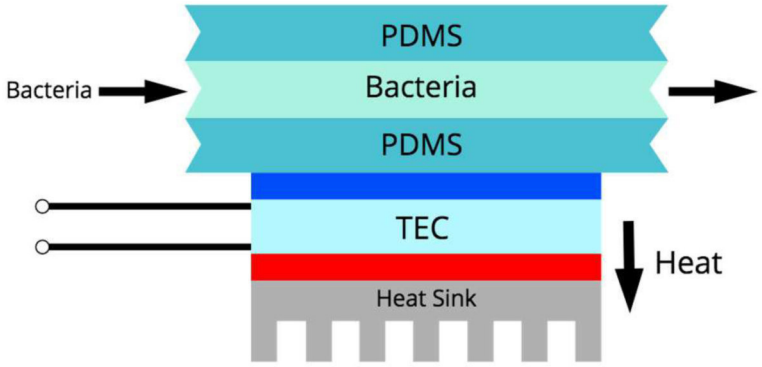

Figure 4.28. Schematic representation of the concept of cooling with a TEC. A heat sink is attached to the hot side of a TEC. Applying an electric current, a desired temperature can be reached during long period of time.

Comparing both presented cooling system with each other and their own advantages and disadvantages, it was clear that the advantages of the TEC outweigh the water-cooling system as well as its own disadvantages. The TEC system is smaller and does not require extra devices. Moreover, the heated or cooled area is determined by the size of the TEC. Finally, the temperature at the surface of the TEC can be accurately controlled. Thus, it was selected as the cooling system for the heat shock.

Thermoelectric cooler (TEC) heating and cooling

As it was established that the cooling was performed by a TEC, the idea of heating with a TEC as well was eagerly studied. The heating process lays chronologically between two cooling stages. To ensure an optimal heat transfer, heating and cooling zones were preferred rather than having a single zone where the heat shock happens. Therefore, the heating unit was physically situated between two cooling units. Although the use of Joule resistors is mostly widespread for heating, using a TEC simplified the design of this specific system.

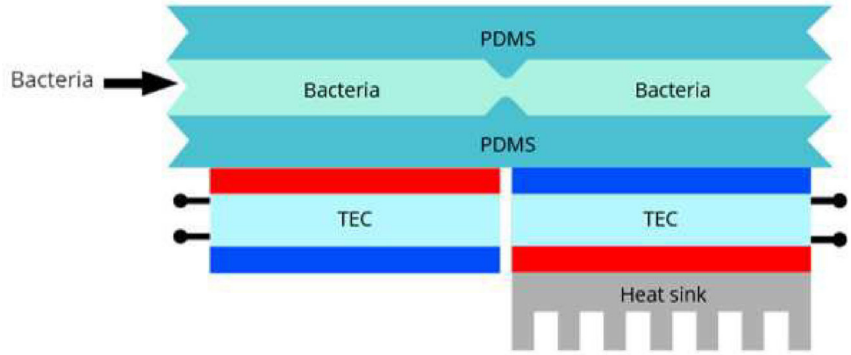

Figure 4.29. Schematic concept of the heating and cooling unit for the heat shock. Both mechanisms work with a TEC.

4.5.4. Characterization

The development of the heat shock mechanism was also an iterative process and was supported by a bachelor thesis [134]. To ensure the compatibility of the heating and the cooling systems, every effort was made to develop them at the same time. Nevertheless, the cooling system was determined first, and the heating system was adapted to it. Different tests were performed to characterize the heat shock system. First, two important tests were performed to provide a basis for the rest: a standard procedure for the transformation and a comparison between the behavior of water and bacteria. With these results, not only the purpose of the system was defined, but it was also determined that water could be used as the substance to test. Afterwards, the heating and cooling performance, as well as the effect on the water, was tested.

4.5.4.1. Standard protocol

The aim of this system is to conduct a heat shock at least as efficient as the standard one. The temperature profile of the liquid inside the Eppi during the heat shock must be known to be able to compare it with the behavior of the liquid inside the PDMS microchannels. Therefore, first, a comparable volume to be used in the T-Module was exposed to a heat shock following the protocol used at the ITG. An Eppi was filled with 15 µl of distilled water and submerged in a 42 °C water bath, after 45 s it was placed on ice. The temperature was logged with a thermocouple type K[9] submerged in the water inside the Eppi. This procedure was done several times.

The mean results of these tests are shown in Figure 4.30. Starting the tests, the water was at ~7 °C, and after 45 s, it reached an average temperature of 41.6 °C (1). The graph is 5 s shifted as the Eppi was placed for heating 5 s after starting the measurement. The Eppi was then put on ice and the temperature dropped to ~0 °C after nearly 70 s (2). 2 minutes after being on ice, an average temperature of -0.06 °C was reached (3). This temperature profile was the aim of the heat shock system.

[9]RS Pro - ANSI Type K Fine Gauge Exposed Welded Tip Thermocouple

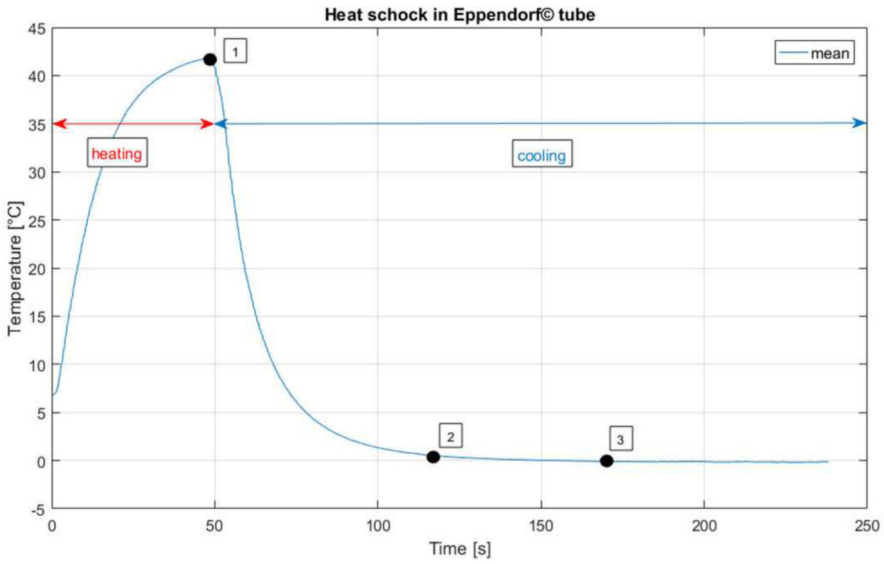

Figure 4.30. Standard protocol: Heat shock with Eppi and distilled water. (1) After the Eppi was in water bad at 42 °C for 45 s, the water reached an average temperature of 41.6 °C (5 s shifted as the Eppi was placed for heating 5 s after starting the measurement). (2) ~0 °C after nearly 70 s being on ice. (3) Average temperature (-0.06 °C) after 2 minutes on ice.

4.5.4.2. Behavior comparison between water and bacteria

The characterization of the heating and cooling systems involved numerous different tests to determine an overall functionality. Using the competent bacteria, or even the *E. coli* EP60, for every test would have been very costly and cumbersome. Therefore, the aim was to test first with water and then with bacteria. In order to relay on the water tests, it was necessary to compare the behavior of water with the bacteria at least in one test. A thermocouple[10] was placed at the end of meandering channels, and the temperature was measured while heating and cooling.

Distilled water was used for the first test. Then, for the test with bacteria, *E. coli* was employed. These were cultured as described in Chapter 4.3.4. The results show a similar temperature profile by heating as well as by cooling for both water and bacteria (Figure 4.31). Therefore, based on these results, the rest of the experiments were performed with distilled water.

[10]RS Pro - IEC PTFE Exposed Welded Tip Thermocouple Type K

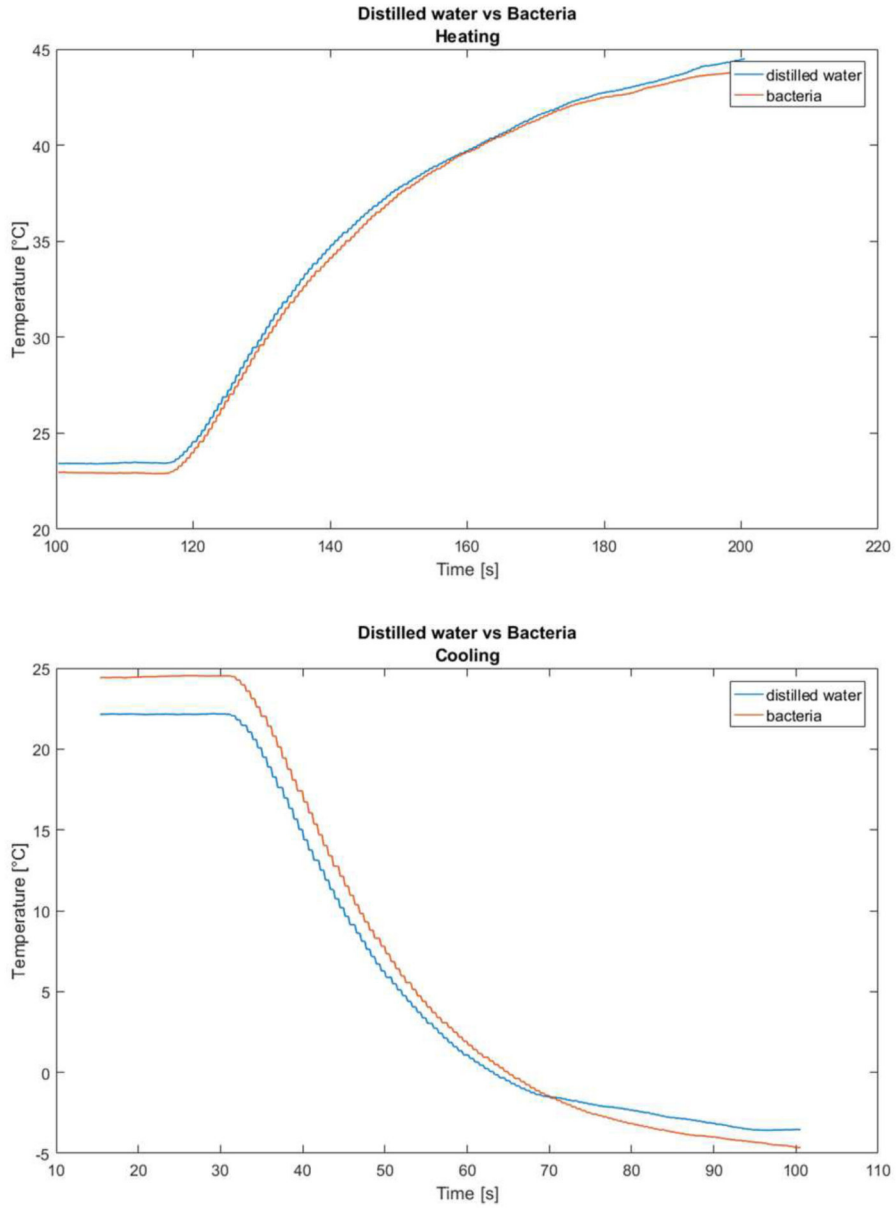

Figure 4.31. Comparison of the temperature profile of water and bacteria. The results show that both fluids behave similarly during both heating and cooling.

4.5.4.3. Heating

The maximal power needed to heat the water inside the microchannels of one process from the initial temperature T_{Hi} = 0 °C to the final temperature T_{Hf} = 42 °C was determined with Equation 2.14:

$$\dot{Q}_{Hmax} = \lambda_{PDMS} A_{HA} \frac{T_{Hf} - T_{Hi}}{d_{PDMS}} =\approx 1.65\ W \tag{4.6}$$

with λ_{PDMS} = 0.15 W/mK, A_{HA} = 104.5 mm^2 as the complete area of the PDMS where the channels are located (not only the channel area), and d_{PDMS} = 0.4 mm as the thickness of the PDMS wall. The actual area of the channel is A_{HCH} = 51 mm^2, thus, even less power, $\dot{Q}_H \approx 0.8$ W is needed.

Hot plate

The first experiments for heating were performed with a hot plate, as the idea of the TEC was yet to be defined. The tests were performed as follows: distilled water was pumped manually into the channels with a syringe. To log the temperature values a thermocouple as the one used for the previous test was placed in the channel, directly after the inlet. The measurements started, followed by the pumping of water 14 s. As can be seen in Figure 4.32, the temperature decreases as the water enters the channel (1). Then, it sinks gradually until the flow stops, i.e. until the channels are completely filled (2). After this point, the temperature of the water starts rising again reaching the initial temperature. This occurs in approximately 30 s. This time is in an acceptable range, if compared with a conventional process.

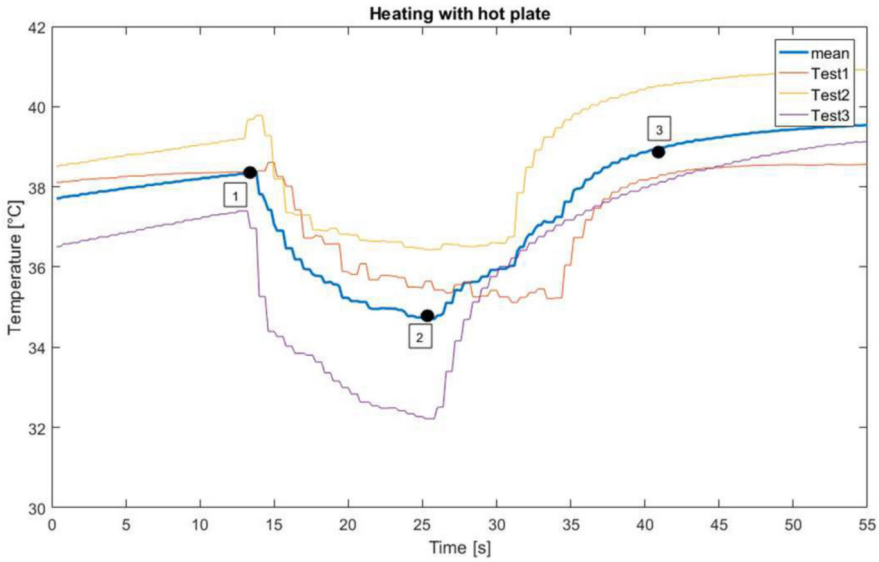

Figure 4.32. Temperature profile of distilled water inside the microchannels, heating with a hot plate. (1) The temperature decreases as the water starts filling the microchannel. (2) The temperature sinks gradually until the flow stops. (3) The temperature of the water starts rising again reaching the initial temperature. The different profiles occur because the Temperature Control System (TCS) was not yet accurate enough.

At this point, the TCS was not yet accurate enough; therefore, the difference between the tests is noticeable. Nonetheless, a proper tendency can be assumed. With these tests, it was concluded that the geometry of the microchannels, and generally the heat transfer inside the device were promising. Therefore, the next step was to test if the hot side of a TEC could be considered for heating.

TEC

For these tests, a commercially available TEC[11] with an active area of 15 x 15 mm and a maximal power of 10.9 W was used (see section A.4). As calculated from Equation 4.6, the required heating power is significantly less than the maximal power delivered by the TEC.

The results of this test are shown in Figure 4.33. Supplying the TEC with 1.3 A and 0.75 V, the desired temperature, 42 °C at the surface of the TEC was reached within ~10 s. The measurement continued for approximately 85 s, a time frame considerably larger than the required one. The temperature was stable, although the TCS was still not accurate. A mean temperature of 42 °C with a standard deviation of 0.4 °C was achieved during this time. The tests were performed using the final TCS described below. These experiments showed that the TEC was a great alternative for heating, as it responds quickly and can be easily controlled. The microheater idea was discarded as its fabrication was more complex as using a TEC.

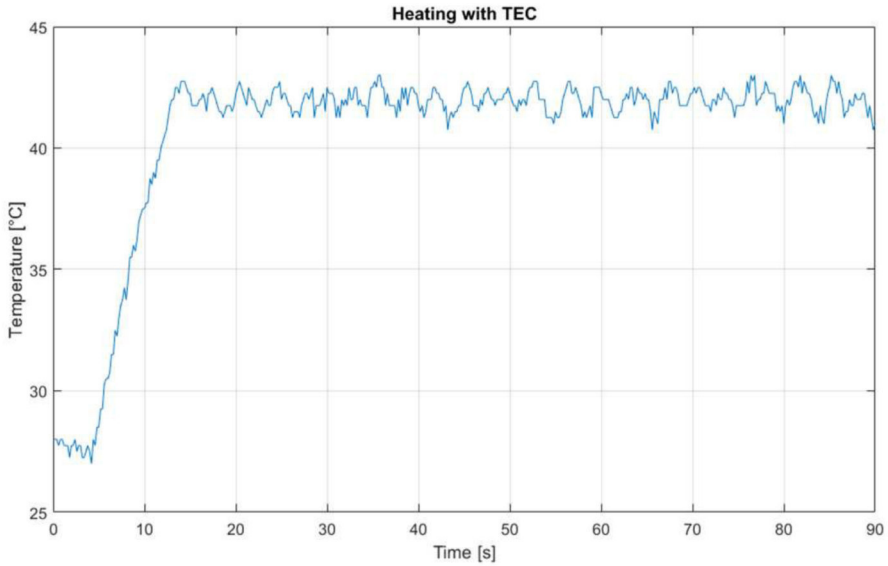

Figure 4.33. Temperature profile of the TEC hot side. The desired temperature, namely 42 °C is reached within ~10 s. The temperature remains stable for a long period. The temperature is stable, although the TCS was still not accurate enough.

Heating effects

A major problem with heating in the microfluidics world is the generation of air bubbles inside the channels depending on the temperature. Normally, a certain amount of gas is dissolved in water. By increasing the temperature this gas is emitted and cannot exit easily the microchannels, therefore generating air bubbles. This phenomenon was analyzed to determine if it could affect the heating process. The hot plate was heated to 42 °C. Once the temperature was stable, the PDMS chip was placed on it and the distilled water was pumped in with a syringe. The distilled water was colored in blue for a better visualization. In the first 45 s of heating, no bubble generation nor any visible changes in

[11] Melcor CP1.4-17-045

the fluid was observed. After 100 s, the first bubbles were noticed, and the rest appeared slowly within the next minute. As expected, there was bubble generation inside the microchannels; however, it starts long after the time most heat shock protocols specify, i.e. 45-90 s. Therefore, even though the problem was indeed observed, it does not affect the times in which the AIMD is supposed to work.

4.5.4.4. Cooling

The cooling power needed was also calculated with Equation 2.14. In this case, the cooling area, where the channels are located, A_{CA} is ~95 mm^2. Therefore, for an initial temperature T_{Ci} = 42 °C and a final temperature T_{Cf} = 0 °C, and with λ_{PDMS} and d_{PDMS} unmodified, the maximal cooling capacity needed is $\dot{Q}_C$ = ~1.5 W. This is only for one process, thus, as the dimension of the TEC cover two processes, ~3 W are needed.

The same TECs were used as for heating, which have a maximum power (10.9 W) enough for cooling, as well. However, for cooling, having enough power is not enough. The most important issue to ensure a proper cooling with a TEC is the heat dissipation on its hot side. Without a suitable heat dissipation mechanism, no cooling is achieved, and the cold side starts getting extremely hotter than room temperature. Therefore, different tests were performed regarding this issue.

Heat sink and forced convection

Normally, for cooling, a heat sink is attached to the hot side of the TEC. The first tests were performed with only an aluminum heat sink[12]. After several tests measuring the cold side of the TEC with a thermocouple, the temperature could not drop lower than 7 °C nor could it be maintained stable longer than a few seconds. As shown in Figure 4.34, after 20 s the temperature increases almost linearly and after 50 s is again by room temperature. Hence, it was determined that an additional dissipation method was required. The heat sink was then submerged in a water container to cause forced convection. The same tests were performed as before, and a clear difference was observed. The minimum temperature was almost the same; however, the temperature did not rise as quickly as without the water container. For all tests 2.2 V and 5 A were applied to the TEC. The minimum temperature was not yet as low as desired; still, it was established that the water container was needed.

[12] ABL - BGA heat sink supplied with thermal tape BGA-STD-010

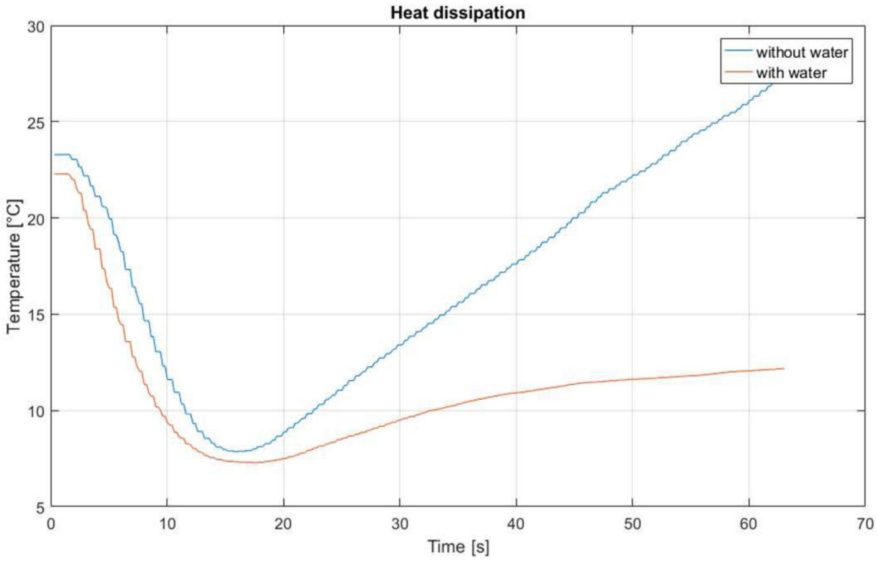

Figure 4.34. Heat dissipation with and without forced convection. Forced convection: the heat sink was submerged in a water container causing the heat to dissipate better. The temperature does not rise as quickly as without it.

Bonding the TEC with heat sink

The next step was to examine why the lowest temperature reached was only 7 °C. The maximum power of the TEC was not being reached, even with the maximum values for voltage and electric current. After different consideration, the bonding between the TEC and the heat sink was analyzed. The heat sinks are supplied with a thermal tape attached to the flat surface. The tape is made up of a thin aluminum foil coated on both sides with an adhesive resistant to very high temperatures. The thermal conductivity of the tape is 0.95 W/mK, according to its data sheet (see Appendix A.5). A heat conducting paste[13] and a thermal conductive glue[14] with a thermal conductivity of 0.61 W/mK and 1.15 W/mK, respectively, were also tested.

Again, the temperature at the surface of cold side of the TEC was measured. As it can be seen in Figure 4.35, the tape attached to the heat sink by the manufacturer delivered the worst results. The thermal glue, on the other hand, was able to dissipate the heat extremely efficiently. After 80 s, the temperature remained almost stable during the three experiments. At this point, the minimum temperatures reached were approximately 5.8 °C, −1.8 °C, and −8.3 °C for the thermal tape, paste and glue, respectively. These tests delivered clear results: the original thermal tape was detached from the heat sink, and instead, thermal glue was applied to bond the heat sink with the TEC.

[13] Fischer Elektronik
[14] EPO-TEK® H20E

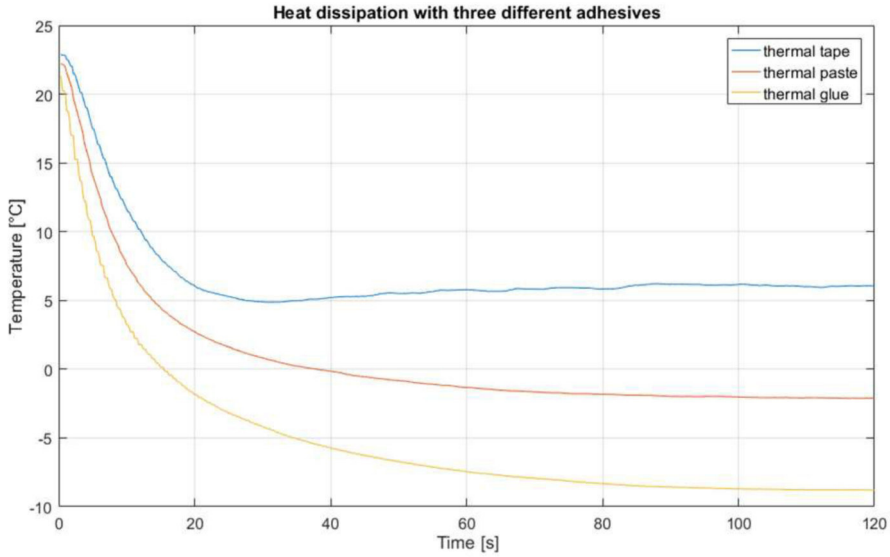

Figure 4.35. Heat dissipation comparing three different adhesives for TEC and heat sink. The thermal tape supplied by the manufacturer delivered the worst heat dissipation, whereas the thermal glue resulted extremely efficient.

Cooling performance

Finally, the cooling performance of the TEC was tested. Two sensors were positioned directly after the inlet and before the outlet. The TEC was supplied with 1 V and 3 A as the measured started. These results are shown in Figure 4.36. First, the TEC was turned on. After 20 s, water was pumped into the microchannels (1). Therefore, a temperature peak can be seen in the temperature profile (2). Within 30 s the water dropped to the desired temperature (3). A time frame shorter than the needed with the standard protocol. The sensor at the end of the channel did not log significant temperature changes as water with the same temperature as the microchannels reaches the sensor. After 150 s, a longer time window than the one needed after the heat shock, the temperature at the begin of the channel as well as at the end remains stable and at 0 °C. To maintain the cooling for more than 5 minutes, the heat dissipation mechanism with the small water container is not enough. For these tests, a larger heat sink was used.

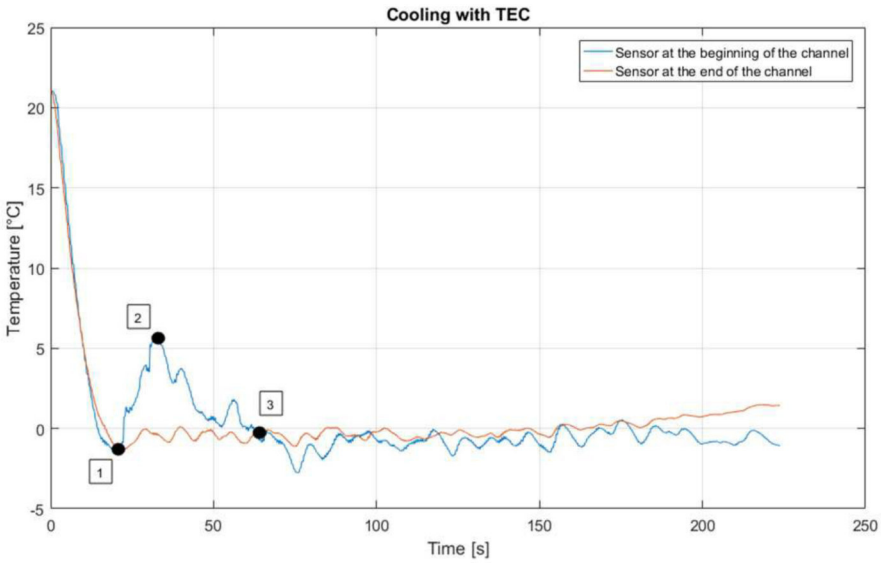

Figure 4.36. Temperature profile inside the channels by cooling. First, the glstec is turned on. (1) After 20 s, the water starts pumping into the channels. (2) Warmer water is being pumped in; therefore, a peak in the temperature profile appears. (3) The desired temperature is reached after ~30 s. Afterwards, the temperature remains stable for at least 150 s.

4.5.4.5. Heating and Cooling

Both systems were tested together; however, for heating, the hot plate was used instead of the TEC. This setup can be seen in Figure 4.37 (left). For these tests, four thermocouples were put inside the microchannels: at the beginning (TC1) and at the end (TC2) of the heating zone, and at the beginning (TC3) and at the end (TC4) of the cooling zone (see Figure 4.37 (right)). The tests were performed as follow: the hot plate was heat up to 42 °C. Once a stable temperature was reached, distilled water was pumped in using the extracting system described in Chapter 4.3. Then, the water was pushed further by pumping air.

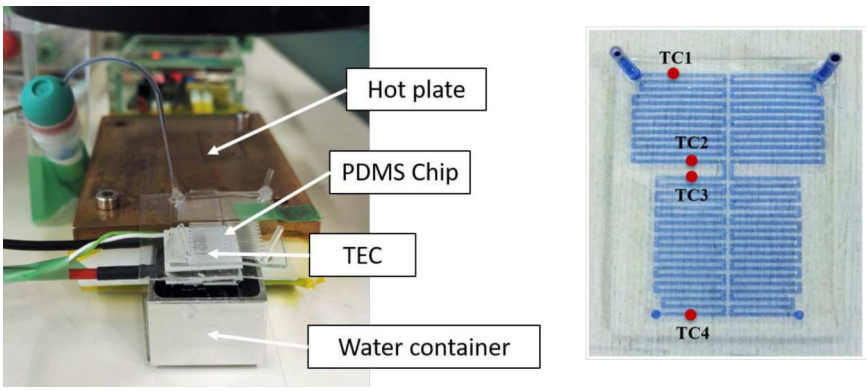

Figure 4.37. Left: Setup for heating and cooling tests. The hot plate, TEC, PDMS device, and the water container are shown. Right: Thermocouples locations on-chip.

The temperature profile of TC1 and TC4 can be seen in Figure 4.38. The measurement starts at 0 s; however, the water is pumped into the channels 11 s later. As the water enters the channels, the temperature decreases approximately 4 °C (1). After ~25 s, the water reaches the initial temperature (2). After 45 s, on the profile at the 56 s mark, the water is pumped out of the heating zone into the cooling zone (3). At ~45 s after starting the measurement, the TEC was turned on. The water reaches the end of the cooling zone 15 s after it had entered (4). After 2 minutes, in the cooling zone, the water is still at ~0 °C.

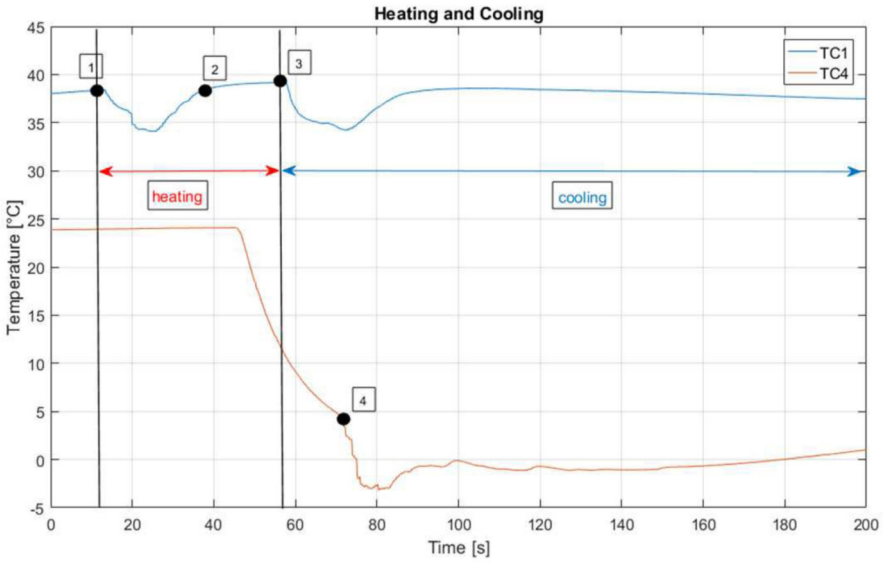

Figure 4.38. Temperature profile of thermocouple TC1 and TC4 during heating and cooling. (1) The water starts flowing, causing a temperature dropped. (2) After ~25 s the water reaches the initial temperature. (3) Water is pumped out of the heating zone into the cold zone. (4) The water reaches the end of the cooling zone. Afterwards, the temperature remains stable at least for 2 minutes after reaching the cooling zone.

These results were also endorsed using the same setup, but an infrared (IR)[15] camera, instead of the thermocouples. For these tests, 8 different points were logged, four in the hot zone and four in the cold zone. The locations of these points are illustrated in Figure 4.39 (A). The area of the PDMS device captured by the camera is shown in (B), whereas a take from the camera can been seen in (C). The red area marks the hot zone and the blue, the cold one.

The water was pumped in the microchannels as mentioned in the previous tests, after 35 s of measuring. Then, after 45 s of heating, the water was pumped into the cold zone. The temperatures of the points at the end of the heating zone, Sp3 and Sp4, are cooler than the desired temperature, whereas the ones at the beginning of the cooling zone, Sp5 and Sp6, are much warmer. This phenomenon happens because the hot plate emits more heat than desired. However, this problem is resolved with the TEC, as the heating is much more focused on a specific area.

[15]FLIR A655sc infrared camera

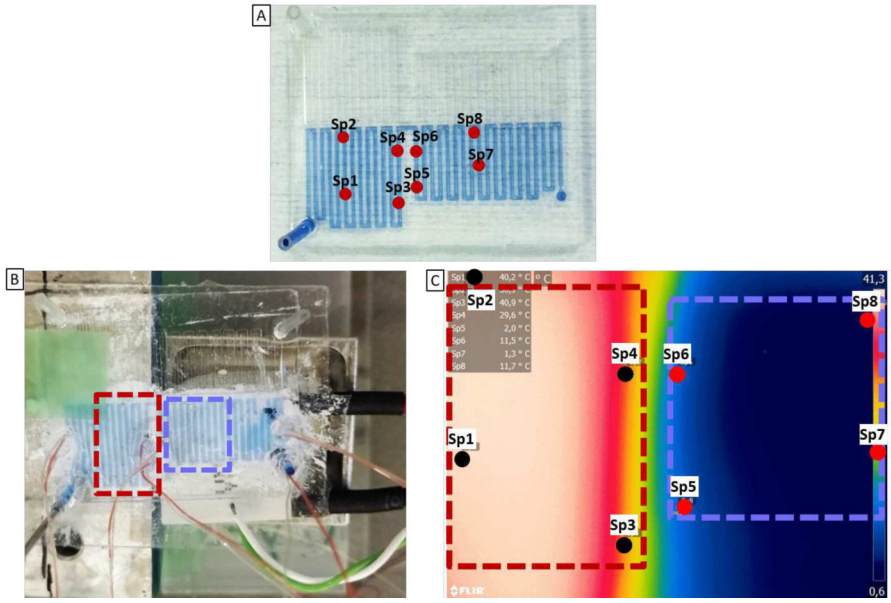

Figure 4.39. Setup for measurement with IR camera. A) Location of the 8 measured points. B) PDMS chip on the hot plate and TEC with the hot and cold zone marked in red and blue, respectively. C) Area captured by the IR camera.

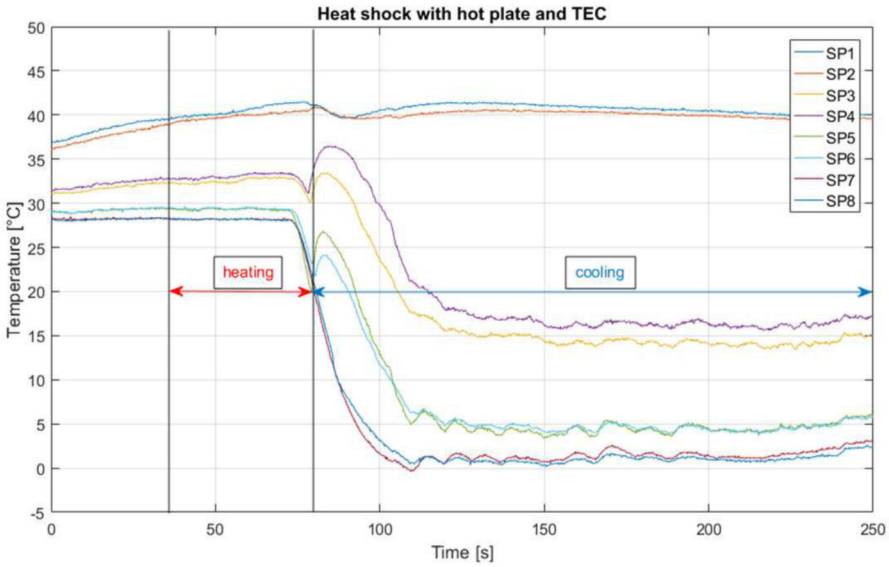

Figure 4.40. Heating and cooling results with IR camera. 8 different points were measured, 4 in the hot zone and 4 in the cold zone. Water was pumped in the microchannels after 35 s of measuring. After 45 s of heating, the water was pumped out of the hot zone into the cold zone. It remains there for at least 2 minutes.

4.5.5. Temperature control system (TCS)

The TCS plays a crucial role for properly heating and cooling the microchannels. The first control system consisted of a relay to act as a simple switch to provide or cut the current supply for the TEC. This control system had an extremely basic principle. Us-

ing an Arduino microcontroller[16], the relay was turned on until the desired temperature was reached. Once this temperature was exceeded, the relay was switched off. If the temperature dropped more than the desired temperature, the relay was turned on again. As mentioned above, the temperature was measured with type K thermocouples. These require a cold junction compensation and every change in temperature corresponds to an extremely small change in voltage. For this purpose, a digital amplifier[17] specially designed for this kind of thermocouples was used.

This control system showed promising results; however, the temperature drifted +/- 2 °C, and not always could stabilize the temperature. Therefore, a new PID[18] control system was developed. The main difference is that the relay was replaced by a Pulse-width modulation (PWM), allowing a smoother and more accurate controlling. The circuit diagram for the control system can be found in Appendix A.6 [135].

As shown in Figure 4.41, by heating it takes the control system approximately 100 s to stabilize the desired temperature. However, afterwards, it can be controlled with a deviation of only +/-0.5 °C for prolonged amounts of time. On the other hand, for cooling, the desired temperature is reached after approximately 45 s (Figure 4.42). The temperature drifting is slightly higher, namely +/-1 °C but is maintained stable for a long period as well. For these tests, a larger heat sink submerged in water was used. This assembly is very cumbersome; hence, this should be replaced by a fan for a simpler setup, if it should be cooled longer than 3-4 minutes. For the biological test, this TCS was used as it was proved to be extremely efficient.

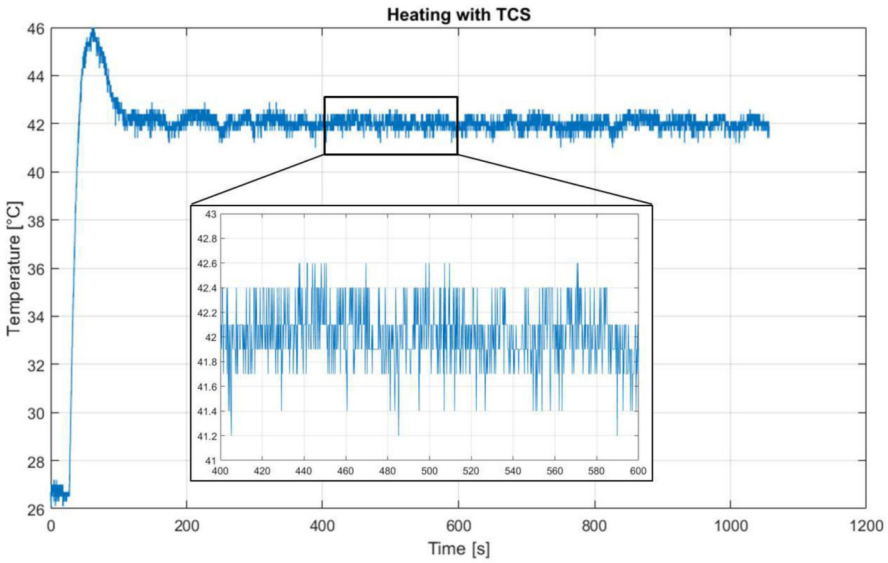

Figure 4.41. Heating for prolonged amount of time with TCS and its respective drifting +/-0.5 °C.

[16] Arduino Nano
[17] MAX6675
[18] proportional–integral–derivative

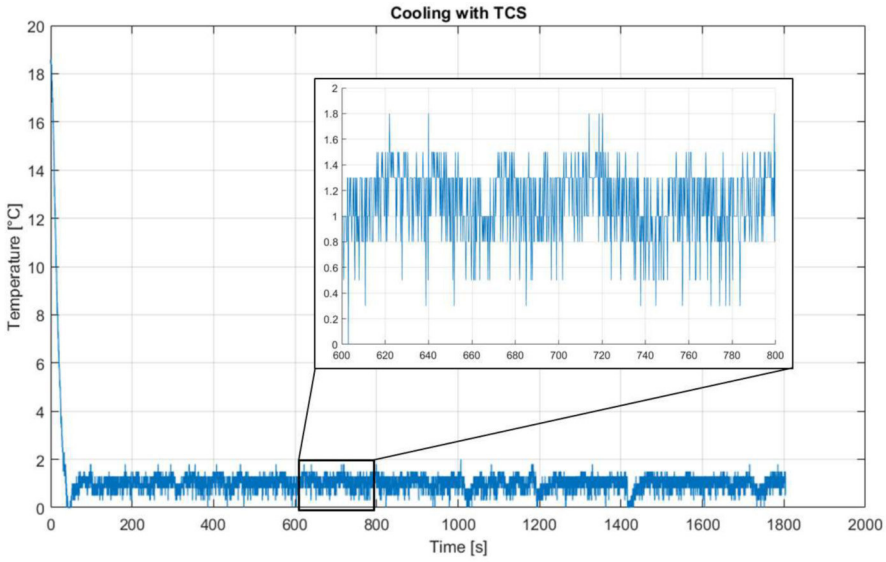

Figure 4.42. Cooling for prolonged amount of time with TCS and its respective drifting +/-1 °C.

5. Modules

After developing the basic components for mixing, control, and transport of fluids as well as the systems for heating and cooling, each module for the molecular cloning process was developed. In this chapter, the attempts to develop the D-Module as well as the problems encountered are described. Subsequently, the final design of the L-Module is presented as well as its characterization with biological tests. Then, the T-Module is introduced. The results of the biological tests performed on-chip are also presented. Finally, the integration of the modules is described as well as the concept for the control system.

5.1. Digestion

The development of the AIMD started with the first module, i.e. the D-Module. This module is intended for the digestion of the vector. It requires a mixer to combine the vector with the restriction enzymes; a temperature-controlled zone, where the biological reaction can occur at 37 °C; and a CE separation, to divide the longer, needed parts of the vector from the others. The latter is the most complex component of the D-Module; therefore, the development started there.

In the past years, there had been different projects at the IMT regarding CE [82–84,136]. Therefore, the CE for this work is based on those works, i.e. CE with C^4D. Contrary to the widespread optical detection, the C^4D allows the detection of the fragments without labeling and comprises a much simpler setup. The previous works were applied for ion separation and no biological tests were performed. Nevertheless, as the measurement setup of the previous works was still available, this was used. The first experiments were performed using different concentrations of Hydroxyethyl Cellulose (HEC) as the sieving matrix and a DNA ladder as sample. Although some peaks were observed, no reproducible results were obtained.

As the project is limited by a specific time frame, priorities were set. After discussion with the biologist, it was determined to focus on the L-Module and T-Module because an automation and parallelization of these two steps is extremely useful. Moreover, based on the literature, the CE with C^4D is feasible; therefore, investing time on this module is for sure valuable. However, in the framework of this work, its development stopped, and it continued with the next ones.

5.2. Ligation

The L-Module is responsible for the ligation process, i.e. mixing the required reagents and allowing the reaction to occur. Usually, a standard ligation protocol such as the pGEM®-T

Easy Vector System I introduced in Chapter 4.1.2.1 uses 10 µl. However, one of the goals of this work was to reduce the volume required to lessen costs. It was more suitable to work with volumes in multiples of four, as it facilitates the even distribution of the volumes. Hence, the total volume was reduced from 10 µl to 4 µl, reducing the total volume by 60%. Regarding the biological substances, the reduction was of 50%. For the vector and the ligase, the volume was reduced from 1 µl to 0.5 µl, respectively. The insert was reduced to 1 µl, instead of the 2 µl normally needed. Only 2 µl buffer was used, and the process ran without distilled water. The volumes in µl of the individual components before and after the reduction are summarized in Table 5.1.

	Original	**Reduced**
Insert	2	1
Vector	1	0.5
Ligase	1	0.5
Buffer	5	2
Water	1	0
Total	10	4

Table 5.1. Original and reduced volumes in µl of the individual components

5.2.1. Design and Fabrication

The L-Module consists of three layers. The Cover, the Vector-Ligase-Buffer Mixture (VLB)-layer, and the DNA-layer (see Figure 5.1). The vector, ligase and buffer do not vary within the parallel processes. Therefore, to simplify the design, these reagents are dosed, mixed and separated in four identical volumes in the VLB-layer. Then, the four VLB are transported to the DNA-layer, where they are mixed with their respective inserts. Additionally, the reaction zones for the ligation are also located in this layer.

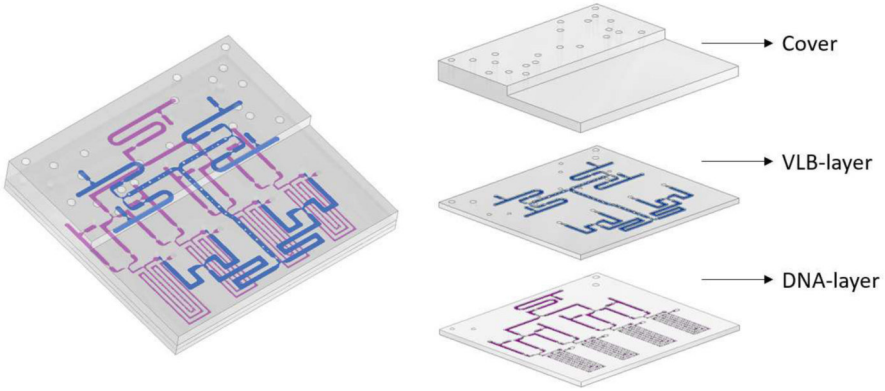

Figure 5.1. Left: 3D-model of the L-Module. Right: Exploded view of the L-Module. Three layers of the module are shown: Cover, VLB-layer, and DNA-layer.

VLB-layer

For four cloning processes, a total of 4x0.5 µl vector and 4x0.5 µl ligase are required. Even though the tests results showed that the ligase could flow without diluting, it is preferable to mix it as soon as possible with the buffer to maintain the flow conditions within the module as homogenous as possible. Thus, the vector as well as the ligase are mixed with 2 µl buffer, respectively, forming an 8 µl VLB. After flowing through the mixer, the VLB is divided in four equal volumes to be then delivered to the next layer.

The VLB-layer is shown in Figure 5.2. It consists of four dosing units for 2 µl each one. They are indicated in different shades of blue depending on the reagent to be dosed: buffer in dark blue, ligase in blue, and vector in light blue. These dosing units are connected to a large mixer. It is followed by an 8 µl distribution unit with two levels (shown in green). This layer has also different holes that allow tubing to reach the next layer or layers. The dimensions of this layer are 42.3 mm x 38.8 mm x 1 mm in length, width and thickness, respectively. The original form of the mixer (see Chapter 4.1.3.1) was changed to adapt it to the needs of the module. However, with ~20 mm, it has almost the same length as the mixer tested. The channel width remained unaltered as well. The dosing and distribution units are identical to the ones tested.

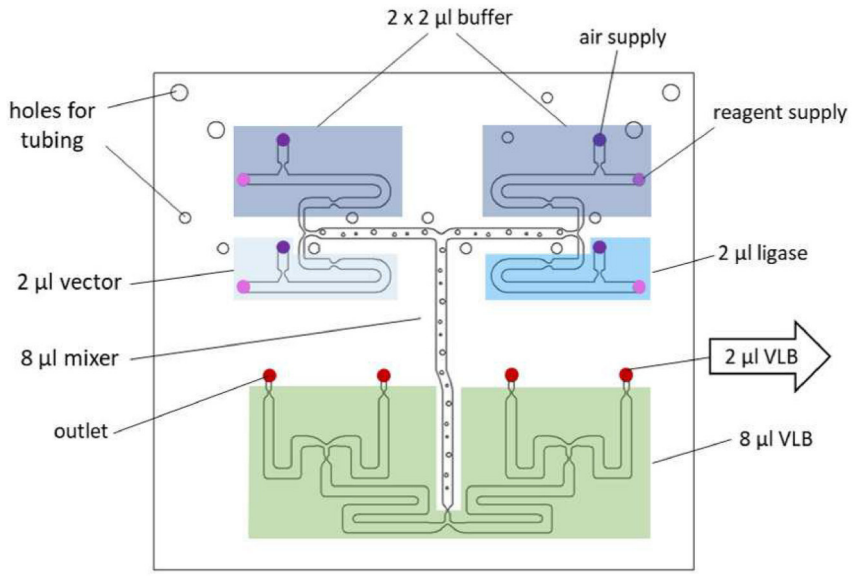

Figure 5.2. Top view of the VLB-layer showing the dosing units in different shades of blue, the mixer, the distribution system shown in green, and the holes for tubing. The inlets reserved for pumping air to the channels are shown in purple, whereas the ones intended for the reagents in pink. The outlets are marked with red.

DNA-layer

The function of this layer is to mix the VLB with the insert and let the ligation happen. For this purpose, the different inserts must be dosed independently. To mix the 2 µl VLB from the previous layer without problems, e.g. without air bubbles, the inserts are mixed beforehand with 1 µl buffer. Then, the 2 µl VLB is mixed with the 2 µl mixture of inserts

and buffer. Finally, the Ligation Mixture (LM) is kept in the reaction zone as long as established by the protocol.

This layer is shown in Figure 5.3. It consists of four independent dosing units for 1 µl (blue) and a 4 µl dosing unit for the buffer (dark blue). This volume is then distributed to the four processes equally (green). Then, the 4 µl mixer (see Chapter 4.1.3.1) follows. Lastly, the reaction zone with a blocking valve at the end secures the LM until the reaction occurs. The dosing units and the mixers with their reaction zones were not modified for this layer. A distribution unit for 4 µl with two levels was designed following the same characteristics as the one for 8 µl, whereby only the length of the channels varied. The dimensions of this layer are the same as the VLB-layer, and the channels of the former are covered by the latter.

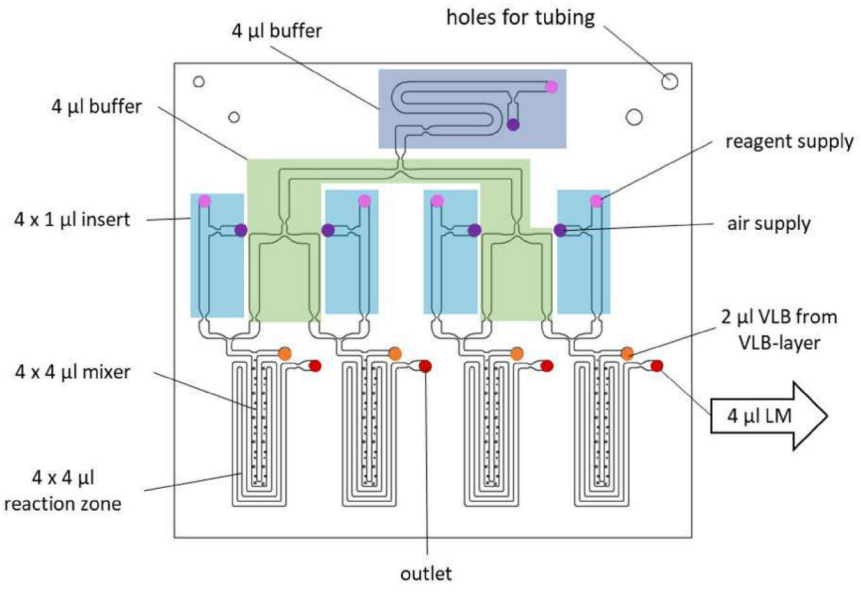

Figure 5.3. Top view of the DNA-layer showing the four 1 µl dosing units (blue), the 4 µl dosing unit (dark blue), and the respective 4 µl distribution system (green). Additionally, the mixers with their respective reaction zone are shown as well as the holes for tubing, the air supply (purple), the inlets for reagents (pink), the inlets for the VLB (orange), and the outlets (red).

Cover

The cover primary function is to close the channels of the VLB-layer. It is also responsible for holding the tubing needed to reach the inlets in all layers. This layer has the same length and width as the VLB- and the DNA-layer, but has two different thickness, being the only layer in the entire system with this characteristic. Half of the layer, where all the inlets and outlets, and therefore the holes, are located is, 4 mm thick for a better stabilization of the tubing. The other half is only 2 mm as the layer below can stabilize the tubing. The main and most important reason or the difference in thickness is to not waste material. Moreover, such a thick PDMS layer reduces significantly the visibility of the layers underneath. For testing, being able to observe the channel was still an important issue. The holes for the tubing have two different diameters, each one 2 mm deep. The first one, i.e. the one in contact with the outside, has a diameter of 1.3 mm, whereas the

other half one of 0.85 mm. In Figure 5.4 the cover is shown with its thickness. The holes for the reagents tubing are shown in purple, whereas the ones for the air supply in pink. The holes for the tubing for the other modules are shown in green.

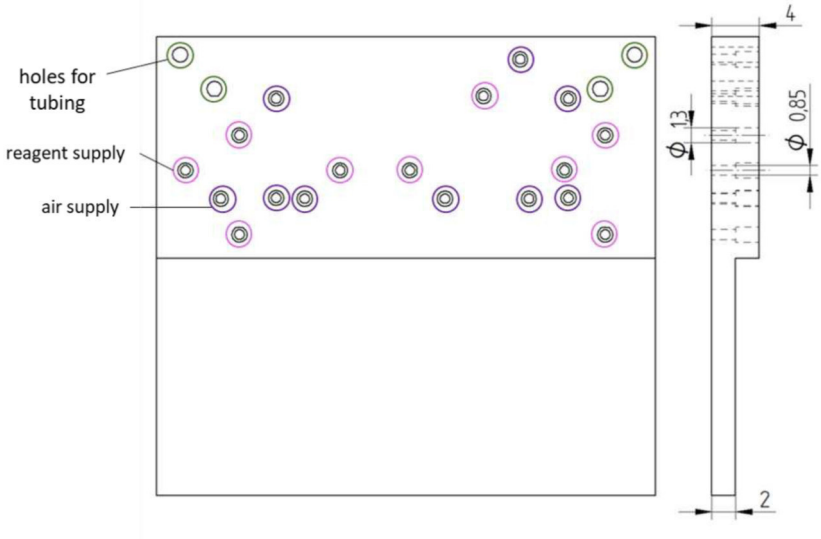

Figure 5.4. Cover with holes for holding the tubing. Top view and side view of the cover. The holes for the reagent tubing are shown in purple, whereas the ones for the air supply in pink. The holes for the tubing for the other modules are shown in green.

A PMMA mold was milled for each layer. All molds were thoroughly observed through a microscope to ensure that all structures were well fabricated without defects. The most crucial structures are the blocking valves and the pins of the mixers. Then, the PDMS parts were casted and bonded using the alignment holder. All fabrication steps followed the procedure explained in Chapter 3.5. The final L-Module in PDMS can be seen in Figure 5.5.

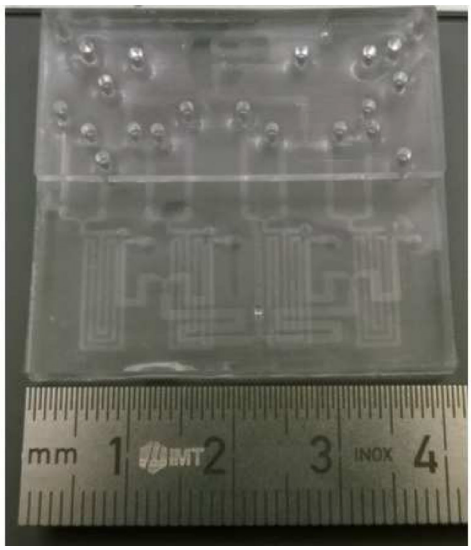

Figure 5.5. Final L-Module PDMS device

5.2.2. Fluid flow

The flow of the reagents within the L-Module is illustrated in Figure 5.6. First, the reagents are dosed on the first layer. For this purpose, the vector (dark pink), ligase (light pink), and buffer (blue) are pumped out their respective Eppis, using the same hydraulic circuit presented in Figure 4.20, i.e. the air supply to the Eppis is turned on. For a better understanding, the air supplies are identified with the letter E for Eppi, followed by the first letter of each reagent. Therefore, the air supplies of the Eppi Vector (EV), Eppi Ligase (EL), Eppi Buffer 1 (EB1), and Eppi Buffer 2 (EB2) are activated simultaneously until all dosing systems are filled (1). Subsequently, the control valve is switched, activating the air supplies for pushing the fluid out of the dosing systems and deactivating the ones connected to the Eppi. The air supplies connected directly to the module are identified with the letter A, for air, and the first letter of the reagent: Air Vector (AV), Air Ligase (AL), Air Buffer 1 (AB1), and Air Buffer 2 (AB2). This activation causes for the reagents to be pumped into the mixer, resulting in the VLB (purple) (2), and then divide it into four equal parts (3). The air supplies are turned off and the VLB remains there. The next step is to turn on the air supply for the buffer (blue), Eppi Buffer 3 (EB3), on the DNA-layer. Once the dosing system is filled, the air supply, Air Buffer 3 (AB3), is turned on to continue the flow and distribute it to the four processes (4, 5). Following this, the AB3 is turned off and the dosing of the different DNA fragments begins (different green shades). Hereby, the air supply for each Eppi, Eppi DNA 1 (ED1), Eppi DNA 2 (ED2), Eppi DNA 3 (ED3), and Eppi DNA 4 (ED4), is switched on (6). Finally, the air supplies to pump the DNA, Air DNA 1 (AD1), Air DNA 2 (AD2), AB3, Air DNA 4 (AD4), and AB3 as well as AV, AL, AB1, and AB2 are activated to enable the mixing of all reagents (yellow) (7). As the LM leaves the mixers, all supplies are deactivated to let the reaction occur (8). The names of the air supplies are summarized in Table 5.2.

Air supply to pump reagents:

out of Eppis		**further (directly to module)**		
EV	Eppi Vector	AV	Air supply Vector	
EL	Eppi Ligase	AL	Air supply Ligase	
EB i	Eppi Buffer i	AB x	Air supply Buffer i	i=1..3
ED j	Eppi DNA j	AD j	Air supply DNA j	j=1..4

Table 5.2. Overview of the air supplied for the ligation module. These vary between connection to an Eppi or directly to the module.

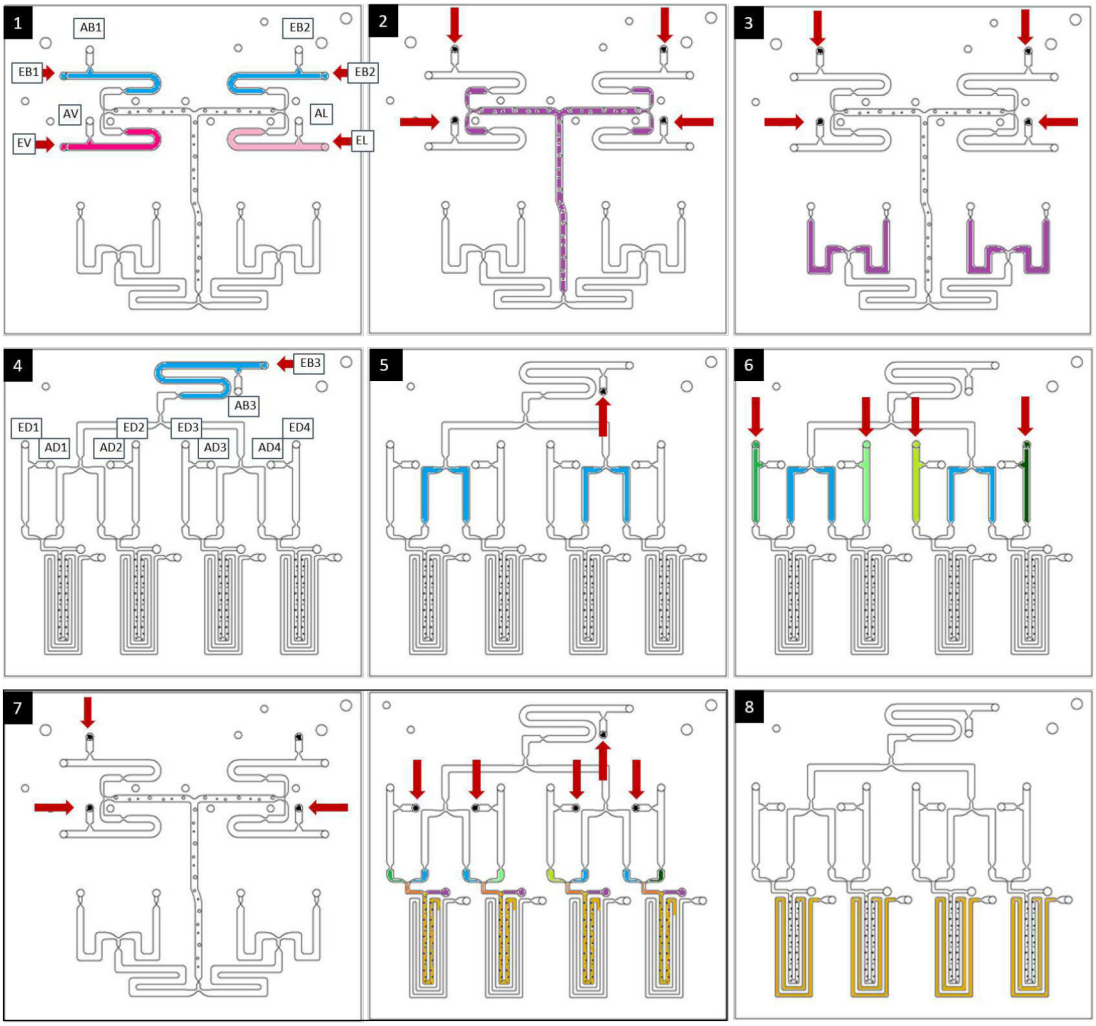

Figure 5.6. Illustration of the reagent flow within the L-Module. The air supplies activated are indicated with an arrow. The air supplies connected directly to the module are marked in black. The ones connected to an Eppi show different colors, one for each reagent. For a detailed description refer to the text (Chapter 5.2.2).

5.2.3. Biological tests

The functionality of the L-Module was tested using the pGEM®-T Easy Vector System I with the volumes mentioned before. First, the vector, the ligase, and the buffer were dosed in the respective dosing units through the extracting system. For this, the buffer was divided in two different Eppi to provide both dosing units at the same time. Subsequently, air was pumped simultaneously to all four dosing units. Air was pumped whilst the reagents reached the end of the channels on the first layer. At this point, the air supply stopped, and the dosing of the inserts on the second layer began, followed by the dosing of the buffer. Immediately, air was pumped to the dosing unit of the buffer and its distribution started. As the buffer reached the ends of the second level of the distribution system, air was pumped to the dosing units of the inserts. By reaching the junction of the mixer, the air supplies on the top layer were activated again, causing the VLB to flow into

the next layer and start mixing with the inserts. The air supply continued until the end of the reaction zone was reached. The LM remained in the reaction zone for one hour. Following this, all air supplies were turned on again and the LM was pumped into four separate Eppis.

The success of the ligation was determined with blue-white screening and gel electrophoresis (see Chapter 2.1.2). The transformation was performed manually, following a standard protocol to avoid adding extra error sources to the process. This protocol is described in Chapter 2.1.1.3. The agar plates were left for more than 24 hours in the incubator; thus, satellite colonies[1] grew on the plates. The results were not as favorable as expected. Two of the four agar plates showed an expected number of colonies, however, only blue ones, i.e. without the insert. In the other two considerably less colonies grew, and they were mostly blue. Nevertheless, on one plate a small white colony grew (see Figure 5.7), whose insert can be appreciated in the results of the gel electrophoresis (Figure 5.8 (lane 1)). For the gel electrophoresis, four colonies for each agar plate were picked and analyzed. For three of the four agar plates, all colonies picked were blue as no white colony grew. For the L1.3, the white colony and three blue ones were picked. The results show, as expected, only one insert.

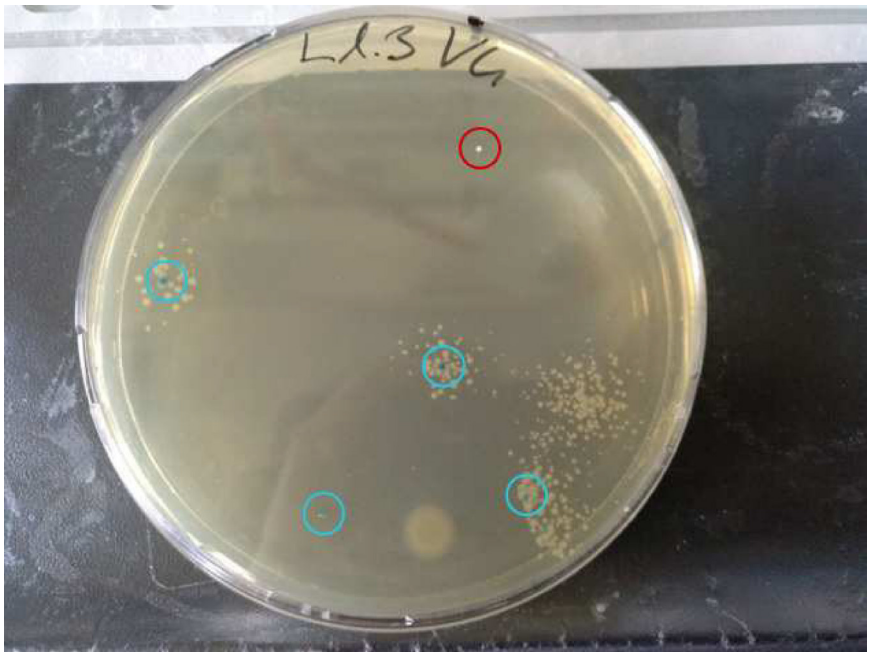

Figure 5.7. Results of the first ligation experiments. One white colony, marked in red, grew on the agar plate. The other were blue colonies, marked in blue.

The pGEM®-T Easy Vector System I, although not expired, had been opened for a few months. Therefore, the results were repeated with a new kit and the reaction time was extended to two hours. The rest of the experiment ran as the first one. In this case, almost half of the colonies were white, whereas the other half blue. In Figure 5.9 and Figure 5.10, two agar plates are shown with white and blue colonies. For a better visualization some white colonies are marked in red and some blue colonies in blue.

[1]These colonies appear as the antibiotic is depleted, allowing non-transformed bacteria to grow.

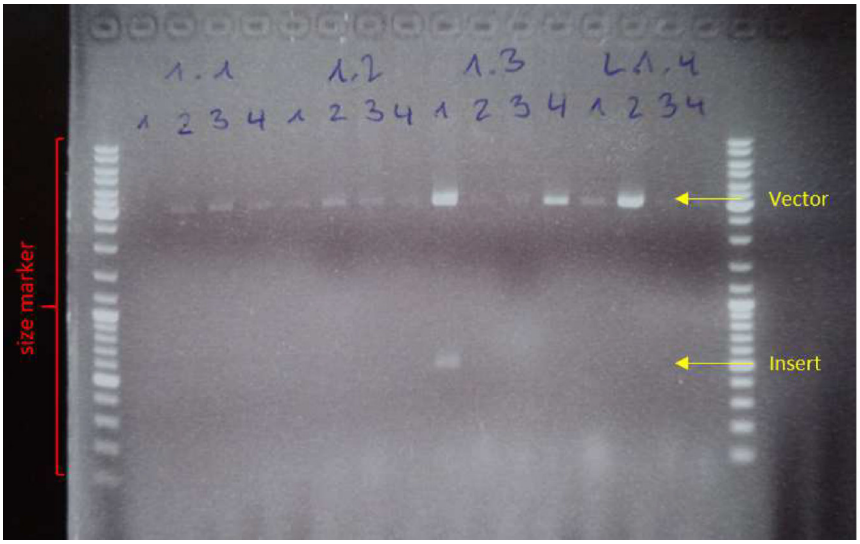

Figure 5.8. Results of the gel electrophoresis for the first ligation results. Four colonies of each agar plate were picked. For three of the four agar plates (1.1, 1.2, and 1.4), all colonies were blue. For one agar plate, 1.3, one colony picked was white (1), whereas the rest were blue (2-4).

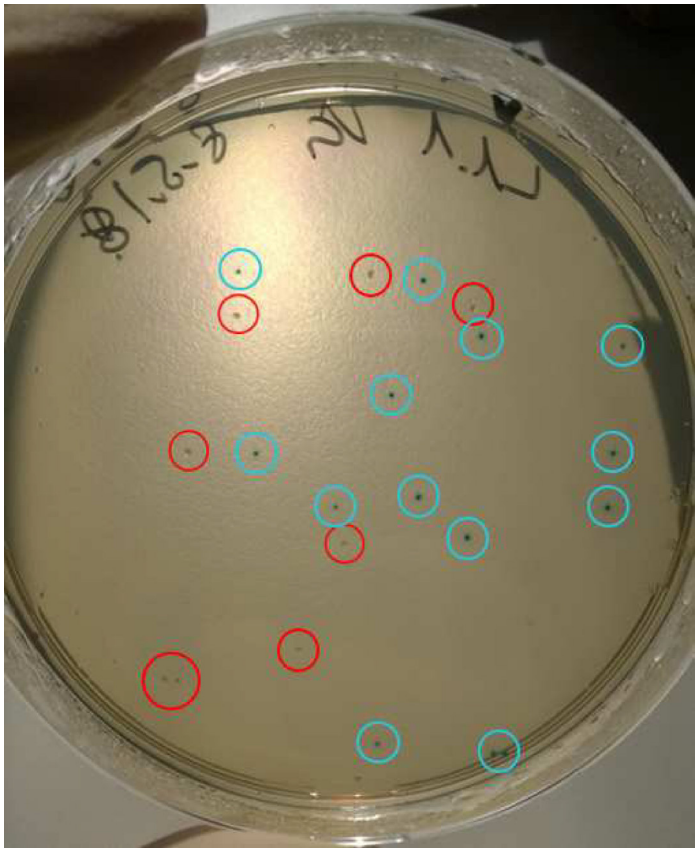

Figure 5.9. Ligation results. Two agar plates showing more white colonies than before, but also blue ones. For a better visualization some of the white colonies are marked in red and some of the blue ones in blue.

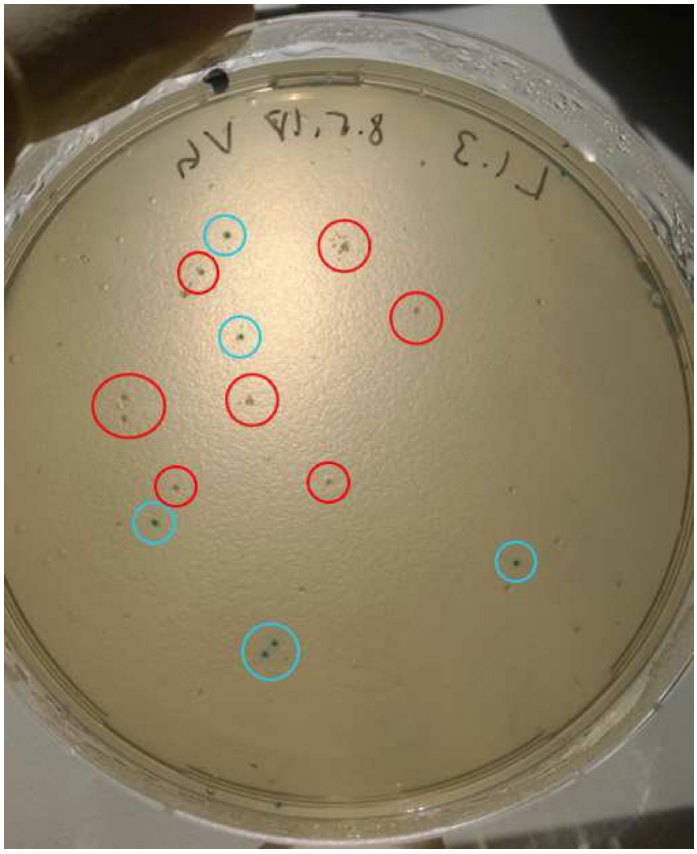

Figure 5.10. Ligation results. Two agar plates showing more white colonies than before, but also blue ones. For a better visualization some of the white colonies are marked in red and some of the blue ones in blue.

From the results above, it can be concluded that a successful ligation can be achieved with the L-Module. Compared with a standard procedure, fewer colonies grew on the agar plates. However, this is completely normal, and acceptable, as less inserts are available for the transformation. Moreover, in average, 50% of the colonies were white. This is a relative lower ligation efficiency compared with a standard protocol. A solution to improve this drawback could be to work with a slightly higher concentration of insert.

5.3. Transformation

The next step of the cloning process, namely the transformation, takes places in the T-Module. The main functions of this module are to mix the LM with the competent bacteria whilst at ~4 °C, and to enable a heat shock to which the Bacterial Mixture (BM) is exposed.

Trying to decrease the costs pro experiment, the aim of the AIMD was also to reduce the volume needed. The total ligation volume was reduced by 60%, whereas the volume of the biological substances by 50% (see Chapter 5.2). The volume of the competent bacteria was reduced even more. Normally, this volume varies from protocol to protocol; it ranges from 35 µl to 100 µl. The standard protocol used at the ITG requires 50 µl for 10 µl LM. In this work, the volume was reduced to 12 µl for 4 µl LM, i.e. ~75% less competent cells.

As the competent bacteria needed for the transformation are very costly, this feature is a great advantage of the AIMD.

The T-Module is a multilayer device that can be divided in two submodules according to their main function: mixing and heat shock. Both submodules can be operated independently or together as one module. Moreover, both consist of a non-reusable PDMS device and a reusable heating and/or cooling unit.

5.3.1. Bacterial Mixture (BM) Incubation

The first submodule, BM-Incubation, is responsible for mixing the competent bacteria with the LM and then incubate it at low temperatures. To achieve this, the competent bacteria are mixed in two stages. The first one occurs in the BM-layer 1 as competent bacteria come together with the LM. Afterwards, this BM is mixed with extra competent bacteria in the BM-layer 2. This submodule can work independently from the L-Module. For this purpose, it needs two extra layers: one for dosing the LM and the cover. Figure 5.11 shows the 3D-model of the BM-Incubation submodule and an exploded view of the layers. The layers required for a standalone T-Module are marked in blue. After mixing, the BM must be incubated at ~4 °C for 20-30 minutes, depending on the protocol. Hence, a cooling unit is attached to the bottom of the PDMS device.

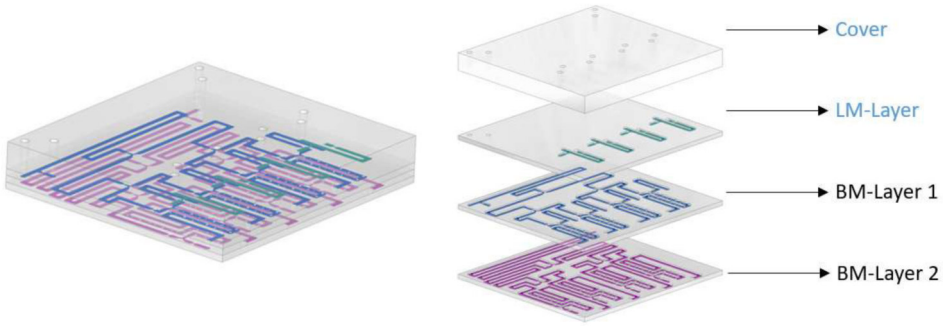

Figure 5.11. 3D-model and exploded view of the submodule, BM-Incubation, for mixing without cooling unit. Four layers of the module are shown: Cover, LM-layer, BM-layer 1, and BM-layer 2. The extra layers required for a standalone T-Module are marked in blue.

LM-layer

This layer has a simple structure, as it consists of only four 4 µl dosing units for the LM. It is employed when the T-Module acts as a standalone device without the L-Module. The width of the channels is 0.8 µm and the height 0.32 µm. The length was adapted to obtain a dosing area of 12.5 mm^2. The layer has the same dimension as the rest of the system (Figure 5.12). Provided that the L-Module and T-Module are integrated, this layer is not required.

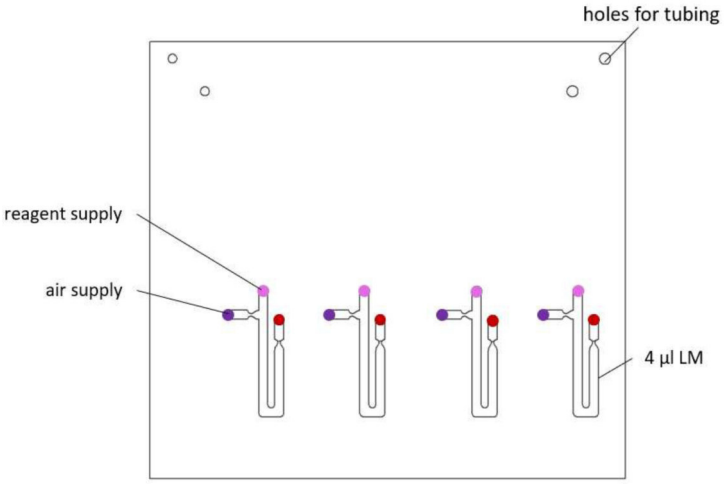

Figure 5.12. Top view of LM-layer with 4 µl four dosing units. Additionally, the holes for tubing, the air supply, the inlets for reagents, and the outlets are shown in purple, pink, and red, respectively.

BM-layer 1

In this layer, the first mixing between the LM and competent bacteria occurs. The ratio LM to competent bacteria are 1:4; therefore, to ensure an efficient mixing between the two parts, the mixing occurs in two phases. First, in this layer, only 4 µl competent bacteria are added to the 4 µl LM. The rest is mixed in the next layer. Thus, as the competent bacteria are dosed as the rest of the reagents, this layer consists of a 16 µl dosing unit (blue), followed by a 16 µl distribution unit with two levels (green). For this layer, the larger mixers are applied exactly as the test mixers introduced in Chapter 4.1.3.1. There are holes for tubing as well, as more bacteria must be dosed to the next layer. The LM-layer, if present, covers the channels of this layer. The dimensions of this layer are the same as the complete system (see Figure 5.13).

BM-layer 2

The next layer, BM-layer 2, is where the rest of the competent bacteria are added to the BM (see Figure 5.14). Hence, in this layer, 32 µl competent bacteria are dosed with a 32 µl dosing unit (shown in blue). It is then connected to a 32 µl distribution unit with two levels (shown in green) to deliver 8 µl extra competent bacteria to each BM coming from the previous layer. For mixing, four larger mixers with the same width, height, and length as the test mixers were used; however, the design was modified for the inlets (orange) and outlets (red) to fit the previous and next layers, respectively. The channels of this layer are covered by the BM-layer 1. The dimensions of this layer are the same as the entire system as well.

Cover

The cover goes on top of the rest of the layers and closes the channels of the LM-layer. It has the same dimensions as the rest of the layer but is 4 mm thick. The holes dimensions are as the ones from the cover of the L-Module. In case the L-Module and T-Module

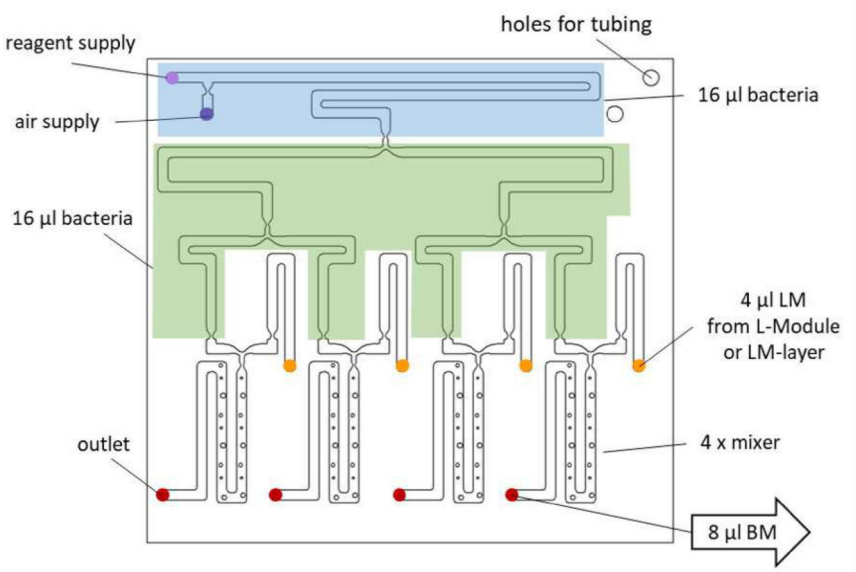

Figure 5.13. Top view of BM-layer 1 displaying a 16 µl dosing unit (blue) and the respective 16 µl distribution system (green) with two levels. These are followed by the larger mixers. The holes for tubing, the air supply (purple), the inlets for reagents (pink), the inlets for the LM (orange), and the outlets (red) are marked as well.

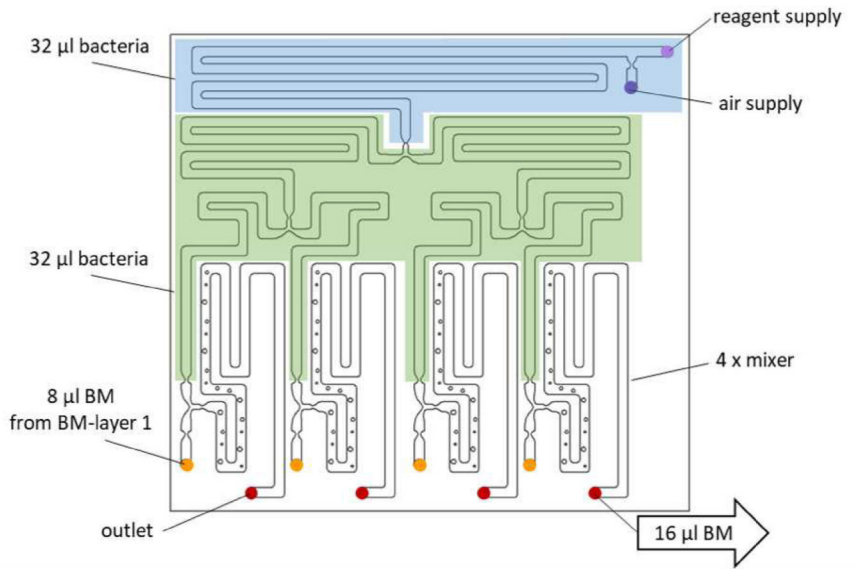

Figure 5.14. Top view of BM-layer 2. The 32 µl dosing unit, followed by a 16 µl distribution system with two levels are shown in blue and green, respectively. In addition, the mixers, holes for tubing, the air supply (purple), the inlets for reagents (pink), the inlets for the BM (orange), and the outlets (red) are shown as well.

work together, this layer is not needed.

Cooling unit

The BM-Incubation submodule can be put on ice to incubate the BM at the desired temper-

ature. However, this hinders the integration with the submodule for heat shock. Therefore, a cooling system is part of this submodule as well. It consists two TECs, 20 x 20 mm^2 in length and width, with their respective aluminum heat sinks. These have a contact surface of the same dimensions as the TECs and are 10 mm high. As the BM has a long incubation period, a small fan is needed to maintain the TECs working properly. The fan has standard dimensions with a 40 mm diameter. In Figure 5.15 the PDMS device with the cooling unit are shown.

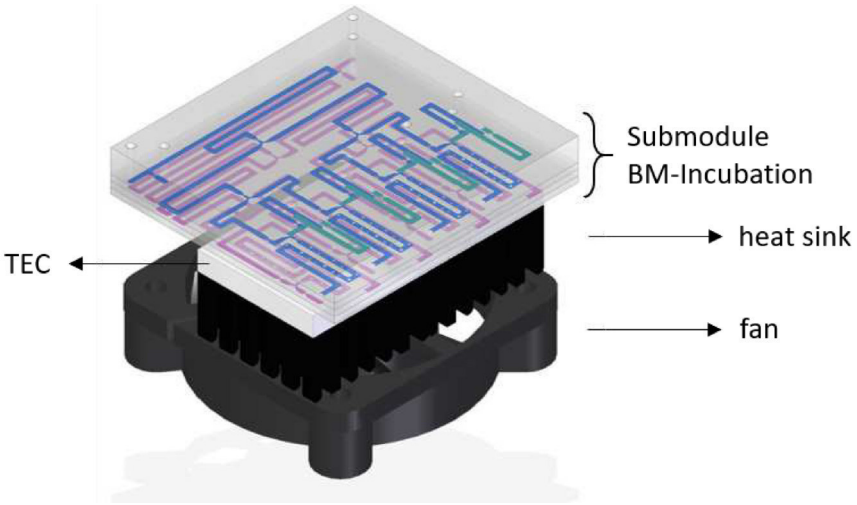

Figure 5.15. 3D-model of the BM-Incubation submodule for mixing, including the cooling unit for incubation. It consists of two TECs, their respective heat sinks, and a fan to improve the heat dissipation.

5.3.2. Heat shock

The next submodule is intended for the heat shock. Hereby, the bacteria are exposed to a temperature around 42 °C for about 45-90 s, both parameters vary depending on the protocol used. Afterwards, the bacteria are cooled down to ~0 °C again to for a few minutes. This module consists of a PDMS microfluidic device and a heating and cooling system. The design and characterization of the latter is described in detail in Chapter 4.5. Based on those tests, this submodule was modified to enable the parallelization of four transformation processes and the integration with the submodule for incubation. The PDMS device consists of a layer with the meandering microchannels with two zones and a cover. In Figure 5.16 the layer of the microchannels is shown. The heating zones are shown in red, whereas the cooling zones in blue. Both areas are divided using a blocking valve (see Chapter 4.2). Additionally, another blocking valve is placed at the end of the cooling zone. Regarding the dimensions of the channels, no modification occurred. This module is also 42.3 x 38.8 mm in length and width; however, it is only 0.72 mm thick. The thickness of this layer was set to maintain the symmetry, i.e. the cover and the bottom of the channels are 0.4 mm thick. This layer has also an opening for the temperature sensor required for the TCS.

The heating and cooling system, shown in Figure 5.17, consists of four TECs with 10 x 10 mm in width and length for heating, and two slightly bigger TECs for cooling (15 x

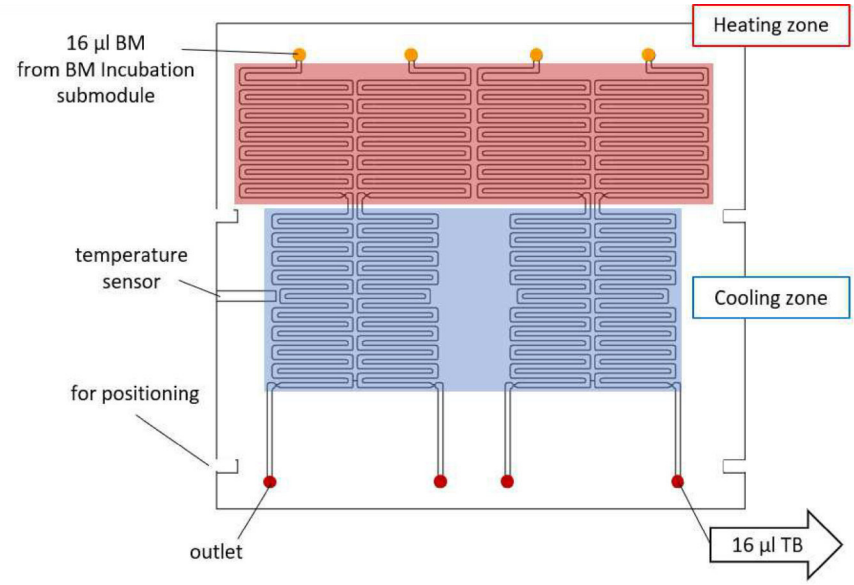

Figure 5.16. Top view of the meandering microchannels for the heat shock. The heating zones are shown in red, whereas the cooling zones in blue. Additionally, the inlets for the 16 µl BM (orange) and the outlets (red) for the TB are also marked.

15 mm in length and width). The TECs for cooling are coupled to heat sinks with a contact surface of 13.5 x 13.5 mm^2 and are 10 mm high. These are submerged in an aluminum water container to improve the heat dissipation. After the heat shock, the time for cooling does not exceed 5 minutes; therefore, a container with static water is enough. No fan nor a water-cooling system is required.

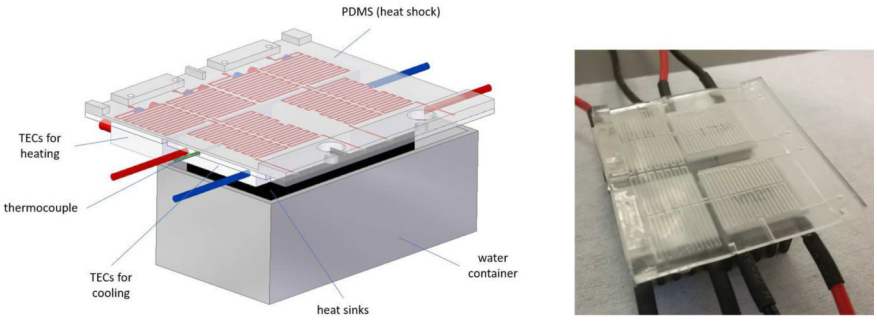

Figure 5.17. Submodule heat shock with all its components. Four TECs for heating are placed below the hot zone of the PDMS microchannels; another two TECs for cooling, coupled to their respective heat sinks are placed below the cold zone. These TECs are submerged in an aluminum water container.

All PDMS parts were fabricated according to the description in Chapter 3.5. The structures were inspected to check their successful fabrication. In Figure 5.18 (left) two adjacent cooling zone are shown in a SEM image with 22x magnification. On the right, a blocking valve at the end of the heating zone is shown (Magnification: 50x).

This final design was attached to the submodule for BM incubation. In Figure 5.19 (left) the whole system is shown. This system differs slightly from the one described

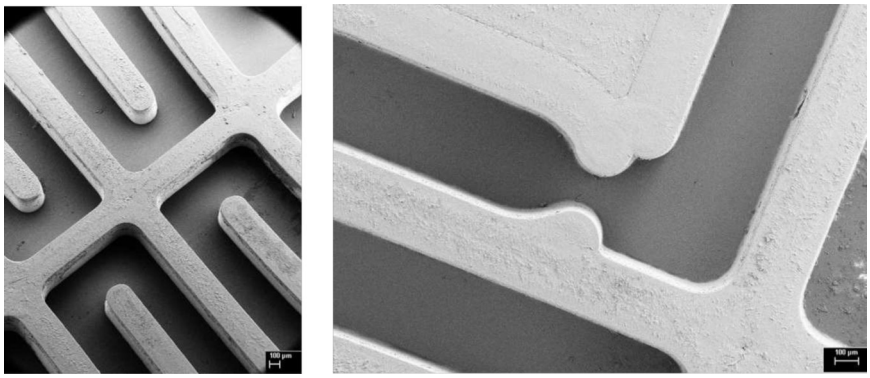

Figure 5.18. Left: SEM image of two adjacent cooling zones. Magnification: 22x. Right: Blocking valve at the end of the heating zone shown in a SEM image with 50x magnification.

in Chapter subsection 5.3.1 as the fan was not used, but instead an oversized heat sink. Additionally, one bigger TEC is used instead of two smaller ones. The multilayer nature of the system can be appreciated in the right image.

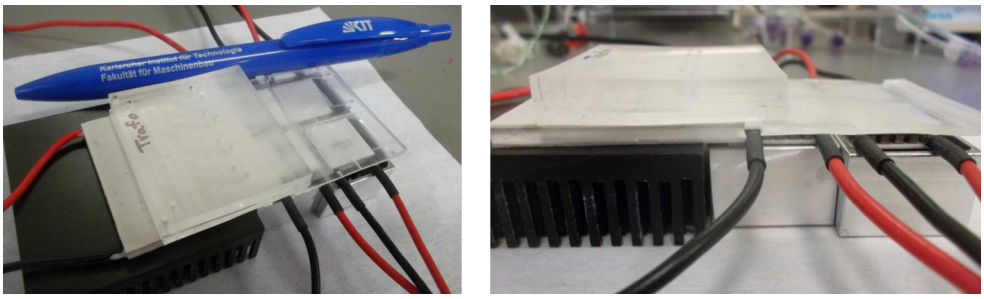

Figure 5.19. Left: T-Module with incubation unit as well as heat shock unit viewed from the top. Right: The same setup viewed from the side. The different layers of the module can be appreciated.

5.3.3. Fluid flow

The reagent flow in this module is explained considering the T-Module a standalone device and is shown in Figure 5.20. First, the four different LMs are dosed on the LM-layer. Following the same procedure as in the L-Module, the air supplies connected to the Eppis, namely, Eppi Ligation Mixture 1 (ELM1), Eppi Ligation Mixture 2 (ELM2), Eppi Ligation Mixture 3 (ELM3), and Eppi Ligation Mixture 4 (ELM4), are activated until the dosing systems are filled (1). Then the air supplies Air Supply Ligation Mixture 1 (ALM1), Air Supply Ligation Mixture 2 (ALM2), Air Supply Ligation Mixture 3 (ALM3), and Air Supply Ligation Mixture 4 (ALM4) are switched on to pump the reagents out of the dosing systems (2) and into the next layer (BM-layer 1). Subsequently, the competent bacteria are dosed on this layer by turning on the air supply Eppi Competent Bacteria 1 (EC1) (3). Then it is distributed to the four processes pumping air through the Air Supply Competent Bacteria 1 (AC1) (4). Once the last level of the distribution system is reached, the air supplies on the LM-layer are activated too (5), obtaining the BM by mixing of the LM with the competent bacteria. The BM is pump further into the BM-layer 2. Then the

activated supplies are deactivated, and more competent bacteria is dosed, following the same procedure, however, this time activating Eppi Competent Bacteria 2 (EC2) (6) and then Air Supply Competent Bacteria 2 (AC2) (7). Once the bacteria reach the end of the distribution system, the other supplies, ALM1, ALM2, ALM3, and ALM4, and AC1, are switched on to pump all reagents further (8). At this point, the BM must be incubated at low temperatures; therefore, all supplies are switched off. During the heat shock, all air supplies directly connected to the module are turned on (9) and then off again, when the end of the heating zone is reached. After the desired time elapsed, they are activated again to pump the Transformed Bacteria (TB) into the cold zone (10).

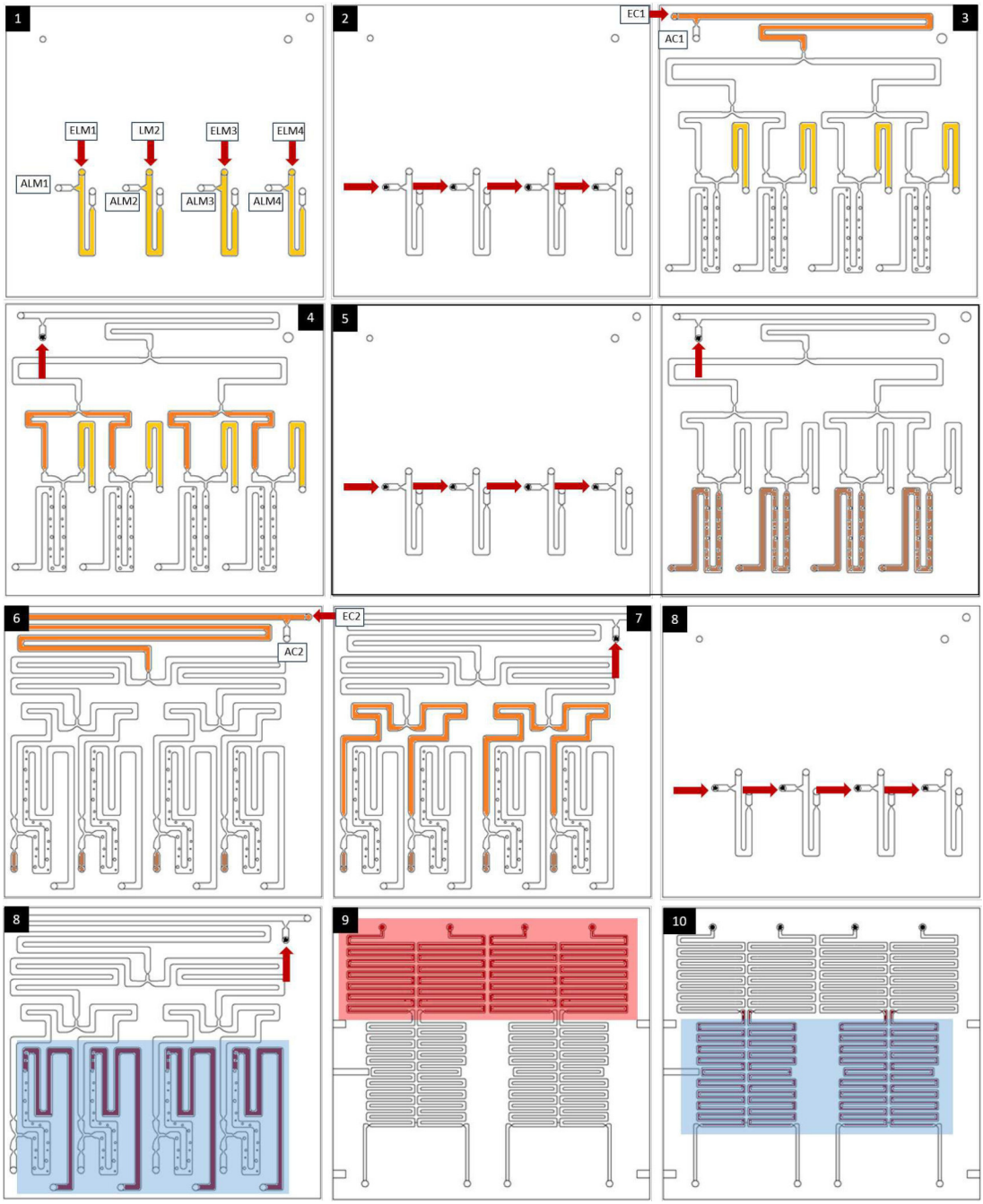

Figure 5.20. Illustration of the reagent flow within the T-Module. The air supplies activated are indicated with an arrow. The air supplies connected directly to the module are marked in black. The ones connected to an Eppi show different colors, one for each reagent. For a detailed description refer to the text (Chapter 5.3.3).

5.3.4. Biological Tests

After all tests described above, the entire system was tested for a real transformation process. The ligation was performed on-chip (see Chapter 5.2.3) as well. For the transformation, the protocol described in Chapter 2.1.1.3 was followed with a few modifications.

50 µl bacteria XL 1 blue, stored in an Eppi, was thawed for 20 minutes. Then, only 12 µl bacteria were pumped into the incubation module as well as the LM, and they were mixed together. The obtained BM was then kept cooled for another 20 minutes. Then the heat shock was performed on-chip. Firstly, the heating as well as the cooling unit were turned on. Once, the temperature was stable for heating, the BM was pumped into the meandering channels until the end was reached, approximately after 25 s. The BM was left heating up for 20 s more. After the time elapsed, the now transformed bacteria was pumped into the cooling zone. Here, the TB was left for 2 minutes. Finally, the TB was transported to Eppis. 32 µl of LB was mixed with the TB manually. The rest of the protocol followed normally. These tests were performed semi-automated, as the directional valve, the micropump, and the TECs were controlled manually.

The results of these tests showed that the transformation on-chip do function, as some blue and white colonies grew on the plates. However, only two colonies grew in each agar plate. In Figure 5.21 two agar plates with the results of two transformation processes can be seen. One agar plate shows one white and one blue colony, whereas the other one shows two blue colonies. The white colony is marked in red, and the blue colonies in blue. This is an unexpected, very low number of colonies, even for less bacteria.

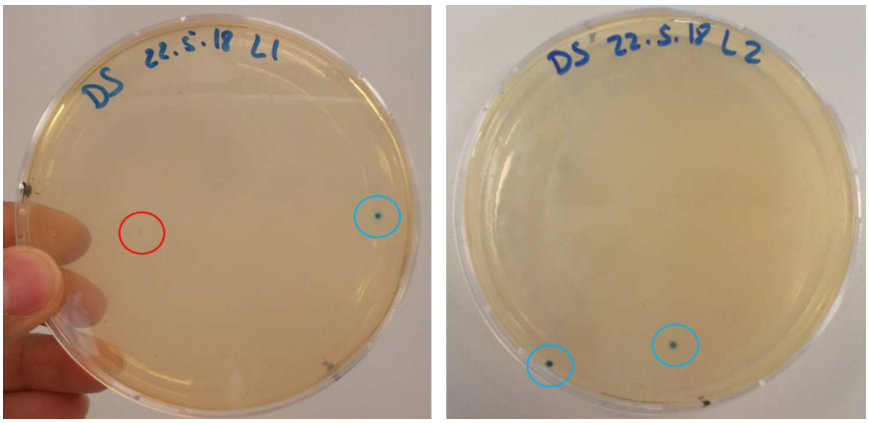

Figure 5.21. First results of the on-chip transformation. The bacteria were spread using small crystal balls. Left: agar plate with one white, marked in red, and one blue colony, marked in blue. Right: agar plate with two blue colonies, marked in blue.

After considering the possible reasons to the low number of cultures, it was decided to modify how the bacteria were spread on the agar plates. The standard procedure involves the mixing of the bacteria with small glass balls. This works efficiently for the standard volume; however, as the total volume was reduced, perhaps using the balls was not as efficient as some µl were lost in the balls. In addition, the agar plates were too large for the smaller volumes. Therefore, all steps of the transformation were done as for the previous tests, but the placement of the bacteria on the agar plates was modified. Two main differences happened: i) only half of the plate was used for one process. ii) the BM was put on the agar plate with a syringe and, then, with a small metal spatula spread through the plate.

The results obtained from these experiments are very successful. As seen in Figure 5.22, a high number of colonies of four different processes grew on the two agar plates. For

the transformation, the color of the colonies is not relevant, as the intake of the bacteria is what matters. Therefore, it was proved that an on-chip transformation with fewer bacteria and ligation products and a slightly modified transformation protocol can be efficiently performed with the AIMD. Modifying the protocol, i.e. avoiding the use of small crystal balls, presents a great opportunity for further automation of the process. The bacteria could be spread on the agar plated with a simple automated process.

Nevertheless, these experiments also delivered new ligation results. In this case, the results are more favorable. T1 and T3 have mostly white colonies. T2 are almost half and half, while T4 has mostly blue colonies. With these results, it was confirmed that a ligation process as well as a transformation process can be performed on the AIMD.

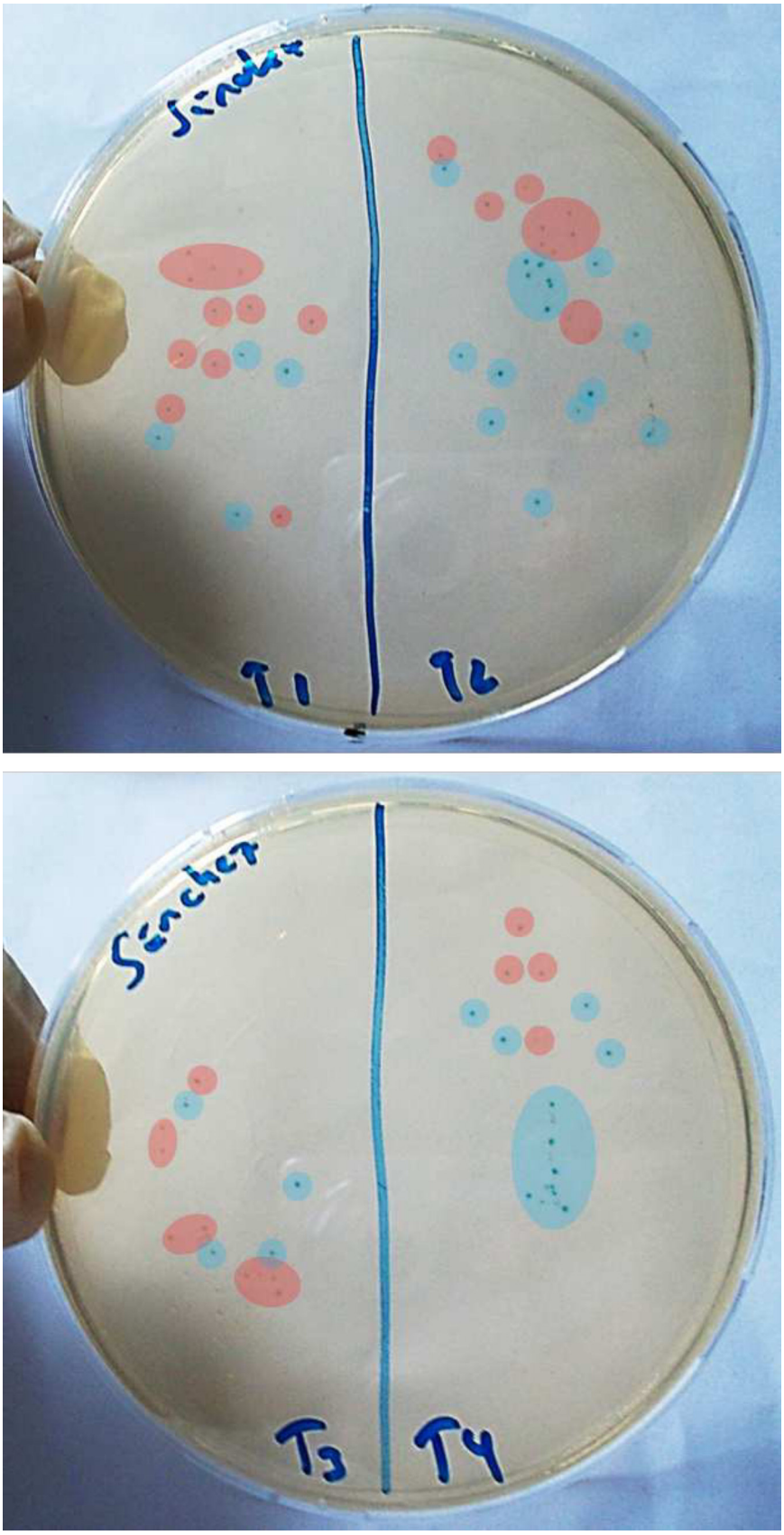

Figure 5.22. Results of the on-chip transformation. All processes show high number of white as well as blue colonies. Left: two transformation processes on one agar plate (T1 and T2). Right: two transformation processes on another agar plate (T3 and T4).

5.4. Integration and Fluid Flow Control

The integration of the L-Module and T-Module module consists on bonding the L-Module without modifications on top of the BM-layer 1 of the T-Module. The heat incubation and heat shock system do not vary. In Figure 5.23 the fluidic components of the AIMD, i.e. the PDMS layers, are seen with the respective fluidic connections between layers. The control flow occurs as described in Chapter 5.2.2 and Chapter 5.3.3.

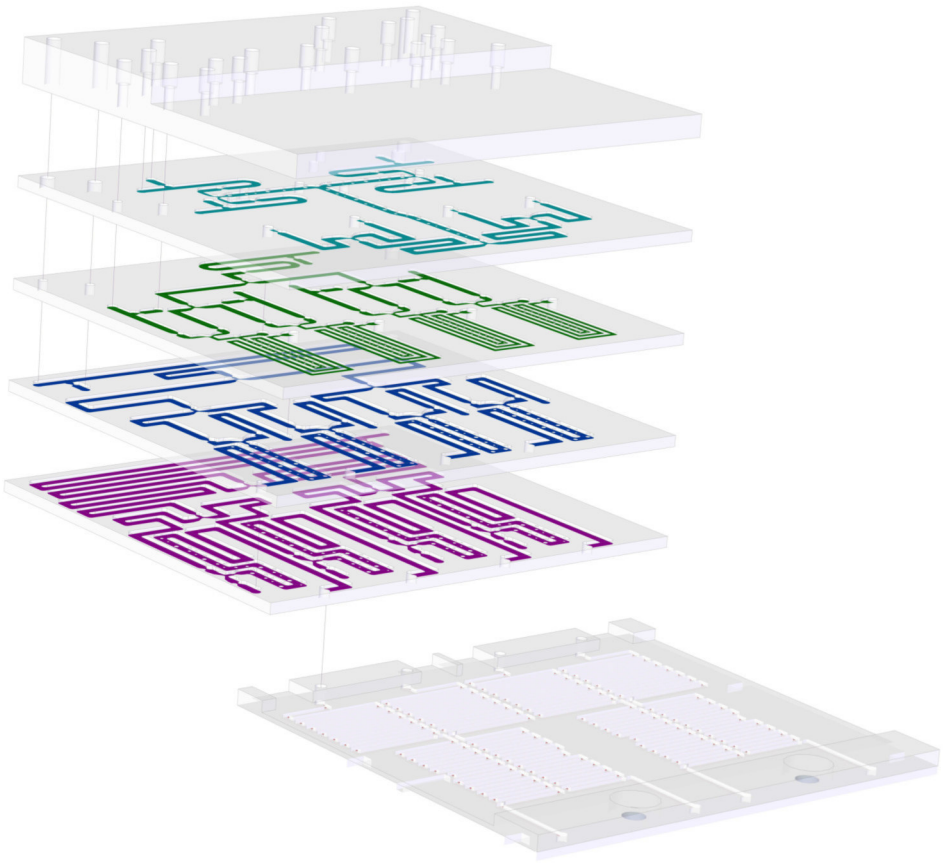

Figure 5.23. Exploded view of the fluidic components of the AIMD. The fluidic connections within the modules, i.e. between the outlets and inlets, are shown.

The air supplies connected to the Eppis and the ones coupled directly to the inlets of the modules must be switched on and off in a specific order. To fully automate the cloning process, this switching must also be automated. A solution for this would be to place a valve at each air supply. However, these would enlarge the systems and increase its costs, as at least 20 valves are required for both modules. Hence, a fluid control system was developed to overcome this problem. It consists of one micropump and a directional valve for the whole fluid control. In order to use only these two components, a switch was developed to control the air supply of the different inlets. This mechanism consists of two hollow shafts with holes for tubing. One hollow shaft, *E-shaft*, is for the connections to the

Eppis, i.e. all the air supplies named EXX, whereas the other, *A-shaft*, is for the air supply of the channels, i.e. for the connections AXX directly to the module (see Figure 5.24).

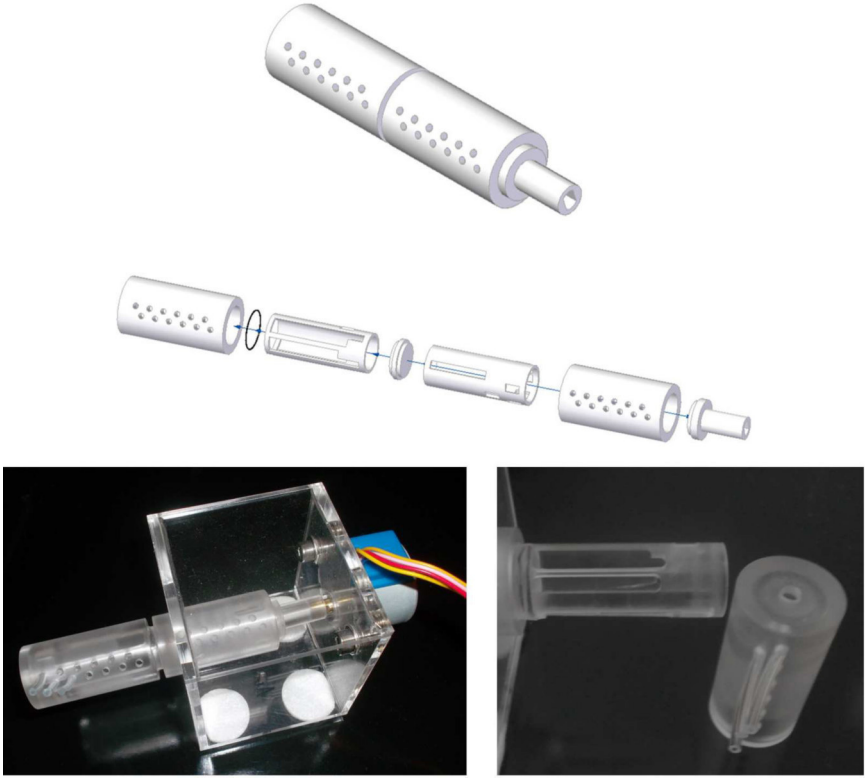

Figure 5.24. 3D-module, exploded view and actual setup of the fluid control system. Two hollow shafts, one for the connection with the Eppis and the other for the connections with the channels

For the ligation and transformation processes, 12 steps, i.e. 12 different valve configurations, are required. To achieve this, inside each hollow shaft, an inner hollow shaft with different gaps can be found. These gaps are responsible for opening the air supply to specific tubing. They have a different pattern every 60°to obtain the required 12 different configurations, i.e. 6 configurations per hollow shaft. The micropump is connected to the directional valve; in turn, its two connections go to each inner shaft. Hence, either the E-shaft provides air to the system: reagents are pumped out of the Eppis; or the A-shaft does: reagents are pumped out of the microfluidic components. In Table 5.3, an overview of the shaft and valve positions and the resulting air supply configurations. "E" represents that the control valve is set to provide air to the E-shaft, whereas "A" describes when the control valve is switched to supply air to the A-shaft. The different 6 positions of each shaft are described with the respective degree. The air supplies are named as explained in Chapter 5.2.2.

Due to its compact design, this control system can be placed next to the AIMD without taking too much space. Moreover, the electrical motor, the directional valve, the TECs, and the TCS can be controlled with, e.g. a LabVIEW program.

Step	1	2	3	4	5	6	7	8	9	10	11	12
Valve position	E	A	E	A	E	A	E	A	A	E	A	A
Shaft position	0°	0°	60°	60°	120°	120°	180°	180°	240°	240°	300°	240°
EV	●	○	○	○	○	○	○	○	○	○	○	○
EL	●	○	○	○	○	○	○	○	○	○	○	○
EB1	●	○	○	○	○	○	○	○	○	○	○	○
EB2	●	○	○	○	○	○	○	○	○	○	○	○
AV	○	●	○	○	○	●	○	○	●	○	○	●
AL	○	●	○	○	○	●	○	○	●	○	○	●
AB1	○	●	○	○	○	●	○	○	●	○	○	●
AB2	○	●	○	○	○	●	○	○	●	○	○	●
EB3	○	○	●	○	○	○	○	○	○	○	○	○
AB3	○	○	○	●	○	●	○	○	●	○	○	●
ED1	○	○	○	○	●	○	○	○	○	○	○	○
ED2	○	○	○	○	●	○	○	○	○	○	○	○
ED3	○	○	○	○	●	○	○	○	○	○	○	○
ED4	○	○	○	○	●	○	○	○	○	○	○	○
AD1	○	○	○	○	○	●	○	○	●	○	○	●
AD2	○	○	○	○	○	●	○	○	●	○	○	●
AD3	○	○	○	○	○	●	○	○	●	○	○	●
AD4	○	○	○	○	○	●	○	○	●	○	○	●
EC1	○	○	○	○	○	○	●	○	○	○	○	○
AC1	○	○	○	○	○	○	○	●	●	○	○	●
EC2	○	○	○	○	○	○	○	○	○	●	○	○
AC2	○	○	○	○	○	○	○	○	●	○	●	●

Table 5.3. Overview of the shaft and valve positions and the resulting air supply configurations. "E" represents that the control valve is switch to the E-shaft, and "A" to the A-shaft. The different 6 positions of each shaft are described with the respective degree. ● - the tubing is open; ○ - the tubing is closed. EXX are the connections going to the Eppis and AXX the ones going directly to the modules. V: Vector, L: Ligase, B: buffer, D: DNA, C: competent bacteria.

6. Conclusion and Outlook

Microfluidic devices are gradually becoming more important in the biomedical field. The possibility to work with micro-, or even nano-volumes, and thus reduce costs, makes microfluidic devices extremely attractive. Moreover, these types of systems are easier to automate and facilitate the parallelization of different processes, effectively reducing research times as well.

In cooperation with the biologists at the Institute of Toxicology and Genetics (ITG), it was concluded that a system allowing them not only to automate the molecular cloning process, but also to perform simultaneous processes, would minimize significantly their workload. Hence, the aim of this work was set to develop a microfluidic device that enables up to four different molecular cloning processes to be performed at the same time, with minimal intervention from the end-user. The molecular cloning process to be automated would start with the digestion step up to the transformation and bacterial growth.

Firstly, an intensive literature review of the existing systems was conducted. It was concluded that there are some existing systems for each step of the cloning process, namely digestion, ligation and transformation, but not an integrated system. These systems have complex designs; are difficult to integrate with each other; or cannot be automated. Therefore, in this work, a new system was developed, i.e. Automated Integrated Microfluidic Device (AIMD)

The system was designed with a modular structure. Each module corresponds to a step of the process. This enables the application of single steps without needing the whole system. The concept of **Module Digestion (D-Module)**, was developed, consisting of a mixer to combine the vector and the enzymes followed by a size separation by means of Capillary Electrophoresis (CE) to set apart the cut parts from the longer, needed ones. However, due to technical problems with the existing measurement setup, priorities were defined. For the biologists, an automated ligation and transformation was more important. Hence, this module was left on the planning phase.

The **Module Ligation (L-Module)** was designed as a multilayer device. On the first layer, the vector, ligase, and buffer are dosed and then, mixed together. Then, this Vector-Ligase-Buffer Mixture (VLB) is divided in four equal volumes and transported to the next layer. On the next one, the VLB is mixed with the different inserts separately. Each Ligation Mixture (LM) is then left to react for a certain amount of time in the corresponding reaction zones. This time depends on the protocol used.

The next module, the **Module Transformation (T-Module)** consists of different layers as well. A volume fraction of the competent bacteria is mixed with the LM on the first layer. Then, this Bacterial Mixture (BM) is mixed with the rest volume of the competent bacteria. The BM is incubated at low temperature for 20-30 minutes, depending on the protocol. Subsequently, the BM is exposed to a heat shock, followed by another incuba-

tion time. The heating mechanism consists of placing the hot side of a Thermoelectric cooler (TEC) at the bottom of the microfluidic device. The cooling mechanism works the same as for heating, but with the cold side of the TEC instead. Depending on the cooling time, different heat dissipation mechanisms are implemented.

The material selected for the system was Polydimethylsiloxane (PDMS) as it is biocompatible, transparent, and, principally, has a simple fabrication method, allowing the rapid fabrication of different parts. Plasma bonding was used as the bonding technique. The molds needed for the PDMS casting were micro-milled in Polymethyl methacrylate (PMMA).

Different components were developed for mixing, controlling, and transporting the substances within the chip. A mixer, consisting of a straight channel with cylindrical obstacles positioned asymmetrically along the channel, was developed. Based on positive simulations results and characterization tests, this mixer was further used. An extracting system to pump the reagents directly from the Eppendorf® tube (Eppi) was implemented. Moreover, to dose and meter the exact reagent volume, a dosing system based on the channel geometry was developed. In combination with the extracting system, the required reagent volumes were dosed and metered exactly and contamination-free. A distribution system, based on a T-junction, with a delay valve and different levels was designed to divide the total volume in equal volumes. All systems were tested with water and a water/glycerin solution, delivering positive results. Additionally, the distribution system was tested with bacteria as well.

Furthermore, different tests were performed to analyze the performance of the heating and cooling systems. The standard protocol was tested to be able to compare the results on-chip with the desired results. Then, the temperature profiles of water and bacteria were also compared to be able to perform the tests with water instead of bacteria. Moreover, heating and cooling times and capacity as well as the Temperature Control System (TCS) were tested.

As the results of the components characterization were positive, they were implemented in the modules as needed. The L-Module was tested with biological substances. These tests were performed semi-automated, as the directional valve was controlled manually. Although bacteria grew on the agar plates; the ligation efficiency was not high enough as almost 50% of the colonies resulted without insert. For the T-Module, biological tests were also performed. The transformation was done on-chip. After slightly modifications of the standard protocol, the results obtained were very successful. Therefore, it was proven that four ligation and transformation processes can be efficiently performed on-chip, with a semi-automated fluid control. The volumes were reduced as follows:

- Vector was reduced from 1 µl to 0.5 µl.
- Insert was reduced from 2 µl to 1 µl.
- Ligase was reduced from 1 µl to 0.5 µl.
- Buffer was reduced from 2 µl to 1 µl.
- Ligation mixture was reduced in total from 10 µl to 4 µl.

- Competent bacteria was reduced from 50 µl to 12 µl.
- Culture medium was reduced from 250 µl to 32 µl.

These results reflect positively in the performance of the molecular cloning in a biological lab. The reduction of the reagent volumes is directly reflected in the costs pro experiment. Additionally, the parallelization of at least four processes accelerate the research, as more experiments can be performed simultaneously, and the researchers can focus their time in other activities.

Even though the results were satisfactory, there are different areas were the device must be optimized. First, the fully automated control system, described in Chapter 5.4 must be tested, as for the tests the micropump, the directional valve, and the TECs were controlled manually. Moreover, to improve the ligation results, different DNA concentration should be tested to maintain the same volumes but increase the ratio regarding the vector. Furthermore, the material, and thus the fabrication method, should be replaced with others that enable mass production. Until now, the PDMS device was a great option, as it allowed a quick fabrication of numerous different parts. However, if the design is not to be modified again, a fabrication method suitable for mass production, such as hot embossing or injection molding, should be taken into consideration. This allows the use of polymers such as Polycarbonate (PC) or Polyethylene terephthalate (PET), which are also great for microfluidic devices and have a high biocompatibility. By using other material, the bonding process can be optimized. Procedures such as thermal bonding or ultrasonic bonding could be implemented to bond the layers.

Lastly, the D-Module should be successfully developed. Its design and some basic characteristics were thus far defined. Hydroxyethyl Cellulose (HEC) was selected as sieving matrix for the CE. This linear polymer allows an easy filling and emptying of the channels. Moreover, as mentioned before, Capacitively Coupled Contactless Conductivity Detection (C^4D) was the detection method chosen to avoid marking the samples and to maintain simple the setup. The Module Bacterial Recovery and Growth (BRG-Module) was also designed and fabricated, but not tested. It consists of meandering channel for mixing the Transformed Bacteria (TB) with culture medium and a zone for bacterial growth with enough oxygen. The zone for bacterial growth is deeper as the channels to allow air to reach the bacteria. Possibly, these channels could be covered with a membrane permeable for air. This would ensure the oxygen supply to the bacteria. At the end of this module, the Eppis are located to receive the TB mixed with the culture medium. In Figure 6.1 (left) the 3D-model of the designed BRG-Module as well as the design of the untested channels are shown (right). The entire system with the three modules as 3D-model is illustrated in Figure 6.2. In Appendix A.7 an explosion view of this entire system can be found.

With modification, optimization, and expansions, the AIMD could go from a lab prototype with efficient results to an actual product for performing high-throughput molecular cloning.

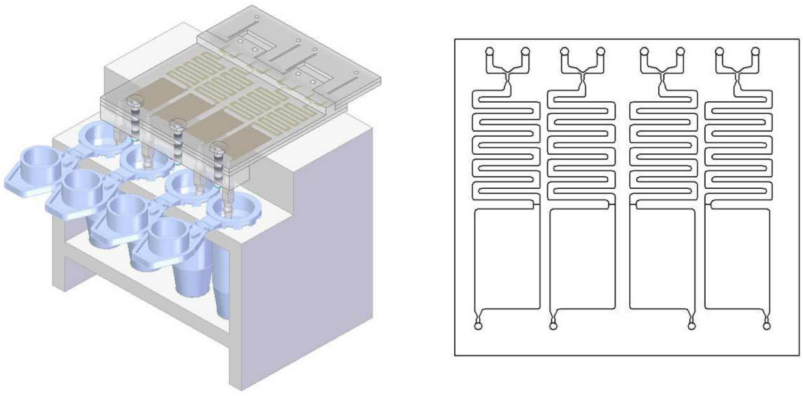

Figure 6.1. BRG-Module. Left: 3D-model; Right: design of the microchannels.

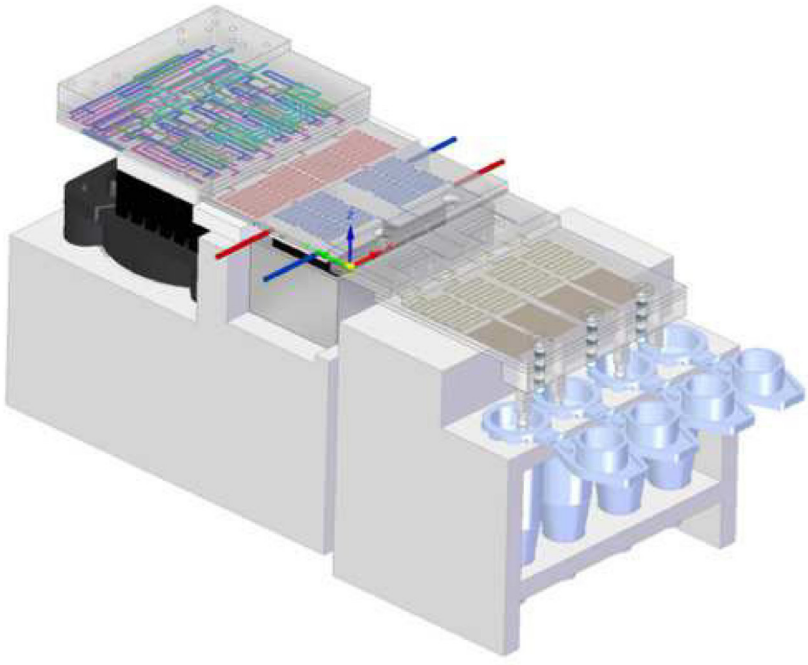

Figure 6.2. System with three modules. L-Module, T-Module, and BRG-Module

Bibliography

[1] A. McLennan, P. Turner, and A. Bates. *Molecular Biology*. Taylor & Francis, New York, fourth edition, 2012.

[2] A. Divan and J. Royds. *Molecular Biology: A Very Short Introduction*. Oxford University Press, New York, 2016.

[3] J. Sambrook and D.W. Russell. *Molecular Cloning: A Laboratory Manual*, volume Bd. 1. Cold Spring Harbor Laboratory Press, New York, 2001.

[4] H.F. Lodish. *Molecular cell biology*. W.H. Freeman, New York and Basingstoke, fourth edition, 1999.

[5] S. Colin. *Microfluidics*. ISTE, Wiley, London, Hoboken, 2013.

[6] A. Manz, N. Graber, and H.M. Widmer. Miniaturized total chemical analysis systems: A novel concept for chemical sensing. *Sensors and Actuators B: Chemical*, 1(1–6):244–248, 1990.

[7] L. Chen, A. Manz, and P.J.R. Day. Total nucleic acid analysis integrated on microfluidic devices. *Lab on a Chip*, 7(11):1413, 2007.

[8] V.N. Hoang, G.V. Kaigala, A. Atrazhev, L.M. Pilarski, and C.J. Backhouse. Strategies for enhancing the speed and integration of microchip genetic amplification. *Electrophoresis*, 29(23):4684–4694, 2008.

[9] C. Zhang, J. Xu, W. Ma, and W. Zheng. Pcr microfluidic devices for dna amplification. *Biotechnology Advances*, 24(3):243–284, 2006.

[10] Y. Zhang and P. Ozdemir. Microfluidic dna amplification—a review. *Analytica Chimica Acta*, 638(2):115–125, 2009.

[11] H. Tachibana, M. Saito, K. Tsuji, K. Yamanaka, Q. Le Hoa, and E. Tamiya. Self-propelled continuous-flow pcr in capillary-driven microfluidic device: Microfluidic behavior and dna amplification. *Sensors and Actuators B: Chemical*, 206:303–310, 2015.

[12] J. Wu, W. Guo, C. Wang, K. Yu, Y. Ma, T. Chen, and Y. Li. Research to improve the efficiency of double stereo pcr microfluidic chip by passivating the inner surface of steel capillary with noa61. *Cell Biochemistry and Biophysics*, 72:605–610, 2015.

[13] Y. Li, W. Jones, F. Rasti, I. Blaga, G. Bogdan, D. Eberhart, B. Kobrin, D. Lee, B. Nielsen, E. van Gelder, S. Jovanovich, and S. Stern. A flexible microfluidic processor for molecular biology: application to microarray sample preparation. *Lab on a Chip*, 11(15):2541, 2011.

[14] C.J. Easley, J.M. Karlinsey, J.M. Bienvenue, L.A. Legendre, M.G. Roper, S.H. Feldman, M.A. Hughes, E.L. Hewlett, T.J. Merkel, J.P. Ferrance, and J.P. Landers. A fully integrated microfluidic genetic analysis system with sample-in-answer-out capability. *Proceedings of the National Academy of Sciences*, 103(51):19272–19277, 2006.

[15] C. Chang, L. Chiou, C. Lin, D. Shieh, and G. Lee. Three-dimensional microfluidic chip for the extraction of mitochondrial dna. *Microfluidics and Nanofluidics*, 9(2-3):489–498, 2010.

[16] S. von der Ecken, D. Sánchez, P. Teunissen, H. Raat, R. Ahrens, and A.E. Guber, editors. *Low-cost and easy producible paper-printed digital microfluidic chips*, Dublin, 2016. Paper presented at MicroTAS.

[17] H. Xie, B. Li, R. Zhong, J. Qin, Y. Zhu, and B. Lin. Microfluidic device for integrated restriction digestion reaction and resulting dna fragment analysis. *Electrophoresis*, 29(24):4956–4963, 2008.

[18] C. Lin, Y. Wang, and L. Fu. Integrated microfluidic chip for rapid dna digestion and time-resolved capillary electrophoresis analysis. *Biomicrofluidics*, 6(1):12818, 2012.

[19] V.E. Papadopoulos, I.N. Kefala, G. Kaprou, G. Kokkoris, D. Moschou, G. Papadakis, E. Gizeli, and A. Tserepi. A passive micromixer for enzymatic digestion of dna. *Microelectronic Engineering*, 124:42–46, 2014.

[20] Y. Liu, D. Yao, H. Lin, W. Chang, and H. Chang. Dna ligation of ultramicro volume using an ewod microfluidic system with coplanar electrodes. *Journal of Micromechanics and Microengineering*, 18(4):45017, 2008.

[21] Y. Ko, J. Maeng, Y. Ahn, and S.Y. Hwang. Dna ligation using a disposable microfluidic device combined with a micromixer and microchannel reactor. *Sensors and Actuators B: Chemical*, 157(2):735–741, 2011.

[22] K. Nagamine, S. Onodera, Y. Torisawa, T. Yasukawa, H. Shiku, and T. Matsue. On-chip transformation of bacteria. *Analytical Chemistry*, 77(13):4278–4281, 2005.

[23] S. Li, L. Meadow Anderson, J. Yang, L. Lin, and H. Yang. Dna transformation via local heat shock. *Applied Physics Letters*, 91(1):13902, 2007.

[24] J. Sha, Y. Wang, J. Wang, L. Ren, Q. Tu, W. Liu, X. Wang, A. Liu, L. Wang, and J. Wang. Capillary-composited microfluidic device for heat shock transformation of escherichia coli. *Journal of Bioscience and Bioengineering*, 112(4):373–378, 2011.

[25] A. Wang, C. Cheng, I. Lin, F. Lu, H. Tsai, C. Lin, C. Yang, P. Pan, C. Kuan, Y. Chen, Y. Lin, C. Chang, Y. Wu, T. Kurniawan, C. Lin, A.M. Wo, and L. Chen. A novel dna selection and direct extraction process and its application in dna recombination. *Electrophoresis*, 32(3-4):423–430, 2011.

[26] F. Yang, Y. Zhang, S. Rafeah, H. Ji, S. Xie, Y. Ning, and G. Zhang. Accelerated dna recombination on a functionalized microfluidic chip. *RSC Advances*, 4(41):21541, 2014.

[27] J.W. Hong, Y. Chen, W.F. Anderson, and S.R. Quake. Molecular biology on a microfluidic chip. *Journal of Physics: Condensed Matter*, 18(18):S691–S701, 2006.

[28] S.C.C. Shih, G. Goyal, P.W. Kim, N. Koutsoubelis, J.D. Keasling, P.D. Adams, N.J. Hillson, and A.K. Singh. A versatile microfluidic device for automating synthetic biology. *ACS synthetic biology*, 4(10):1151–1164, 2015.

[29] D. Tagu and C. Moussard. *Techniques for Molecular Biology*. Taylor & Francis, Bristol, 2006.

[30] ”Restriction Digest of Plasmid DNA”, Addgene, 10.11.16. https://www.addgene.org/protocols/restriction-digest/.

[31] “pGEM®-T Easy Vector Systems. Quick Protocol.” Promega Corporation, 2013. https://www.promega.de.

[32] T. Brown. *Gene Cloning and DNA Analysis: An Introduction*. John Wiley & Sons, Oxford and Hoboken, sixth edition edition, 2010.

[33] P. Tabeling. *Introduction to microfluidics*. Oxford University Press, Oxford, U.K and New York, 2005.

[34] N.T. Nguyen. *Mikrofluidik: Entwurf, Herstellung und Charakterisierung*. Vieweg+Teubner Verlag, Wiesbaden, 2013.

[35] W.C. Tian and E. Finehout. *Microfluidics for Biological Applications*. Springer US, New York, 2008.

[36] S. Kandlikar, S. Garimella, D. Li, S. Colin, and M.R. King. *Heat Transfer and Fluid Flow in Minichannels and Microchannels*. Butterworth-Heinemann, Oxford, second edition, 2013.

[37] B.J. Kirby. *Micro- and Nanoscale Fluid Mechanics: Transport in Microfluidic Devices*. Cambridge University Press, New York, 2010.

[38] R.A. Granger. *Fluid Mechanics*. Dover Publications, New York, second edition, 2012.

[39] W.B.J. Zimmerman. *Microfluidics: History, theory and applications*, volume 466 of *CISM courses and lectures*. Springer, Wien, 2006.

[40] V. Jokinen and S. Franssila. Capillarity in microfluidic channels with hydrophilic and hydrophobic walls. *Microfluidics and Nanofluidics*, 5(4):443–448, 2008.

[41] H. Butt, K. Graf, and M. Kappl. *Physics and chemistry of interfaces*. Wiley-VCH, Weinheim, 2003.

[42] E.W. Washburn. The dynamics of capillary flow. *Physical Review*, 17(3):273–283, 1921.

[43] B. Hagmeyer, F. Zechnall, and M. Stelzle. Towards plug and play filling of microfluidic devices by utilizing networks of capillary stop valves. *Biomicrofluidics*, 8(5):056501, 2014.

[44] H. Mehrer. *Diffusion in Solids: Fundamentals, Methods, Materials, Diffusion-Controlled Processes*. Springer Berlin Heidelberg, 2007.

[45] G. Cai, L. Xue, H. Zhang, and J. Lin. A review on micromixers. *Micromachines*, 8(9):274, 2017.

[46] J. Li, G. Xia, and Y. Li. Numerical and experimental analyses of planar asymmetric split-and-recombine micromixer with dislocation sub-channels. *Journal of Chemical Technology & Biotechnology*, 88(9):1757–1765, 2013.

[47] N.T. Nguyen. Micromixers: Fundamentals, design, and fabrication, 2012.

[48] A. Alam, A. Afzal, and K. Kim. Mixing performance of a planar micromixer with circular obstructions in a curved microchannel. *Chemical Engineering Research and Design*, 92(3):423–434, 2014.

[49] D. Will, R. Nollau, N. Gebhardt, and D. Herschel. *Hydraulik: Grundlagen, Komponenten, Schaltungen*. Springer, Berlin and Heidelberg, fifth edition, 2011.

[50] K.W. Oh and C.H. Ahn. A review of microvalves. *Journal of Micromechanics and Microengineering*, 16(5):R13–R39, 2006.

[51] C. Zhang, D. Xing, and Y. Li. Micropumps, microvalves, and micromixers within pcr microfluidic chips: Advances and trends. *Biotechnology Advances*, 25(5):483–514, 2007.

[52] A.K. Au, H. Lai, B.R. Utela, and A. Folch. Microvalves and micropumps for biomems. *Micromachines*, 2(4):179–220, 2011.

[53] P. Liu and R.A. Mathies. Integrated microfluidic systems for high-performance genetic analysis. *Trends in biotechnology*, 27(10):572–581, 2009.

[54] P. Böckh and T. Wetzel. *Heat Transfer: Basics and Practice*. Springer Berlin Heidelberg, 2011.

[55] M. Kaviany. *Principles of heat transfer*. A Wiley-Interscience publication. Wiley, New York, 2002.

[56] A.F. Mills. *Heat Transfer*. Irwin, Homewood Boston, 1992.

[57] D.M. Rowe. *Thermoelectrics Handbook: Macro to Nano*. Taylor & Francis, Boca Raton, London, and New York, 2006.

[58] S.D. Minteer. *Microfluidic Techniques: Reviews and Protocols*, volume 321 of *Methods in molecular biology*. Humana Press Inc., Totowa, NJ, 2006.

[59] "PDMS: A review" Elveflow, 2018. https://www.elveflow.com/microfluidic-tutorials/microfluidic-reviews-and-tutorials/the-poly-di-methyl-siloxane-pdms-and-microfluidics/ [Online; accessed 4-June-2018].

[60] "Product Information" Dow Corning, Silicone Encapsulants, 2005. https://consumer.dow.com/en-us.html.

[61] "Product Information" Dow Corning, Sylgard® 184 Silicone Elastomer, 2017. https://consumer.dow.com/en-us/pdp.sylgard

[62] "Product description" Wacker, ELASTOSIL® RT 601, 2014. https://www.wacker.com/cms/en/products/product/product.jsp?product=10461.

[63] J.C. McDonald, D.C. Duffy, J.R. Anderson, D.T. Chiu, H. Wu, O.J. Schueller, and G.M. Whitesides. Fabrication of microfluidic systems in poly(dimethylsiloxane). *Electrophoresis*, 21(1):27–40, 2000.

[64] S.K. Sia and G.M. Whitesides. Microfluidic devices fabricated in poly(dimethylsiloxane) for biological studies. *Electrophoresis*, 24(21):3563–3576, 2003.

[65] D.C. Duffy, J.C. McDonald, O.J. Schueller, and G.M. Whitesides. Rapid prototyping of microfluidic systems in poly(dimethylsiloxane). *Analytical chemistry*, 70(23):4974–4984, 1998.

[66] C.S. Effenhauser, G.J. Bruin, A. Paulus, and M. Ehrat. Integrated capillary electrophoresis on flexible silicone microdevices: analysis of dna restriction fragments and detection of single dna molecules on microchips. *Analytical chemistry*, 69(17):3451–3457, 1997.

[67] M.A. Eddings, M.A. Johnson, and B.K. Gale. Determining the optimal pdms–pdms bonding technique for microfluidic devices. *Journal of Micromechanics and Microengineering*, 18(6):067001, 2008.

[68] M.A. Unger, H.P. Chou, T. Thorsen, A. Scherer, and S.R. Quake. Monolithic microfabricated valves and pumps by multilayer soft lithography. *Science (New York, N.Y.)*, 288(5463):113–116, 2000.

[69] S. Satyanarayana, R.N. Karnik, and A. Majumdar. Stamp-and-stick room-temperature bonding technique for microdevices. *Journal of Microelectromechanical Systems*, 14(2):392–399, 2005.

[70] K. Kreppenhofer. *Modular Biomicrofluidics - Mikrofluidikchips im Baukastensystem für Anwendungen aus der Zellbiologie*, volume 18. KIT Scientific Publishing, Karlsruhe, Baden, 2012.

[71] B. Samel, M.K. Chowdhury, and G. Stemme. The fabrication of microfluidic structures by means of full-wafer adhesive bonding using a poly(dimethylsiloxane) catalyst. *Journal of Micromechanics and Microengineering*, 17(8):1710–1714, 2007.

[72] J.S. Go and S. Shoji. A disposable, dead volume-free and leak-free in-plane pdms microvalve. *Sensors and Actuators A: Physical*, 114(2-3):438–444, 2004.

[73] L. Xiong, P. Chen, and Q. Zhou. Adhesion promotion between pdms and glass by oxygen plasma pre-treatment. *Journal of Adhesion Science and Technology*, 28(11):1046–1054, 2014.

[74] S. Bhattacharya, A. Datta, J.M. Berg, and S. Gangopadhyay. Studies on surface wettability of poly(dimethyl) siloxane (pdms) and glass under oxygen-plasma treatment and correlation with bond strength. *Journal of Microelectromechanical Systems*, 14(3):590–597, 2005.

[75] S. von der Ecken and A.E. Guber. *Entwicklung einer digitalen Mikrofluidikplattform für die synthetische Biologie.* Dissertation, KIT-Bibliothek, Karlsruhe, 2017.

[76] G. Li, R. Ran, J. Zhao, and Y. Xu. Design, simulation, and optimization of a miniaturized device for size-fractioned dna extraction. *Electrophoresis*, 28(24):4661–4667, 2007.

[77] D. Sánchez, A. Guber, R. Ahrens, and U. Strähle. Automatisiertes, integriertes mikrofluidisches system für die hochdurchsatz-klonierung, 05.12.2017. Patent Pending (102017011226.6) Germany.

[78] D.J. Guckenberger, T.E. de Groot, A.M.D. Wan, D.J. Beebe, and E.W.K. Young. Micromilling: a method for ultra-rapid prototyping of plastic microfluidic devices. *Lab on a chip*, 15(11):2364–2378, 2015.

[79] A. Waldbaur, H. Rapp, K. Länge, and B.E. Rapp. Let there be chip—towards rapid prototyping of microfluidic devices: One-step manufacturing processes. *Analytical Methods*, 3(12):2681, 2011.

[80] T.D. Boone, Z.H. Fan, H.H. Hooper, A.J. Ricco, H. Tan, and S.J. Williams. Peer reviewed: Plastic advances microfluidic devices. *Analytical Chemistry*, 74(3):78 A–86 A, 2002.

[81] T. Rajabi, V. Huck, R. Ahrens, M.C. Apfel, S.E. Kim, S.W. Schneider, and A.E. Guber. Development of a novel two-channel microfluidic system for biomedical applications in cancer research. *Biomedical Engineering / Biomedizinische Technik*, 57(SI-1 Track-E), 2012.

[82] H. Mühlberger. Mikrofluidische CE-Systeme aus polymeren mit elektrischer detektion für life-science-anwendungen, 2007. Dissertation, KIT-Bibliothek, Karlsruhe.

[83] W. Hwang and V. Saile. Effizientes multikanal-lab-on-chip-system für die bioanalytik, 2010. Dissertation, KIT-Bibliothek, Karlsruhe.

[84] L. Petrova-Belova. *Mehrlagige mikrofluidische Systeme aus Polymeren zur zweidimensionalen Kapillarelektrophorese.* KIT Scientific Publishing, Karlsruhe, 2010.

[85] W. Wang and S.A. Soper. *Bio-MEMS: Technologies and applications.* CRC/Taylor & Francis, Boca Raton, 2007.

[86] H. Huang and D. Densmore. Integration of microfluidics into the synthetic biology design flow. *Lab on a Chip*, 14(18):3459–3474, 2014.

[87] A. Mata, A.J. Fleischman, and S. Roy. Characterization of polydimethylsiloxane (pdms) properties for biomedical micro/nanosystems. *Biomedical Microdevices*, 7(4):281–293, 2005.

[88] N.E. Steidle and A.E. Guber. *Micro- and Nanostructured Microfluidic Devices for Localized Protein Immobilization and Other Biomedical Applications.* PhD thesis, KIT-Bibliothek, Karlsruhe, 2014.

[89] T. Rajabi. *Entwicklung eines mikrofluidischen Zweikammer-Chipsystems mit integrierter Sensorik für die Anwendung in der Tumorforschung*, volume 23. KIT Scientific Publishing, Karlsruhe, 2014.

[90] S.E. Kim. *Konzeption und prototypische Fertigung einer nicht-invasiven mikrofluidischen Plattform für die Elektrophysiologie (NIMEP) zur Zellenanalyse*, volume 31. KIT Scientific Publishing, Karlsruhe, 2015.

[91] K.H.J. Buschow. *Encyclopedia of materials: Science and technology*, volume 11. Elsevier, Amsterdam, 2001.

[92] S.V. Gohil, S. Suhail, J. Rose, T. Vella, and L.S. Nair. Polymers and composites for orthopedic applications. In S. Bose and A. Bandyopadhyay, editors, *Materials and devices for bone disorders*, pages 349–403. Academic Press, Amsterdam, 2016.

[93] A. Subramaniam and S. Sethuraman. Biomedical applications of nondegradable polymers. In *Natural and Synthetic Biomedical Polymers*, pages 301–308. Elsevier, 2014.

[94] W. Kaiser. *Kunststoffchemie für Ingenieure.* Carl Hanser Verlag GmbH & Co. KG, München, third edition, 2011.

[95] "Properties of Polmethacrylate" Polymer Properties Database, 2017. http://polymerdatabase.com/polymer[Online, accessed 07-June-2018].

[96] H. Domininghaus, P. Elsner, P. Eyerer, and T. Hirth. *Kunststoffe: Eigenschaften und Anwendungen.* VDI-Buch. Springer, Berlin, Heidelberg, eight edition, 2012.

[97] "Polycasa Cast - Technical information" Polycasa, 2014. https://plastics.ulprospector.com/datasheet/e277713/polycasa-cast.

[98] "Gegossenes Acryl contra extrudiertes Acryl." Induflex A/S, 2018. http://www.pmma.dk/default.aspx?Lang=de-DE.

[99] F. Jiao and K. Cheng. An experimental investigation on micro-milling of polymethyl methacrylate components with nanometric surface roughness. *Proceedings of the Institution of Mechanical Engineers, Part B: Journal of Engineering Manufacture*, 228(5):790–796, 2013.

[100] P. Chen, C. Pan, W. Lee, and K. Li. An experimental study of micromilling parameters to manufacture microchannels on a pmma substrate. *The International Journal of Advanced Manufacturing Technology*, 71(9-12):1623–1630, 2014.

[101] E. Korkmaz, R. Onler, and O.B. Ozdoganlar. Micromilling of poly(methyl methacrylate, pmma) using single-crystal diamond tools. *Procedia Manufacturing*, 10:683–693, 2017.

[102] E. Joanni, J. Peressinotto, P.S. Domingues, G. de Oliveira Setti, and D. Pereira de Jesus. Fabrication of molds for pdms microfluidic devices by laser swelling of pmma. *RSC Adv*, 5(32):25089–25096, 2015.

[103] A.A.S. Bhagat and I. Papautsky. Enhancing particle dispersion in a passive planar micromixer using rectangular obstacles. *Journal of Micromechanics and Microengineering*, 18(8):85005, 2008.

[104] J. Aubin, D.F. Fletcher, and C. Xuereb. Design of micromixers using cfd modelling. *Chemical Engineering Science*, 60(8-9):2503–2516, 2005.

[105] A.A.S. Bhagat, E.T.K. Peterson, and I. Papautsky. A passive planar micromixer with obstructions for mixing at low reynolds numbers. *Journal of Micromechanics and Microengineering*, 17(5):1017–1024, 2007.

[106] C.K. Chung and T.R. Shih. A rhombic micromixer with asymmetrical flow for enhancing mixing. *Journal of Micromechanics and Microengineering*, 17(12):2495, 2007.

[107] S. Hossain, M.A. Ansari, and K. Kim. Evaluation of the mixing performance of three passive micromixers. *Chemical Engineering Journal*, 150(2-3):492–501, 2009.

[108] W. Jeon and C.B. Shin. Design and simulation of passive mixing in microfluidic systems with geometric variations. *Chemical Engineering Journal*, 152(2-3):575–582, 2009.

[109] J.H. Jung, G. Kim, and T.S. Seo. An integrated passive micromixer–magnetic separation–capillary electrophoresis microdevice for rapid and multiplex pathogen detection at the single-cell level. *Lab on a Chip*, 11(20):3465, 2011.

[110] B. Zhou, W. Xu, A.A. Syed, Y. Chau, L. Chen, B. Chew, O. Yassine, X. Wu, Y. Gao, J. Zhang, X. Xiao, J. Kosel, X. Zhang, Z. Yao, and W. Wen. Design and fabrication of magnetically functionalized flexible micropillar arrays for rapid and controllable microfluidic mixing. *Lab Chip*, 15(9):2125–2132, 2015.

[111] L. Fu and C. Lin. A rapid dna digestion system. *Biomedical Microdevices*, 9(2):277–286, 2007.

[112] N.T. Nguyen, M. Kim, J. Park, and N.E. Lee. An effective passive microfluidic mixer utilizing chaotic advection. *Sensors and Actuators B: Chemical*, 132(1):172–181, 2008.

[113] C. Wang and Y. Hu. Mixing of liquids using obstacles in y-type microchannels. *Tamkang Journal of Science and Engineering*, 13:385–394, 2010.

[114] "pGEM®-T Easy Vector Systems. Technical manual" Promega Corporation, 2015. https://www.promega.de.

[115] D. Sánchez, S. Rastegar, V. Gerber, R. Ahrens, U. Strähle, and A. Guber, editor. *Automatisiertes mikrofluidisches System zur Hochdurchsatz-DNA-Ligation*, 2017.

[116] G.L. Lukacs, P. Haggie, O. Seksek, D. Lechardeur, N. Freedman, and A.S. Verkman. Size-dependent dna mobility in cytoplasm and nucleus. *The Journal of biological chemistry*, 275(3):1625–1629, 2000.

[117] H. Kuhn, H. Försterling, and D.H. Waldeck. *Principles of physical chemistry*. Wiley, Hoboken, N.J., second edition, 2009.

[118] G. Heinzmann and B. Tartsch. "Antikörper, DNA und Proteine - Masse und Struktur von komplexen Biomolekülen in Lösung exakt analysieren" Analytik News. Viscotek GmbH, 2007. https://www.analytik-news.de/Fachartikel/Volltext/viscotek2.pdf [Online; accessed 20-November-2017].

[119] "Whisper Valve 6712 - Data sheet: 2/2 way Whisper Valve with media separation" Bürkert, 2018. https://www.burkert-usa.com/en/type/6712.

[120] Y. Zhan. *Development of a Microvalve for a DNA Ligation Microfluidic Device*. Master thesis, Karlsruhe Institut of Technology, Karlsruhe, 2016.

[121] Y Xu. *Development of a Microvalve for a DNA Cloning Microfluidic Device*. Master thesis, Karlsruhe Institut of Technology, Karlsruhe, 2017.

[122] N. Siegel. *Entwicklung eines Dosier- und Verteilsystems für die Automatisierung von DNA-Ligationen*. Master thesis, Karlsruhe Institut of Technology, Karlsruhe, 2017.

[123] N. Tsai and C. Sue. Review of mems-based drug delivery and dosing systems. *Sensors and Actuators A: Physical*, 134(2):555–564, 2007.

[124] S. Haeberle and R. Zengerle. Microfluidic platforms for lab-on-a-chip applications. *Lab on a chip*, 7(9):1094–1110, 2007.

[125] "Microfluidic Reservoir for 1.5 mL Eppendorf® – XS" Darwin Microfluidics, 2018. https://darwin-microfluidics.com/collections/microfluidic-reservoirs/products/1-5-ml-eppendorf-microfluidic-reservoir-xs.

[126] A.E. Guber, M. Heckele, D. Herrmann, A. Muslija, V. Saile, L. Eichhorn, T. Gietzelt, W. Hoffmann, P.C. Hauser, J. Tanyanyiwa, A. Gerlach, N. Gottschlich, and G. Knebel. Microfluidic lab-on-a-chip systems based on polymers—fabrication and application. *Chemical Engineering Journal*, 101(1-3):447–453, 2004.

[127] K.R. Aneja. *Experiments in microbiology, plant pathology and biotechnology*. New Age International, New Delhi, 4th ed. edition, 2007.

[128] M. Rahimzadeh, M. Sadeghizadeh, F. Najafi, S. Arab, and H. Mobasheri. Impact of heat shock step on bacterial transformation efficiency. *Molecular biology research communications*, 5(4):257–261, 2016.

[129] "Bacterial Transformation Workflow-4 Main Steps" Thermo Fischer Scientific, 2016. https://www.thermofisher.com/de/de/home/life-science/cloning/cloning-learning-center/invitrogen-school-of-molecular-biology/molecular-cloning/transformation/bacterial-transformation-workflow.html [Online; accessed 22-February-2018].

[130] R. Phatthanakun, P. Deekla, W. Pummara, C. Sriphung, C. Pantong, and N. Chomnawang. Design and fabrication of thin-film aluminum microheater and nickel temperature sensor. In *2012 7th IEEE International Conference on Nano/Micro Engineered and Molecular Systems (NEMS)*, pages 112–115. IEEE, 2012.

[131] Y. Fu, X. Zhou, and D. Xing. Lab-on-capillary: A rapid, simple and quantitative genetic analysis platform integrating nucleic acid extraction, amplification and detection. *Lab on a Chip*, 17(24):4334–4341, 2017.

[132] J. Wu, W. Cao, W. Wen, D.C. Chang, and P. Sheng. Polydimethylsiloxane microfluidic chip with integrated microheater and thermal sensor. *Biomicrofluidics*, 3(1):12005, 2009.

[133] J. Brandner. Ideas for conducting a heat shock in a microfluidic device, 24.06.2015. Personal Conversation.

[134] E. Bárcena Pérez. *Development of a Heating and Cooling Unit for a DNA-Transformation Microfluidic Device*. Bachelor thesis, Karlsruhe Institut of Technology, Karlsruhe, 2018.

[135] L. Witt and A. Voigt. 2 kanaltemperaturregelung, 2018. Internal Comunication.

[136] K.P. Schierjott. *Miniaturisierte Kapillarelektrophorese zur kontinuierlichen Überwachung von Kationen und Anionen in Prozessströmen*. PhD thesis, KIT Scientific Pub, Karlsruhe, 2010.

List of Figures

List of Tables

List of Symbols

A_c	cross-section area of the channel
α	opening angle of the channel walls at the position of the meniscus
A_{HA}	microchannels complete area for heating
A_{HCH}	microchannels area for heating
A_{CA}	microchannels complete area for cooling
C	concentration
D_h	hydraulic diameter
D	diffusion coefficient
D_{hM}	hydraulic diameter mixer
D_w	Diffusion coefficient DNA in water
D_c	Diffusion coefficient closed coil DNA
D_o	Diffusion coefficient open coil DNA
D_l	Diffusion coefficient linear DNA
η	medium viscosity
R_1	radius 1 of curvature
R_2	radius 1 of curvature
γ	surface tension
h	channel height
J_x	diffusion flux
k_b	Boltzmann constant
L	length dosing section
λ_{PDMS}	PDMS thermal conductivity
μ_w	water dynamic viscosity

μ_g	water/glycerin 50% (w/w) dynamic viscosity
m_b	dosing unit mass before dosing
m_a	dosing unit mass after dosing
D_{2000}	Diffusion coefficient for 2000 bp-DNA
P_w	Wetted perimeter of the channel
Δp_{cap}	Laplace pressure for a rectangular channel
Δp_{capR}	Laplace pressure for a circular channel
Δp_{burst}	Burst pressure
$\dot{Q}$	heating power
$\dot{Q}_H$	required heating power
$\dot{Q}_C$	required cooling power
Re_{cr}	critical Reynolds number
Re	Reynolds number
r_{ch}	channel radius
r	radius of expansion
Re_M	Reynolds number mixer
ρ_w	water density
T_M	medium temperature
r_H	Stokes radius
r_c	Stokes radius closed coil DNA
r_o	Stokes radius open coil DNA
r_l	Stokes radius linear DNA
ρ_g	water/glycerin 50% (w/w) density
ρ	density
θ	contact angle of the liquid and channel
T	local temperature
x	coordinate in the flow direction
T_g	glass-transition temperature
T_{Hi}	initial temperature for heating
T_{Hf}	final temperature for heating
d_{PDMS}	PDMS wall thickness
T_{Ci}	initial temperature for cooling
T_{Cf}	final temperature for cooling
u	characteristic velocity

u_1	velocity inlet 1
V_D	dosing volume
V_t	dosed volume
w	channel width
w_α	effective channel width

List of Acronyms

μ-TAS	Micro Total Analysis System
AB1	Air Buffer 1
AB2	Air Buffer 2
AB3	Air Buffer 3
AC1	Air Supply Competent Bacteria 1
AC2	Air Supply Competent Bacteria 2
AD1	Air DNA 1
AD2	Air DNA 2
AD4	Air DNA 4
AIMD	Automated Integrated Microfluidic Device
AL	Air Ligase
ALM1	Air Supply Ligation Mixture 1
ALM2	Air Supply Ligation Mixture 2
ALM3	Air Supply Ligation Mixture 3
ALM4	Air Supply Ligation Mixture 4
AV	Air Vector
BM	Bacterial Mixture
bp	base pairs
BRG-Module	Module Bacterial Recovery and Growth
C^4D	Capacitively Coupled Contactless Conductivity Detection
CE	Capillary Electrophoresis
CM	Culture Medium
COC	Cyclic olefin copolymer
D-Module	Module Digestion
DNA	Deoxyribonucleic acid
E. coli	Escherichia coli
EB1	Eppi Buffer 1

EB2	Eppi Buffer 2
EB3	Eppi Buffer 3
EC1	Eppi Competent Bacteria 1
EC2	Eppi Competent Bacteria 2
ED1	Eppi DNA 1
ED2	Eppi DNA 2
ED3	Eppi DNA 3
ED4	Eppi DNA 4
EL	Eppi Ligase
ELM1	Eppi Ligation Mixture 1
ELM2	Eppi Ligation Mixture 2
ELM3	Eppi Ligation Mixture 3
ELM4	Eppi Ligation Mixture 4
emf	electromotive force
Eppi	Eppendorf® tube
EV	Eppi Vector
EWOD	Electrowetting-on-dielectric
HEC	Hydroxyethyl Cellulose
HPMC	Hydroxypropyl Methyl Cellulose
IMT	Institute of Microstructure Technology
IR	infrared
ITG	Institute of Toxicology and Genetics
KIT	Karlsruhe Institute of Technology
LM	Ligation Mixture
L-Module	Module Ligation
LB	Lysogeny broth
MAD	Mean Average Deviation
MEMS	Micro-Electro-Mechanical Systems
mtDNA	Mitochondrial deoxyribonucleic acid
OD	optical density
PC	Polycarbonate
PCR	Polymerase chain reaction
PDMS	Polydimethylsiloxane

PE	Polyethylene
PET	Polyethylene terephthalate
PMMA	Polymethyl methacrylate
PS	Polystyrene
PVP	Polyvinylpyrrolidone
PWM	Pulse-width modulation
RNA	Ribonucleic acid
SEM	Scanning Electron Microscope
SOC	Super Optimal Broth
TB	Transformed Bacteria
T-Module	Module Transformation
TBE	Tris-Borate-Ethylenediaminetetraacetic acid (EDTA)
TCS	Temperature Control System
TEC	Thermoelectric cooler
UV	ultraviolet
VLB	Vector-Ligase-Buffer Mixture
WLI	White Light Interferometry

A. Appendix

A.1. PDMS properties

Property	Unit	Result
One or Two Part Two		two
Color		colorless
Viscosity (Base)	cP	5100
Viscosity (Mixed)	cP	3500
Thermal Conductivity	W/m K	0.27
Specific Gravity (Cured)		1.03
Working Time at 25 °C	hours	1.5
Cure Time at 25 °C	hours	48
Heat Cure Time at 100 °C	minutes	35
Heat Cure Time at 125 °C	minutes	20
Heat Cure Time at 150 °C	minutes	10
Durometer Shore		43
Dielectric Strength	kV/mm	19
Volume Resistivity	Ω*cm	2.9e14
Dissipation Factor at 100 Hz		0.00257
Dissipation Factor at 100 kHz		0.00133
Dielectric Constant at 100 Hz		2.72
Dielectric Constant at 100 kHz		2.69
Linear CTE (by DMA)[1]	ppm/°C	340
Tensile Strength	MPa	6.7
Refractive Index	@ 589 nm	1.4118
Refractive Index	@ 632.8 nm	1.4225
Refractive Index	@ 1321 nm	1.4028
Refractive Index	@ 1554 nm	1.3997
UL RTI Rating[2]	°C	150

Table A.1. Typical properties of PDMS *Sylgard*® 184 Silicone. ([1]UL-Underwriters Laboratories; RTI-Relative Thermal Index; [2]CTE-Coefficient of Thermal Expansion; DMA-Dynamic Mechanical Analysis) [61]

A.2. PMMA properties

Property	Unit	Result
Density	g/cm^3	1.19
Water absorption	%	0.2
Rockwell hardness	M scale	105
Tensile Strength	MPa	75
Elongation	%	6
Tensile Modulus	MPa	3400
Flexural Strength	MPa	120
Flexural Modulus	MPa	3200
Charpy (unnotched)	kJ/m^2	17
Charpy (notched)	kJ/m^2	2
Vicat Temp. (VST/B 50)	°C	110
Specific Heat Capacity	J/g K	2.16
Linear thermal expansion	mm/m°C	0.19
Max. service temperature continuous use	°C	80
Max service temperature short term use	°C	90
Degradation temperature	°C	> 280
Light transmission	%	92
Refractive index	n^D_{20}	1.492
Surface resistivity	Ω	10^{14}
Volume resistivity	Ω*m	10^{15}
Electrical strength	kV/mm	10
Dielectric strength	kV/mm	30
Dielectrical dissipation, factor 50 Hz		0.06
Dielectrical dissipation, factor 1 kHz		0.04
Dielectrical dissipation, factor 1 MHz		0.02
Relative permittivity, factor 50 Hz		2.7
Relative permittivity, factor 1 kHz		3.1
Relative permittivity, factor 1 MHz		2.7

Table A.2. Typical properties of PMMA Polycasa Cast®. ([1]UL-Underwriters Laboratories; RTI-Relative Thermal Index) [97]

A.3. pGEM® -T Easy Vector System

Promega

Quick PROTOCOL 1

pGEM®-T and pGEM®-T Easy Vector Systems

INSTRUCTIONS FOR USE OF PRODUCTS A1360, A1380, A3600 AND A3610.

Cloning PCR Products with pGEM®-T and pGEM®-T Easy Vectors

Ligation Using 2X Rapid Ligation Buffer

1. Briefly centrifuge the pGEM®-T or pGEM®-T Easy Vector and Control Insert DNA tubes to collect contents at the bottom of the tube.
2. Set up ligation reactions as described below. Vortex the 2X Rapid Ligation Buffer vigorously before each use. Use 0.5ml tubes known to have low DNA-binding capacity.

Reagents	Standard Reaction	Positive Control	Background Control
2X Rapid Ligation Buffer, T4 DNA Ligase	5µl	5µl	5µl
pGEM®-T or pGEM®-T Easy Vector (50ng)	1µl	1µl	1µl
PCR product	Xµl	–	–
Control Insert DNA	–	2µl	–
T4 DNA Ligase (3 Weiss units/µl)	1µl	1µl	1µl
Deionized water to a final volume of	10µl	10µl	10µl

3. Mix the reactions by pipetting. Incubate the reactions 1 hour at room temperature. Alternatively, incubate the reactions overnight at 4°C for the maximum number of transformants.

Transformation of JM109 High Efficiency Competent Cells

1. Prepare LB/ampicillin/IPTG/X-Gal plates.
2. Centrifuge the ligation reactions briefly. Add 2µl of each ligation reaction to a sterile 1.5ml tube on ice. Prepare a control tube with 0.1ng of uncut plasmid.
3. Place the JM109 High Efficiency Competent Cells in an ice bath until just thawed (5 minutes). Mix cells by gently flicking the tube.
4. Carefully transfer 50µl of cells to the ligation reaction tubes from Step 2. Use 100µl of cells for the uncut DNA control tube. Gently flick the tubes and incubate on ice for 20 minutes.
5. Heat-shock the cells for 45–50 seconds in a water bath at exactly 42°C. DO NOT SHAKE. Immediately return the tubes to ice for 2 minutes.
6. Add 950µl room temperature SOC medium to the ligation reaction transformations and 900µl to the uncut DNA control tube. Incubate for 1.5 hours at 37°C with shaking (~150rpm).
7. Plate 100µl of each transformation culture onto duplicate LB/ampicillin/IPTG/X-Gal plates. For the uncut DNA control, a 1:10 dilution with SOC is recommended.
8. Incubate plates overnight at 37°C. Select white colonies.

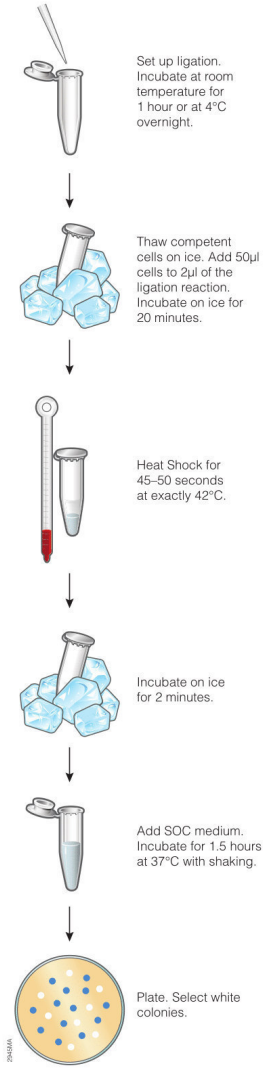

Additional protocol information in Technical Manual #TM042, available online at: **www.promega.com**

Figure A.1. Quick protocol of the pGEM® -T Easy Vector System I [31].

Promega

Quick PROTOCOL 2

pGEM®-T and pGEM®-T Easy Vector Systems

INSTRUCTIONS FOR USE OF PRODUCTS A1360, A1380, A3600 AND A3610.

pGEM®-T Vector Circle Map and Sequence Reference Points

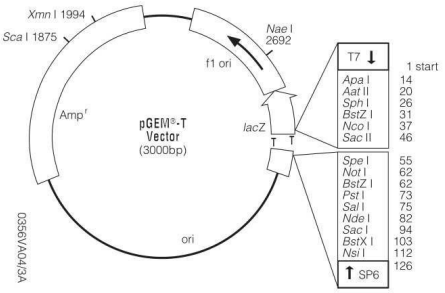

pGEM®-T Vector Sequence reference points:

T7 RNA Polymerase transcription initiation site	1
multiple cloning region	10–113
SP6 RNA Polymerase promoter (–17 to +3)	124–143
SP6 RNA Polymerase transcription initiation site	126
pUC/M13 Reverse Sequencing Primer binding site	161–177
lacZ start codon	165
lac operator	185–201
β-lactamase coding region	1322–2182
phage f1 region	2365–2820
lac operon sequences	2821–2981, 151–380
pUC/M13 Forward Sequencing Primer binding site	2941–2957
T7 RNA Polymerase promoter (–17 to +3)	2984–3

pGEM®-T Easy Vector Circle Map and Sequence Reference Points

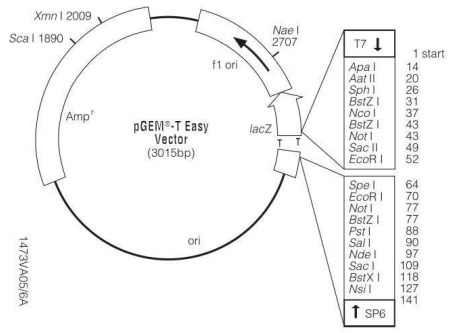

pGEM®-T Easy Vector Sequence reference points:

T7 RNA Polymerase transcription initiation site	1
multiple cloning region	10–128
SP6 RNA Polymerase promoter (–17 to +3)	139–158
SP6 RNA Polymerase transcription initiation site	141
pUC/M13 Reverse Sequencing Primer binding site	176–197
lacZ start codon	180
lac operator	200–216
β-lactamase coding region	1337–2197
phage f1 region	2380–2835
lac operon sequences	2836–2996, 166–395
pUC/M13 Forward Sequencing Primer binding site	2949–2972
T7 RNA Polymerase promoter (–17 to +3)	2999-3

Ordering and Technical Information
www.promega.com • Phone 608-274-4330
Toll free in USA 800-356-9526 • Fax 608-277-2601

Printed in USA. Revised 12/13. Part# 9FB033

Figure A.2. pGEM® -T Easy Vector Circle Map and Sequence Reference Points [31].

A.4. Data sheet TEC

MELCOR

Thermoelectric Cooler

CP1.4-17-045

Performance Specifications

Hot Side Temperature (º C)	25º C	50º C
Qmax (Watts)	9.2	10.9
Delta Tmax (º C)	65	74
Imax (Amps)	8.5	8.5
Vmax (Volts)	2.06	2.19
Module Resistance (Ohms)	0.21	0.23

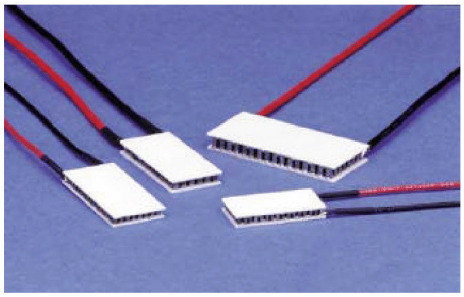

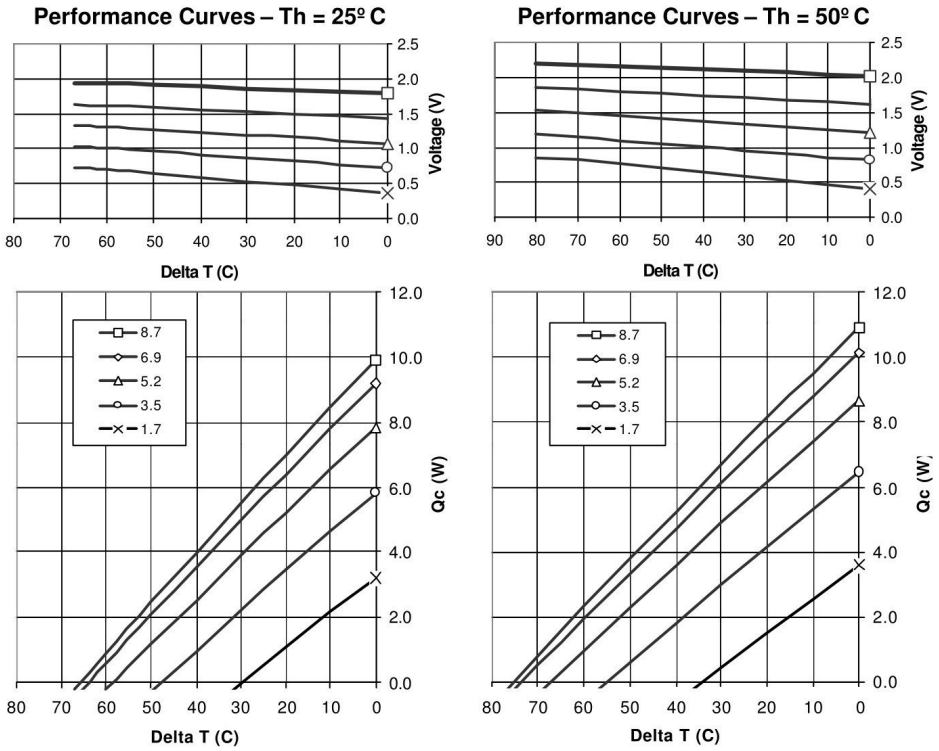

 Rev 1.01

1

Figure A.3. TEC Data sheet 1/2

CP1.4-17-045

Mechanical Drawing

NO DRAWING AVAILABLE

Ceramic Material: Alumina (Al_2O_3)
Solder Construction: 138ºC, Bismuth Tin (BiSn)

Thickness and Surface Finish Specifications

Suffix	Thickness	Flatness & Parallelism	Hot Face	Cold Face	Lead Length
L	0.131” ± 0.010”	0.0015” / 0.0015”	Lapped	Lapped	4.5”
-1	0.131” ± 0.001”	0.001” / 0.001”	Lapped	Lapped	4.5”
-2	0.131” ± 0.0005”	0.0005” / 0.0005”	Lapped	Lapped	4.5”
ML	0.135 ± 0.010”	0.002” / 0.002”	Metallized	Lapped	4.5”
LM	0.135 ± 0.010”	0.002” / 0.002”	Lapped	Metallized	4.5”
MM	0.139 ± 0.010”	0.002” / 0.002”	Metallized	Metallized	4.5”

Operating Tips

- Max. Operating Temperature: 80°C
- Do not exceed Imax or Vmax when operating module.
- Please consult Melcor for moisture and
- corrosion protection options.
- Solder tinning also available on metallized ceramics.

 Rev 1.01

2

Figure A.4. TEC Data sheet 2/2

A.5. Data sheet Heat sink

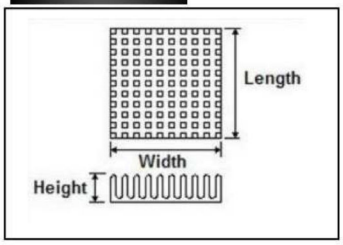

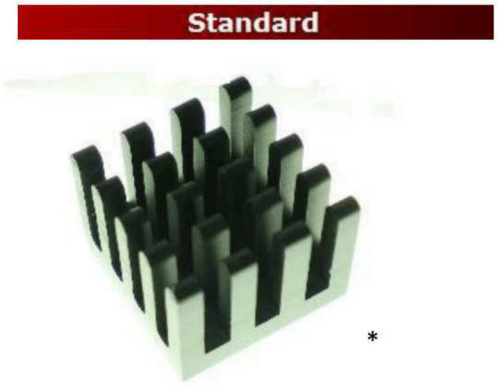

All ABL's BGA heatsinks are supplied with thermal tape

Model	Width [mm]	Length [mm]	Height [mm]	Pad Size [mm]	Wire Form	°C/W Natural	°C/W Forced 2M/s
BGA-STD-010	13.5	13.0	10.0	12x12	-	27.00	14.50
BGA-STD-015	14.0	14.0	10.0	18x18	-	26.50	14.00
BGA-STD-020	21.0	21.0	9.0	20X20	-	24.50	13.00
BGA-STD-025	23.0	23.0	6.0	20x20	-	22.00	10.50
BGA-STD-030	27.0	27.0	6.0	20x20	WF700/WF300	20.00	10.00
BGA-STD-035	26.0	26.0	8.0	20x20	WF700/WF300	18.50	9.70
BGA-STD-040	27.0	27.0	6.0	20x20	WF700/WF300	16.00	10.20
BGA-STD-045	23.0	23.0	18.0	20x20	WF700/WF300	14.70	7.30
BGA-STD-050	20.0	20.0	19.1	18x18	-	14.00	5.80
BGA-STD-055	25.9	23.9	10.0	20x20	WF700/WF300/WF151	14.00	6.00
BGA-STD-060	40.0	40.0	10.0	30x30	-	13.50	7.50
BGA-STD-065	27.8	27.8	11.2	20x20	WF700/WF300	12.20	5.80
BGA-STD-070	40.0	40.0	25.0	30x30	WF700/WF300/WF151	11.50	6.00
BGA-STD-075	40.0	40.0	23.0	18x18	WF700/WF300/WF151	11.00	5.60
BGA-STD-080	27.0	27.0	25.0	20x20	WF700/WF300/WF151	10.50	4.50
BGA-STD-085	30.7	30.7	14.1	20x20	WF700/WF300	10.00	5.20
BGA-STD-090	40.0	23.9	10.0	20x20	-	10.00	5.20
BGA-STD-095	40.0	40.0	10.0	18x18	WF700/WF300	9.70	4.00
BGA-STD-100	38.1	38.1	16.0	30x30	-	9.20	4.10
BGA-STD-105	35.0	35.0	18.0	30x30	WF700/WF300/WF151	9.20	5.20
BGA-STD-110	35.0	35.0	25.0	30x30	WF700/WF300/WF151	8.50	5.00
BGA-STD-115	40.0	40.0	18.0	30x30	WF700/WF300/WF151	8.20	5.10
BGA-STD-120	40.6	38.8	30.5	30x30	-	7.00	3.70

Figure A.5. Heat sink Data sheet

Thermally Conductive Aluminium Foil

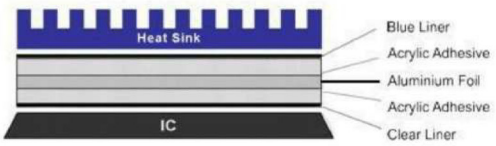

Colour	-	White
Backing Type / Thickness	Mm	Aluminium Foil / 0.10
Adhesive Type / Thickness	Mm	Arylic 0.075 (on clear liner side)
Total Thickness	mm	0,27
Adhesion	Kg/25mm	1,5
Thermal Conductivity	W/m-K	0,95
Thermal Resistance	°C-in^2/W	0,2
Holding Power@23°C	Hour	>72
Holding Power @ 130°C	Hour	>2

All ABL's BGA heatsinks are supplied with thermal tape.

With excellent thermal conductivity, cushioning and gap filling properties, the pad is an ideal thermal interface material specifically designed for heat sink attachment to MPU, chip set and other plastic encapsulated components.

It consists of an aluminium foil backing coated, on both sides, with a very high temperature resistance acrylic adhesive. Due to its high heat performance and adhesive properties this tape can also be use to attach components to a vertical heatsink and to metal enclosure surfaces.

Figure A.6. Thermal tape Data sheet

A.6. Circuit Diagram Temperature PID-Controller

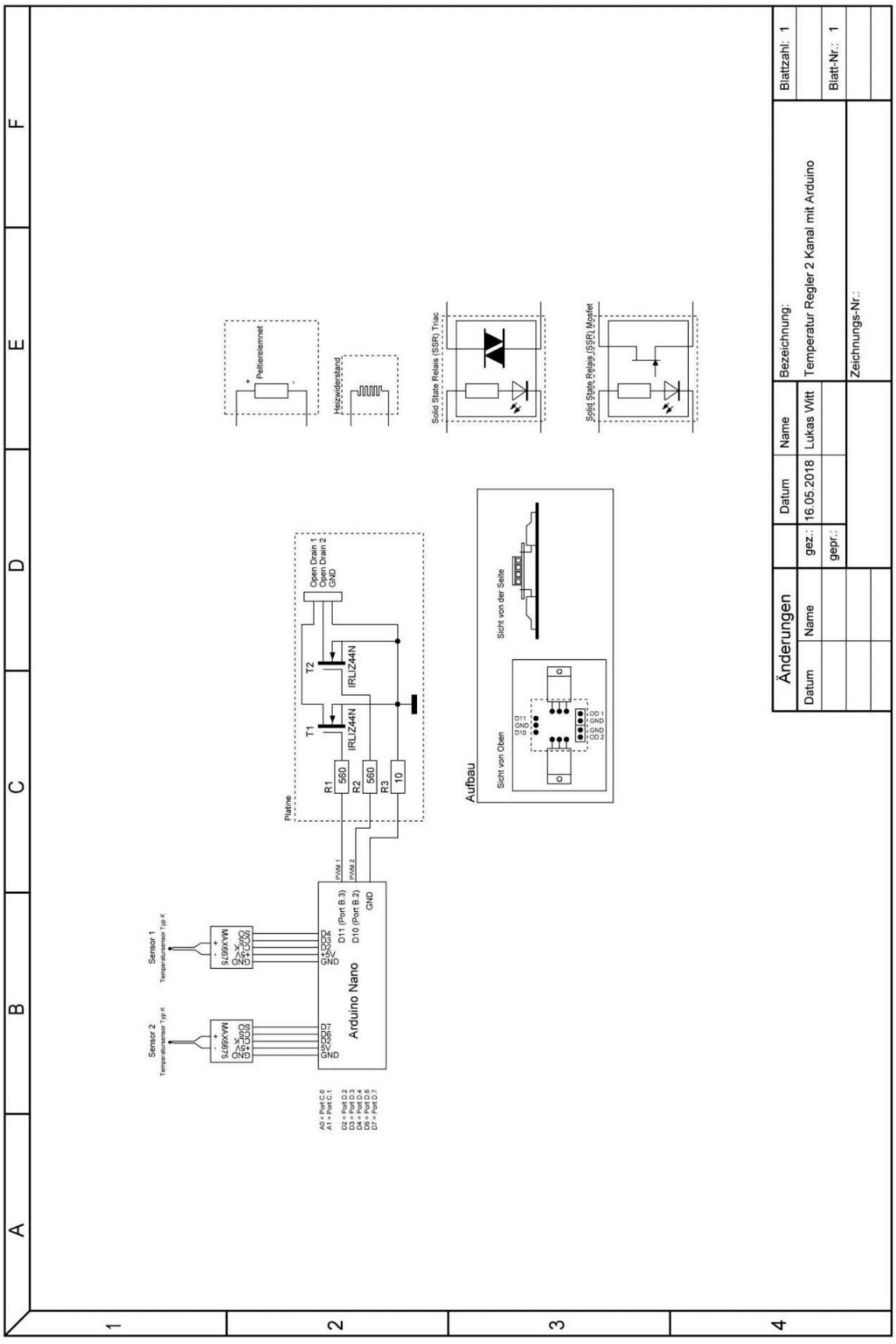

Figure A.7. Circuit diagram of the Temperature Control System [135]

A.7. Explosion view of the entire system

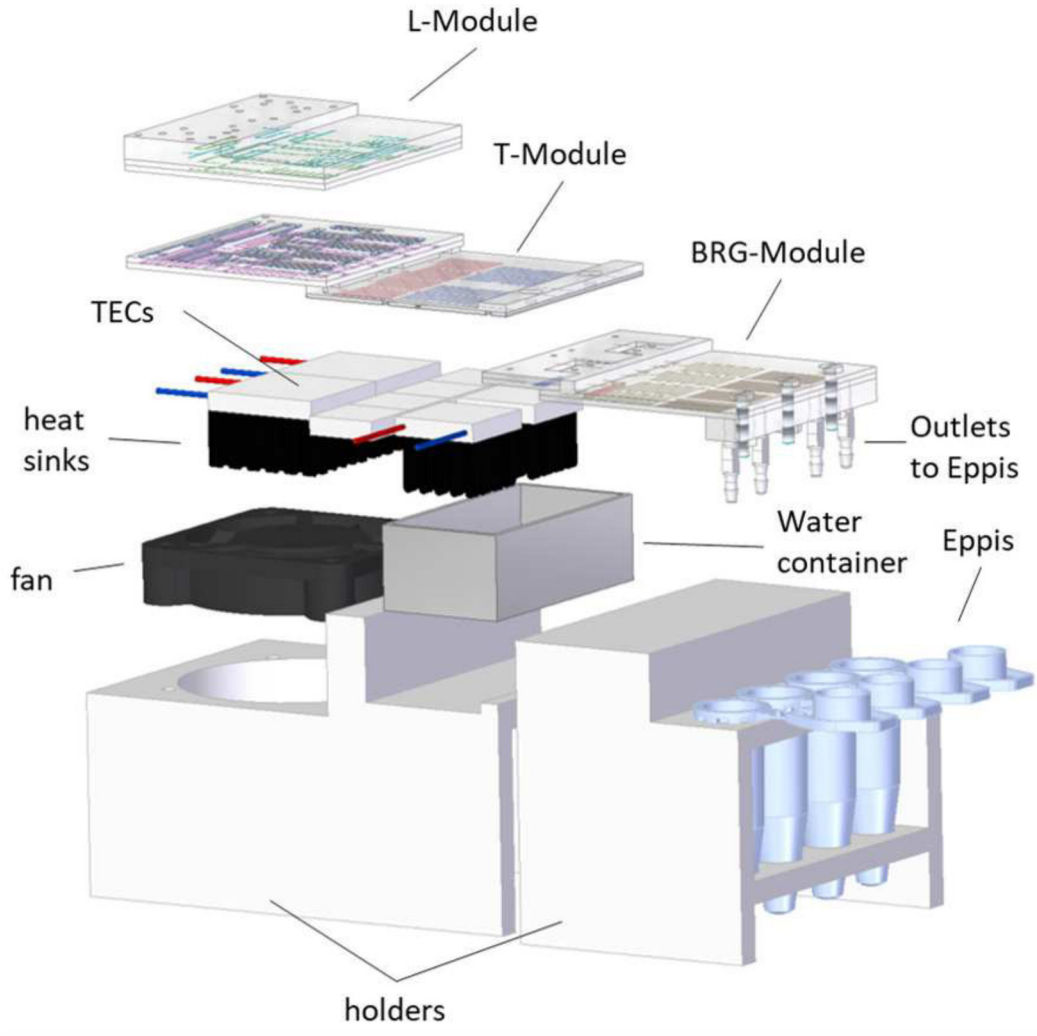

Figure A.8. Explosion view of the entire system. The L-Module, T-Module, and BRG-Module are shown as well as the TECs required for heating and cooling, with their respective heat dissipation mechanisms: heat sinks and water container or fan. The holders to support the entire system are also shown.

A.8. Patent, Contributions and Supervised degree theses

Patent

D. Sánchez, A. Guber, R. Ahrens, U. Strähle, 2017, *Automatisiertes, integriertes mikrofluidisches System für die Hochdurchsatz-Klonierung*, patent pending (102017011226.6), Germany

Contributions

S. von der Ecken, **D. Sánchez**, 2015, *Development of a digital microfluidic platform for the automation of a TALEN ligation process*, Meeting Molecular Interaction Engineering (MIE), Karlsruhe Institute of Technology (KIT) (Poster).

S. von der Ecken, **D. Sánchez**, S. Rastegar, R. Ahrens, A. Guber, 2016, *Continuous-flow and Digital Microfluidics*, International Conference on Molecular Interaction Engineering (MIE), Karlsruhe Institute of Technology (KIT) (Poster).

D. Sánchez, S. Rastegar, V. Gerber, R. Ahrens, U. Strähle, A. Guber, 2016, *Development of an automated, integrated microfluidic system for high-throughput cloning*, Meeting BioInterfaces International Graduate School (BIF-IGS), Althütte, Germany (Poster).

D. Sánchez, 2016, *Development of an automated, integrated microfluidic system for high-throughput cloning*, Seminar BioInterfaces International Graduate School (BIF-IGS), Karlsruhe Institute of Technology (KIT) (Talk).

S. von der Ecken, **D. Sánchez**, P. Teunissen, H. Raat, R. Ahrens und A. E. Guber, 2016, *Low-cost and easy producible paper-printed digital microfluidic chips*, presented in part at the MicroTAS Dublin, Ireland, 9-13 October, 2016, ISBN 978-0-9798064-9-0 (Poster)

D. Sánchez, S. von der Ecken, R. Ahrens, S. Rastegar, U. Strähle, A. Guber, 2017, Microfluidics in OG-4, Meeting Molecular Interaction Engineering (MIE), Teltow (Talk)

D. Sánchez, S. Rastegar, V. Gerber, R. Ahrens, U. Strähle, A. Guber, 2017, Automatisiertes mikrofluidisches System zur Hochdurchsatz-DNA-Ligation, 23-25 October, 2017, MikroSystemTechnik Kongress, München, Germany, ISBN 978-3-8007-4491-6 (Poster)

Supervised degree theses

Ying Zhan, *Development of a Microvalve for a DNA Ligation Microfluidic Device*, Institute of Microstructure Technology (IMT), Karlsruhe Institute of Technology (KIT), Master thesis, 2016.

Ye Xu, *Development of a Microvalve for a DNA Cloning Microfluidic Device*, Institute of Microstructure Technology (IMT), Karlsruhe Institute of Technology (KIT), Master thesis, 2017.

Nicolas Siegel, *Entwicklung eines Dosier- und Verteilsystems für die Automatisierung von DNA-Ligationen*, Institute of Microstructure Technology (IMT), Karlsruhe Institute of Technology (KIT), Master thesis, 2017.

Erika Bárcena Pérez, D*evelopment of a Heating and Cooling Unit for a DNA-Transformation Microfluidic Device*, Institute of Microstructure Technology (IMT), Karlsruhe Institute of Technology (KIT), Bachelor thesis, 2018.